RESEARCH REPORT

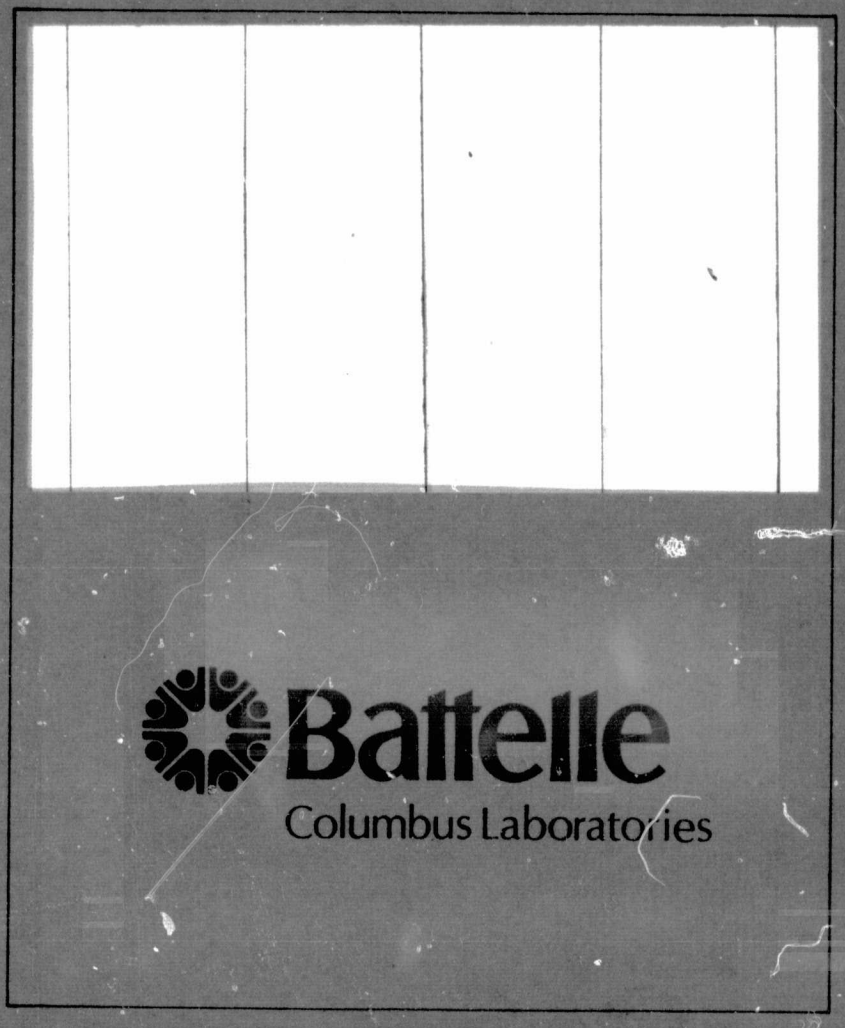

Battelle
Columbus Laboratories

FINAL REPORT

on

INVESTIGATION OF IMMISCIBLE SYSTEMS AND POTENTIAL APPLICATIONS

to

NATIONAL AERONAUTICS AND SPACE ADMINISTRATION
GEORGE C. MARSHALL SPACE FLIGHT CENTER

April, 1975

by

A. J. Markworth, W. Oldfield,
J. Duga, and S. H. Gelles

Contract No. NAS8-29748

BATTELLE
Columbus Laboratories
505 King Avenue
Columbus, Ohio 43201

TABLE OF CONTENTS

FOREWORD vi

ABSTRACT vii

1.0 INTRODUCTION AND SUMMARY 1

1.1 Background 1

1.2 Program Objective 4

1.3 Program Organization 4

1.4 Program Summary 5

1.41 Computer-Simulation Studies 5

1.42 Experimental Studies in the Aluminum-Indium System 8

1.43 Preparation of Immiscible Materials by Unusual Techniques 10

1.44 Analysis of Immiscible Materials 12

2.0 DETAILED PROGRAM DESCRIPTION 16

2.1 Computer-Simulation Study 16

2.11 Introduction 16

2.12 Transformation Processes in Liquid Immiscible Systems 17

2.13 Kinetics of Droplet Growth 21

2.14 Droplet Coalescence 30

2.15 Analysis of Skylab 4 Experiment TV102 36

2.16 Simulation of Collision Kinetics in Liquid Aluminum-Indium 48

2.2 Aluminum-Indium Experimental Studies 51

2.21 Background 51

2.22 Experimental 54

2.23 Results 57

TABLE OF CONTENTS
(Continued)

2.24 Low-G Experiments. 69

2.3 Rapidly Cooled Immiscible Materials. 71

2.4 Analysis of Liquid Phase Immiscible Systems. 83

2.41 Potential Systems for Consideration. 84

2.42 Categories of Applicability. 85

2.43 Characteristic Features of Suggested Applications 86

REFERENCES. 109

LIST OF TABLES

Table 1. Summary of Thermal Treatment Experiments Conducted on Aluminum-Indium Alloys. 56

Table 2. Results of Indium Droplet Size Distribution As Determined by the Quantimet 62

Table 3. Indium Droplet Size Distribution in Samples Al-In-3 and Al-In-4 63

Table 4. Results of Particle Size Analysis Carried Out on Al-In-3 And Al-In-4 Zeiss Particle Size Analyzer 66

Table 5. Results of Particle Size Analysis for Al-In-3 and Al-In-4 Zeiss Particle Size Analysis Carried Out on 500X Photomicrographs 68

Table 6. Summary of Rod Extraction Experiments 77

Table 7. Potential Applications of Immiscible Materials. . . . 85

Table 8. Systems of Immiscible Materials Suggested for Superconducting properties. 87

Table 9. Suggested Electrical Contact Materials Derived from Immiscible Systems. 92

Table 10. Suggested Immiscible Systems for Application to Nuclear Reactor Control Rods. 94

Table 11. Fine Particle Permanent Magnet Material Candidates . 96

LIST OF TABLES
(Continued)

Table 12. Properties of Selected Permanent Magnet Materials. . 100

Table 13. Immiscible Materials Systems for Bearing Alloys. . . 102

Table 14. Selected List of Candidate Systems with Potential Superplastic Behavior. 108

LIST OF FIGURES

Figure 1. Hypothetical Miscibility Gap, Showing Equilibrium Compositions of Host Phase and Second Phase (f_1 and f_2, Respectively) Upon Cooling from T_1 to T_2 at Composition f. 22

Figure 2. Variation of f_1' with Time During Droplet Growth for Three Different Droplet Concentrations. 29

Figures 3. Example of Collision Kinetics Simulated for a Terrestrial Environment Using Lindborg and Torssell Data for Velocity Functions. 34

Figure 4. Effect of Altering the Initial Distribution on Subsequent Distribution Behavior. 35

Figure 5. Simulation of Oil-Water Separation Kinetics in Space 43

Figure 6. Variation of Droplet Concentration with Time for Simulation Illustrated in Figure 5. 44

Figure 7. Simulation of Oil-Water Separation Kinetics in Space 45

Figure 8. Variation of Droplet Concentration with Time for Simulation Illustrated in Figure 7. 46

Figure 9. Aluminum-Indium Equilibrium System. 50

Figure 10. Simulation of Droplet Coalescence in a Liquid Aluminum-Indium System. 52

Figure 11. Variation of Droplet Concentration with Time for Simulation Illustrated in Figure 10. 53

Figure 12. Photomicrographs of Al-In-3 Rapidly Cooled (4.75 C/Sec) Through Miscibility Gap (100X). 58

LIST OF FIGURES
(Continued)

Figure 13. Photomicrographs of Al-In-4 Slowly Cooled (0.12 C/Sec) Through Miscibility Gap (100X). 59

Figure 14. Droplet Size Distribution for Samples Al-In-3 and Al-In-4 as Determined on the Quantimet. 65

Figure 15. Droplet Size Distribution for Samples Al-In-3 and Al-In-4 as Determined on the Zeiss Particle Size Analyzer. 67

Figure 16. Sketch Illustrating the Principles of Crucible Melt Extraction. 73

Figure 17. Schematic Diagram of Pendant Drop Melt Extraction Apparatus 74

Figure 18. Schematic of Vacuum-Melting Equipment 75

Figure 19. Photomicrographs of Extracted Rod No. 5, Pb-Cu (23.5 wt %). 78

Figure 20. Photomicrographs of Extracted Rod No. 7, Al-In (40 wt %). 79

Figure 21. Photomicrographs of Pendant Drop Melt Extracted Fibers Produced from Extracted Rod 6, Pb-Cu (23.5 wt %) . . 81

Figure 22. Typical Properties of Superplastic Al-Zn Alloy. . . . 106

FOREWORD

This report was prepared by Battelle's Columbus Laboratories under NASA Contract No. NAS8-29748 entitled "Investigation of Immiscible Systems and Potential Applications" for the George C. Marshall Space Flight Center of the National Aeronautics and Space Administration. It covers the period June 28, 1973, through March 30, 1975. Mr. I. C. Yates is the principal COR. Data on this program is recorded in Battelle's Columbus Laboratories Research Notebook 31049.

ABSTRACT

Described in this report is a combined analytical and experimental program whose objective is to explore the potential usefulness of systems containing a liquid phase miscibility gap and the role space processing might play in development of useful materials from these systems.

The program consisted of a computer simulation study in which the droplet coalescence kinetics at 0 g and 1 g were considered for two systems which contained liquid droplets in a host liquid. One of these (Al-In) typified a system containing a liquid-phase miscibility gap and the other (oil-water) a mixture of two essentially insoluble liquids. The stability of droplets in the oil-water system had been the subject of a Skylab Scien Demonstration Experiment. A number of coalescence mechanisms potentially prominent at low g in this system were analyzed in the present program and explanations presented for the observed unusual stability of the emulsion.

Ground base experiments were conducted on the coalescence of In droplets in an Al-In alloy during cooling through the miscibility gap at different cooling rates. These were in qualitative agreement with the computer simulation carried out on this system.

Potential applications for systems with liquid phase miscibilit gaps were explored. Possibilities included superconductors, electrical contact materials, superplastic materials, catalysts, magnetic materials, and others. The role of space processing in their production was also analyzed.

FINAL REPORT

on

INVESTIGATION OF IMMISCIBLE SYSTEMS AND POTENTIAL APPLICATIONS

to

NATIONAL AERONAUTICS AND SPACE ADMINISTRATION
GEORGE C. MARSHALL SPACE FLIGHT CENTER

from

BATTELLE
Columbus Laboratories

by

A. J. Markworth, W. Oldfield,
J. Duga, and S. H. Gelles

April, 1975

1.0 INTRODUCTION AND SUMMARY

1.1 Background

The field of immiscible materials and its relation to space processing has been summarized in a recent publication[1]*. Immiscibles represent a broad category of multiphase materials embracing composites, eutectics, monotectics, peritectics, eutectoids, peritectoids, precipitates, and systems with miscibility gaps.

Only materials and reactions that involve fluid phases (liquids or gases) have a special role in space processing. It is only in these that the effects of gravity would be pronounced. The more obvious mechanisms influenced by gravity are

- Segregation in a single phase liquid or gas due to density differences arising from local variations in composition or temperature
- Segregation in a multiphase system due to density differences between droplet and host phases (Stokes migration)

---

* References are listed on page 109.

- Convection currents in both single-phase fluids and those containing liquid or solid droplets due to temperature gradient-induced or composition-induced density variations in the liquid phase
- Segregation of a liquid phase in a porous solid host phase. This mechanism may be applicable to segregation in castings or in liquid-phase sintered compacts.

The work on the present program has concentrated on those systems containing a liquid-phase miscibility gap, i.e., a two-phase field consisting of two liquids which at sufficiently high temperature become a homogeneous single-phase liquid. Our efforts in this area have been concerned with the potential usefulness of such materials, the relationship between their microstructure and properties, the evaluation of these microstructures at 1 g and at 0 g, and the role of space processing in developing unique properties and microstructures in these materials. We have also been active in analyzing a Science Demonstration Experiment performed in Skylab dealing with the stability of oil (Krytox)-water mixtures.

The past work concerning experiments on processing materials with liquid-phase miscibility gaps at low g has been summarized by Reger and Yates[2]. Their review starts with the Apollo 14 experiments on the system paraffin-sodium acetate trihydrate with and without additions of argon or solid tungsten microspheres. It also describes the TRW low-g experiments conducted in the MSFC drop tower on Bi-Ga (50 at. %) and Pb-Zn (50 at. %) alloys and those conducted in KC-135 research aircraft on Au-Ge (40 at. %) (hypereutectic composition in a simple eutectic system), Cu-Pb (50 at. %), and Cr-Cu (55 at. %) alloys. Lastly, Reger and Yates described the Skylab experiments on Au-Ge (23.1 wt %), Pb-Zn (45.1 wt %) - Sb (9.9 wt %), and Pb-Sn (14.8 wt %) - In (15.0 wt %) alloys.

The following observations were made:

- Segregation--In general, the low-g processed material was less segregated than the terrestrially processed samples.

- Microstructure--The dispersed phase was generally more finely distributed in the low-g processed samples than in those processed at 1 g.
- Additional Phases--In the case of the Au-Ge alloys and Pb-Zn-Sb alloys, X-ray diffraction lines from unidentified phases were obtained from the 0-g processed samples and not from the samples processed at 1 g.
- Unusual Properties--The electrical properties of the Bi-Ga alloys processed by Reger in the MSFC drop tower were studied by Lacy and Otto[3]. These authors demonstrated that the finely dispersed structures present in some of the low-g processed samples produced manifestations of semiconducting behavior, while only metallic behavior was observed in the coarser earth-processed alloy. Superconducting transitions were found in both the 1- and 0-g processed alloys. T_c was significantly higher in these mixtures than in the pure metal reference materials.

At the start of the program, there had been little or no analytical work performed aimed at exploring the differences in structure and properties expected when systems containing a miscibility gap are processed at 0 versus 1 g. Certainly the minimization of segregation effects is expected. The observation of the fine microstructure obtained by 0-g processing is not as obvious. However, as will be described in this report, our computer-simulation studies have clearly demonstrated that it also is to be expected as a result of the removal of gravity-driven collision processes which cause droplet coalescence during cooling through, or holding in, a miscibility gap.

No further explanation has been put forth dealing with the unexpected presence of unidentified phases in the 0-g processed materials or the unusual electrical properties observed. Further analysis and experimentation is much needed in this area.

Reger and Yates[2] have expressed cautious optimism that some space-processed immiscible systems will have potentially useful properties as superconductors, permanent magnets, catalysts, etc. A list of systems containing known and suspected miscibility gaps has been compiled by Reger[4] as part of a NASA contract. These have been organized into rather broad categories according to their potentially useful properties. The list was the starting point for Battelle's Columbus Laboratories' analysis of potential applications for immiscible systems.

1.2 Program Objective

The objective of the program is to explore the potential usefulness of systems containing a miscibility gap from four major viewpoints.

(1) To understand the factors that control the size distribution of liquid droplets suspended in a host liquid and, specifically, to determine the effect of gravity on the distribution

(2) To technically assess the potential of immiscible systems for providing materials with superior or unusual properties

(3) To explore methods for producing and evaluating immiscible materials

(4) To explore the potential of space processing for the production of immiscible materials of improved or unusual properties.

1.3 Program Organization

The program was divided into three tasks which dealt with the following subject matter:

- Task 1--Experimental and computer-simulation studies of the behavior of liquid droplets in a host liquid. In particular, the influence of gravity is to be explored.

- Task 2--The development of processes for producing rapidly cooled/nonequilibrium, fine structures.
- Task 3--Exploration of potential applications of immiscible materials.

1.4 Program Summary

1.41 Computer-Simulation Studies

The computer-simulation studies have been concerned with the coalescence of liquid droplets in a host liquid either during the cooling of a single-phase liquid through a liquid-phase miscibility gap or after dispersing a mechanical mixture of two liquid phases as was the case in the Skylab experiment involving Krytox and water. Several processes were treated during the course of this study.

(1) Diffusion-controlled droplet growth in a liquid-phase miscibility gap
(2) Coalescence by collision processes
    (a) Stokes migration in a gravitational field
    (b) Gravity-driven convection-current-induced velocity gradients
    (c) Brownian motion of droplets
    (d) Marangoni effect, i.e., droplet migration in a thermal gradient due to the temperature dependence of the interfacial energy between the droplet and the host phase
(3) Ostwald ripening.

1.411 Major Findings. The following major results have come out of this aspect of the program:

(1) Development of computer coding for handling the changes in distribution of a population of droplets

in a host liquid. This development stressed both computer-time efficiencies and accuracy in the computations.

(2) Diffusional growth of droplets in a host liquid. This treatment showed that the process was complete in approximately 1 second or less. This allowed the separate treatment of this and other coalescence processes.

(3) Gravity-induced collision processes. After the rapid occurrence of the diffusional growth processes, the major agglomeration mechanism is due to gravity-induced collision processes, such as Stokes migration and velocity-gradient collisions caused by convection currents. Since these processes are virtually absent in low g, it is expected that the structures produced in systems containing liquid-phase miscibility gaps would be appreciably finer than those processed on earth under the same thermal conditions. It is also possible that with the finer sizes and the greater importance of surface energy terms that metastable structures could be obtained by space processing.

(4) Sensitivity to original size distributions. The treatment of agglomeration by gravity-induced collision processes is sensitive to the assumed droplet size distribution present at the onset of the collision processes. For very narrow original distributions, the growth of multiple peaks is predicted and compares favorably with experimental observations.

(5) Other coalescence processes. The contribution of Brownian motion to collision processes producing agglomeration and coalescence has been found to

be minimal. Collision processes produced by the Marangoni effect are not well understood. Growth by Ostwald ripening has also been shown to be unimportant.

(6) Contribution of fluid damping. In the analysis of the Skylab Science Demonstration experiment dealing with coalescence in the Krytox-water system, it has been concluded that fluid motion induced by the shaking of the sample vials and which is damped out during the early stages of observation can substantially contribute to coalescence during this stage.

(7) The abnormal stability of the droplet dispersions in the Krytox-water system as pointed out by Lacy and Otto[5] may be explained in terms of a collision model in which the collision efficiency is reduced from the usually assumed value of 1. This reduction results from the tendency of the droplets to follow fluid streamlines and thereby permit two droplets, which from simple geometrical considerations would collide, to in fact pass around each other.

1.412 Recommended Directions for Future Research. Damped Turbulence. Results obtained from our simulation study indicated that damped turbulent currents within the fluid could have important effects upon coalescence kinetics. At present, our model for such effects is relatively crude and requires some significant upgrading. This would yield more realistic predictions of the effects of turbulence (and also boundary-layer effects) on the behavior in time of the droplet size distribution.

Collision-Efficiency Effect. Factors affecting the rate at which droplets collide and coalesce are likely to be of major importance. A detailed study is therefore required of the influence of such factors as droplet size and velocity, fluid viscosity, etc., on the collision efficiency. Inclusion of these factors in our simulation will greatly enhance our predictive capabilities as far as the low-g environment is concerned and may remove the anomalous nature of the Skylab observations.

Separation Kinetics. For situations in which significant separation of the second phase from the host phase takes place, account of this behavior must be taken in the simulation. Removal of second-phase droplets from the host phase into a region containing only completely separated second-phase material affects the size distribution of droplets left behind and, hence, should be accounted for in the simulation

Solidification. All the processes described thus far take place in the liquid state. Also of importance is the effect of solidification of the liquid mixture upon the nature of the second-phase size distribution. Some collisions between droplets or spatial segregation of droplets may occur during solidification, and these phenomena need to be understood in order that we be able to produce two-phase alloys with the finest possible dispersion of second phase and as homogeneous as possible.

Simulation of Aluminum-Indium Separation Kinetics. The experimental portion of the completed research dealt extensively with separation kinetics in the Al-In system. Efforts were also undertaken to apply the computer simulation to this system, and these efforts should be continued, aimed particularly at predicting coalescence kinetics in the low-g environment. The experimental data obtained terrestrially will serve as a useful basis for comparison with results of simulations of earthbound behavior.

1.42 Experimental Studies in the Aluminum-Indium System

These studies are designed as an experimental backup for the computer-simulation studies. The objective is to determine the droplet

size distribution in an Al-In (40 wt %) alloy after cooling through the miscibility gap at different rates. The intention is to do similar experiments in the drop tower or in sounding rockets in order to verify the predictions made by the computer-simulation studies and to provide input data into such studies.

Al-In (40 wt %) alloys have been cooled through the miscibility gap at three rates. The two slower ones were measured as $\sim$ 0.1 and 5 C/sec, whereas the third is estimated to be on the order of 100 C/sec. Metallographic procedures have been developed for this material, and In droplet size distributions have been determined on metallographic sections by two techniques: Zeiss particle size analysis and the Quantimet. Only samples representing the two slower cooling rates have thus far been analyzed by these techniques. Some problems still remain in optimizing the metallographic procedures for unambiguously detecting the finer In droplets and determining the droplet size distribution in the fine size range.

1.421 Major Findings.

(1) Al-In appears to be an acceptable choice of alloy system for studying droplet coalescence in the miscibility gap.

(2) The size distributions in Al-In (40 wt %) alloys change in the following way. The number of fine particles decreases and the number of coarse ones increases as the cooling rate through the miscibility gap decreases. This was determined quantitatively for the slower cooled alloys and qualitatively for the fastest cooled alloy.

(3) Low-g experiments have been formulated to quantitatively deduce the effect of gravity on the coalescence of droplets in a host liquid. The information should not only be a check on the predictions made from the computer-simulation studies, but also allow us to explore the degree of structural fineness attainable in space.

1.422 Recommended Directions for Future Research. Background Experiments. Further work must be carried out in the area of droplet size distribution analysis. The In droplet size distributions had a very wide range of droplet sizes, all the way from a fraction of a micron close to 100 μ. To obtain a complete size distribution, it will be necessary to observe the sample by both metallographic techniques and by scanning electron microscopy. Thus, metallographic techniques would be used to characterize the droplet distribution in the larger size range, and electron micrographic techniques would be used for the finer size range. These two distributions would then have to be combined to obtain the entire droplet size distribution. Additional effort is also required in perfecting metallographic polishing techniques so that the finer particles may be unambiguously distinguished from the background.

Low-G Experiments. Low-g experiments should be carried out both in drop tower and in rocket flights to deduce the effect of gravitational forces and cooling rate on the kinetics of the droplet coalescence process and on the possible presence of nonequilibrium phases. Such work should provide answers to the question of how fine a structure is attainable by space processing and should not only improve our understanding of the effect of gravity on such processes, but should also guide us in selection of potential payoffs for these materials.

Compositional Effects. It would be highly beneficial to determine the effect of composition on the distribution of the droplets and phase morphology of the resulting structure. This information combined with experiments at low g and at different cooling rates should provide us with a good picture of the structural possibilities achievable on earth and in space.

1.43 Preparation of Immiscible Materials by Unusual Techniques

The objective of this portion of the work is to develop methods for producing materials with structures similar to those expected to be produced by space processing. The methods developed could act as screening

techniques for determining which materials might have attractive properties and thus might benefit from processing at 0 g. For this aspect of the work, we have chosen to use fast quenching techniques since these are most apt to duplicate the structures that might be obtained in space. Two techniques have been explored. The first is a rod extraction technique, which one of the principal investigators has used in the past[6] and which produces cooling rates of the order of 100 C/sec. The second technique is a Battelle Development Corporation patented one called melt extraction. Cooling rates as high as 10^6/sec should be achievable by this technique. The rod extraction technique produces rods ∿ 3-mm diameter which can provide a homogeneous feedstock into the second technique. The latter produces wire as fine as 0.1 mm or less.

1.431 Major Findings. Alloys have been fabricated by rod extraction in the systems Al-In, Bi-Ga, and Pb-Cu. Some of the Pb-Cu and Al-In rods have thus far been metallographically examined and generally show a microstructure consisting of fine particles dispersed in a matrix.

The production of fast-quenched wire has been attempted with one of the Pb-Cu alloys and one of the Al-In alloys by the pendant drop melt extraction technique. This was not at all successful for the Al-In and was only partially successful for the Pb-Cu. Instability of the droplet and the tendency for a portion of it to be at the temperature at which two liquids are stable and thus tend to segregate appear to be the major problems.

Some of the finer segments of Pb-Cu alloy prepared by the pendant drop melt extraction technique were examined metallographically. A large variation in composition among the wire segments was noted. This would be the case if a Pb-rich region were extracted, leaving behind a Cu-rich region which was subsequently extracted. The technique did, however, show much promise in that the structure, whether it be Cu rich or Pb rich, was extremely fine. It is expected that with some modification the method could be made to operate well.

1.432 Recommended Directions for Future Research. It is recommended that further effort be expended to produce alloys of liquid-phase immiscible materials rapidly quenched from a temperature above the miscibility gap. The exploration of two production techniques is recommended.

- Melt extraction of wire from a molten bath contained in a crucible
- Pressurized orifice chill block melt spinning.

The second method, which should produce higher quenching rates than the first, depends on the rapid quenching of a stream of molten metal produced by ejecting the metal under pressure through an orifice. The quenching is accomplished by directing the stream onto a cooled moving surface, such as a spinning disk or drum where the jet is shaped and solidified. After a suitable technique is developed, it may be used as a screening tool for sorting out potentially attractive systems. The wire or ribbon generated by these techniques should be suitable for property measurements.

1.44 Analysis of Immiscible Materials

The objective of this part of the program is to determine whether immiscible materials, especially those processed in space, can be effectively used in meaningful applications.

A large number of binary systems containing liquid-phase miscibility gaps as compiled by Reger[4] at TRW were reviewed. The analysis began first with the potential application, then with a consideration of whether a fine structure (a notable asset of space processing) would be of benefit, and last whether the components of a given liquid-phase immiscible system have suitable properties for the application. The following groups of applications/products were considered:

- Superconductors
- III-V semiconductors
- Electrical contact materials
- Catalysts

- Nuclear reactor control rods
- Permanent magnet materials
- Bearing materials
- Superplastic materials.

1.441 Major Findings and Recommendations for Future Research. Superconductors. There appears to be some merit for investigating liquid-phase immiscible materials having at least one component which is a superconductor. There are many systems to choose from. The fine size potentially achievable in space-processed materials may actually produce a superconducting transition where one does not exist in the bulk (e.g., Bi), may spread out the transition so that it is at least partially superconducting to a higher temperature, and may improve current carrying capacity. Other possible benefits may be obtained by introducing small particles in a superconducting matrix. These particles under some circumstances would act as grain refiners and/or flux pinners and lead to enhanced transition temperatures, higher current carrying capacities, and higher critical fields. For the size effect considerations, continuous rods of fine Pb in either Cu or Fe might be useful model materials. For the flux pinning aspects, Cu or Fe particles in Pb would be of interest. Further study of compositional and microstructural effects on the superconducting properties of some of the low-temperature alloys, such as Bi-Ga and Pb-Zn, should prove valuable as models for understanding the relation between the microstructure and superconducting properties of multiphase systems.

III-V Semiconductors. There has been evidence in the literature for the Ga-Bi system that unusual electronic effects may be occurring when the Ga and Bi are intimately mixed. In order to understand this effect, similar studies should be continued with Ga-Bi and initiated with As-Tl and Al-Bi.

Electrical Contact Materials. The area of electrical contact materials is very broad and complex. Many different materials are used, ranging from Cu and Cu alloys to Ag and its alloys and other precious metals, as well as the refractories, such as W and Mo. The costs of these materials range from $\sim$ \$0.50 per lb for Cu to $\sim$ \$1000 per lb for Pt.

The properties sought are good electrical conductivity, corrosion, welding and erosion resistance, good strength and long life. The use of one material over another is based on a complex set of details involving installation costs, operating costs, contact properties, design considerations, etc.

Some liquid-phase immiscible systems are presently being used in electrical contact applications (Cu-W, Ag-W, and Ag-Ni). These are processed mainly by powder metallurgy routes. It is not known whether these or others, such as Ag-Cr or Ag-Rh, could be made to have superior properties (such as longer life) by space processing. It very well may be the case. The objective of any research in this area would be to establish whether superior contact materials can be made by space processing and whether their usage would be economical. The higher cost precious metals and alloys would seem to be the better candidates from this viewpoint. Ag-base systems, such as Ag-Ni or Ag-Cr, however, could be starting points for this research.

Catalysts. Many potential catalytic systems have been listed in Reger's compilation. We have suggested techniques for producing such materials so that their high surface-to-volume requirement can be met. Additional effort will be required to suggest specific applications and specific systems to meet the requirements of these applications.

Nuclear Reactor Control Rods. Several binary systems have been suggested as having possible use in this application. More in-depth study is required to see if there is any potential payoff in this area.

Permanent Magnet Materials. Space processing may be a good way to produce fine elongated particles of a magnetic element or alloy in a matrix such as Pb. It is recommended that further exploration of the potential of such systems as Fe, Co, or Fe-Co alloy in a Pb matrix or Co or Fe in a Cu matrix be conducted.

Bearing Materials. Although there are many candidate bearing materials that potentially could benefit from a fine structure produced by space processing, it is not yet evident that distinct advantages can be obtained by the low-g processing. Study is required in a model system

to see if there are performance advantages to be obtained from space processing. The Pb-Cu or Al-Pb system seem to be reasonable candidates for the study.

Superplastic Materials. Seven immiscible systems (Ag-V, Bi-Zn, Co-Cu, Cr-Y, Cu-Fe, Pb-Zn, and Tl-Zn) have been suggested as good candidates for displaying superplastic behavior when produced to yield a fine microstructure. It is suggested that one or two of these systems be studied further and that the economics of a manufacturing process which involves the forming of a superplastic alloy be studied.

General Discussion. The Analysis of Immiscible Materials portion of this study has further developed our thinking in a number of different potential product areas. Because of the broad nature of the survey, however, the results have been somewhat superficial. It is now time to dig into some of the candidate applications in greater depth. We would thus recommend further study on superconductors, contact materials, bearing materials, and superplastic metals. The other potential product areas are still worthy of further effort, but their understanding and the potential of space processing is less obvious at this time.

2.0 DETAILED PROGRAM DESCRIPTION

2.1 Computer-Simulation Study

2.11 Introduction

A computer-simulation study of a given physical process is comprised of essentially two ingredients: (1) a physical model, which incorporates a description of the major kinetic phenomena giving rise to the process, and (2) an appropriate numerical interpretation of the physical model, which can be used, via the computer, to generate a quantitative description of the manner in which the process under consideration evolves with time for given input conditions. Computer-simulation methods are finding ever-widening applications in the materials science area. This stems partly from the fact that, on the one hand, kinetic processes occurring in materials are generally of an extremely complex nature, whereas on the other hand, increasingly sophisticated technological applications of materials require as complete an understanding of materials behavior as possible. Among the advantages offered by computer-simulation methods are the following:

(1) One is freed from requirements of analytical tractability in the development of theoretical models. The physical model one uses as the basis for his simulation is limited only by the bounds of current knowledge and the time and funds allotted to prepare and execute the program.

(2) Phenomena difficult to reproduce within the laboratory can often be more efficiently carried out by simulation techniques.

(3) It is a relatively simple and inexpensive matter to alter processing and physical parameters in a given computer "experiment", then repeat the "experiment" to observe resulting changes.

(4) Laboratory experimentation can be minimized when computer-simulation methods are used and the

simulations themselves represent a valuable supplement to corresponding laboratory experiments.

The results of space-production processes, in particular, because of the unique processing conditions, cannot be predicted completely via terrestrial experiments. This fact provides the incentive for the use of computer-simulation methods, which can be related to partially relevant experiments to predict, as accurately as possible, the results to be expected in the low-g environment. Such simulations take account of the best available theoretical results and employ laboratory experiments to test the predictions as far as possible. In addition, data obtained under actual low-g conditions can be comprehensively evaluated and understood in terms of current knowledge by means of simulation techniques.

The research described herein constitutes a computer-simulation study of transformation processes occurring in liquid immiscible systems, the emphasis being placed upon behavior to be expected at low g. The simulation developed is applied to corresponding experimental data obtained both terrestrially (i.e., for the Al-In system) and in space [i.e., for oil (Krytox)-water systems studied in Skylab 4].

2.12 Transformation Processes in Liquid Immiscible Systems

Basically, the approach of a liquid immiscible system toward thermodynamic equilibrium involves a series of kinetic processes, including the following:

(1) Nucleation of second-phase droplets within the supersaturated host phase
(2) Growth of the droplets by long-range diffusion of solute within the host phase, with consequent approach of the supersaturation level toward zero
(3) Coalescence of droplets by any of the following processes:
    (a) Direct impingement of growing droplets

(b) Impingement resulting from Brownian motion

(c) Impingement resulting from Stokes flow, in which droplet velocity (within a gravitational field) is a function of its radius

(d) Impingement resulting from velocity gradients within host-fluid flow field

(e) Impingement resulting from temperature-gradient-induced variation in interfacial energy (the Marangoni effect)[7]

(f) Ostwald ripening or growth of larger droplets at the expense of smaller ones[8].

Droplet nucleation results from fluctuations in solute concentration within the host phase, and the resultant competition between the decrease of Gibbs free energy associated with droplet formation and the increase of interfacial energy. Droplets which attain a certain critical size are stable, and their growth continues as the Gibbs free energy of the system decreases toward its equilibrium value. The various coalescence processes which subsequently occur are driven by the reduction in overall interfacial energy, which occurs as particles collide and coalesce. In addition, Stokes migration serves to reduce the overall gravitational energy of the system. It should be noted that droplet migration can be affected by the magnitude of the interfacial energy between the host phase and second phase, with a relatively low energy resulting in reduced migration velocities[9]. Also, certain factors may affect droplet coalescence, including the following: (1) the probability that two migrating droplets approaching one another will actually coalesce may be reduced by effects of the fluid-flow fields in their neighborhood, and (2) a finite time is required to drain the liquid film separating two droplets in close proximity (see Turkdogan's discussion of these phenomena[10]. The first of these two factors will be discussed below in greater detail in terms of Skylab 4 results on separation kinetics of immiscible oil-water mixtures.

The development of a quantitative physical model to describe the separation kinetics of an immiscible system can best be carried out

in terms of a continuous function $f(\bar{r},R,t)$, which describes the size distribution of droplets. To this end, we define this function such that the number dN of droplets (assumed spherical), at time t, having radii within incremental range dR measured about R and lying within volume element $d\bar{r}$ of coordinate space measured at position vector $\bar{r}$, relative to the origin of coordinates, is given by

$$dN = f(\bar{r},R,t)d\bar{r}dR \quad .$$

This function is, of itself, not of primary physical interest, although properties that are of interest [e.g., droplet concentration, $n(\bar{r},t)$, mean radius, $\langle R \rangle$, volume fraction, $f_v(\bar{r},t)$] can be expressed in terms of algebraic moments of the distribution function, the ℓ^{th} moment being given by

$$\mu_\ell(\bar{r},t) \equiv \int_0^\infty R^\ell f(\bar{r},R,t)dR \quad .$$

According to this definition,

$$n(\bar{r},t) = \mu_0(\bar{r},t) \quad ,$$

$$\langle R \rangle = \mu_1(\bar{r},t)/\mu_0(\bar{r},t) \quad ,$$

$$f_v(\bar{r},t) = 4\pi\mu_3(\bar{r},t)/3 \quad .$$

If, on the average, the distribution function is independent of spatial coordinates, then, of course, the moments and the associated properties of the second-phase distribution are functions only of time.

One can easily demonstrate that the distribution function must satisfy a continuity relation having the following form:

$$\frac{\partial f}{\partial t} + \text{div}(\bar{v}f) + \frac{\partial}{\partial R}(\nu f) = \sum_i \psi_i \quad , \tag{1}$$

where $\bar{v}$ is the velocity of a droplet through coordinate space, ν is its rate of growth (i.e., its "velocity" in radius space), and the various "source" functions ψ_i describe the rates at which droplets of given size are created and annihilated, such as through nucleation and collision processes. Clearly, this expression is analogous to the familiar Boltzmann integrodifferential equation which describes the distribution function for molecules of a gas [11].

The source functions for droplet-collision effects, resulting from droplet migration, are well known[12-14], and we shall simply state some known relations at this time. It is important to note that we shall ignore, for now, some factors that affect collision kinetics, such as those resulting from streamlines around migrating droplets in the host fluid. This important subject will be taken up again in our analysis of the Skylab 4 experiment on immiscible oil-water mixtures.

We define a function $Q(R',R'')$, where R' and R'' represent droplet radii, as follows:

$$Q(R',R'') \equiv \iint_s |\bar{v}' - \bar{v}''| ds \quad , \tag{2}$$

where $\bar{v}'$ and $\bar{v}''$ are the velocities of the R' and R'' droplets, respectively. The integration is carried out over area s, which may be regarded as a circular area of radius $R' + R''$, perpendicular to the relative velocity vector, and having its center located at the center of the R' droplet. Taking the distribution function to be independent of spatial coordinates, one can show that the source function ψ_c describing the creation of droplets of radius R is

$$\psi_c = 1/2 \int_0^\infty dR' \int_0^\infty dR'' \delta[R - (R'^3 - R''^3)^{1/3}] Q(R',R'') f(R',t) f(R'',t) \quad ,$$

where δ is the Dirac delta function. Integration over R'' yields

$$\psi_c = \frac{R^2}{2} \int_0^R \frac{dR'}{(R^3 - R'^3)^{2/3}} Q[R', (R^3 - R'^3)^{1/3}] f(R',t)$$

$$f[(R^3 - R'^3)^{1/3}, t] \quad . \tag{3}$$

Likewise, the source function, ψ_a, describing the annihilation of droplets of radius R is

$$\psi_a = - f(R,t) \int_0^\infty dR' Q(R,R') f(R',t) \quad . \tag{4}$$

Another source function can also be written, in principle at least, for droplet nucleation. This function may depend largely upon empirical nucleation data for want of an adequate nucleation theory. Source

functions for creation and annihilation of droplets by direct impingement as growth occurs can also be developed.

The growth velocity in droplet-radius space, v, depends upon such factors as cooling rate, kinetic data (e.g., solute diffusivity within the host fluid), droplet concentration, and phase-diagram data describing the miscibility gap at the temperatures in question. An adequate expression for v can generally be derived, at least under appropriate simplifying assumptions.

We thus have the essence of the physical model describing the breakdown of a liquid immiscible system. It should be noted that the various kinetic processes are likely to occur on different time scales, so that, at any given instant, one or another or some combination of these processes may actually be dominating the overall kinetics. In a given situation, one or another of the processes may never contribute to an appreciable degree; for instance, if the system of second-phase droplets is very disperse, direct impingement of growing droplets may occur only to a negligible extent.

In general, the integrodifferential equation, describing the temporal evolution of the distribution function, cannot be integrated analytically. It is at this point that the computer must be brought in, and solutions generated numerically.

2.13 Kinetics of Droplet Growth

2.131 The Equilibrium Configuration. Consider a hypothetical liquid immiscible system, for which a portion of the phase diagram is illustrated in Figure 1. The system contains two types of atoms, which we denote by A and B. Let us analyze the growth kinetics of second-phase droplets when the system is cooled from temperature T_1 above the miscibility gap, down to temperature T_2 within the gap at atomic fraction f of B atoms, where

$$f = \frac{N_B}{N_A + N_B} \quad , \tag{5}$$

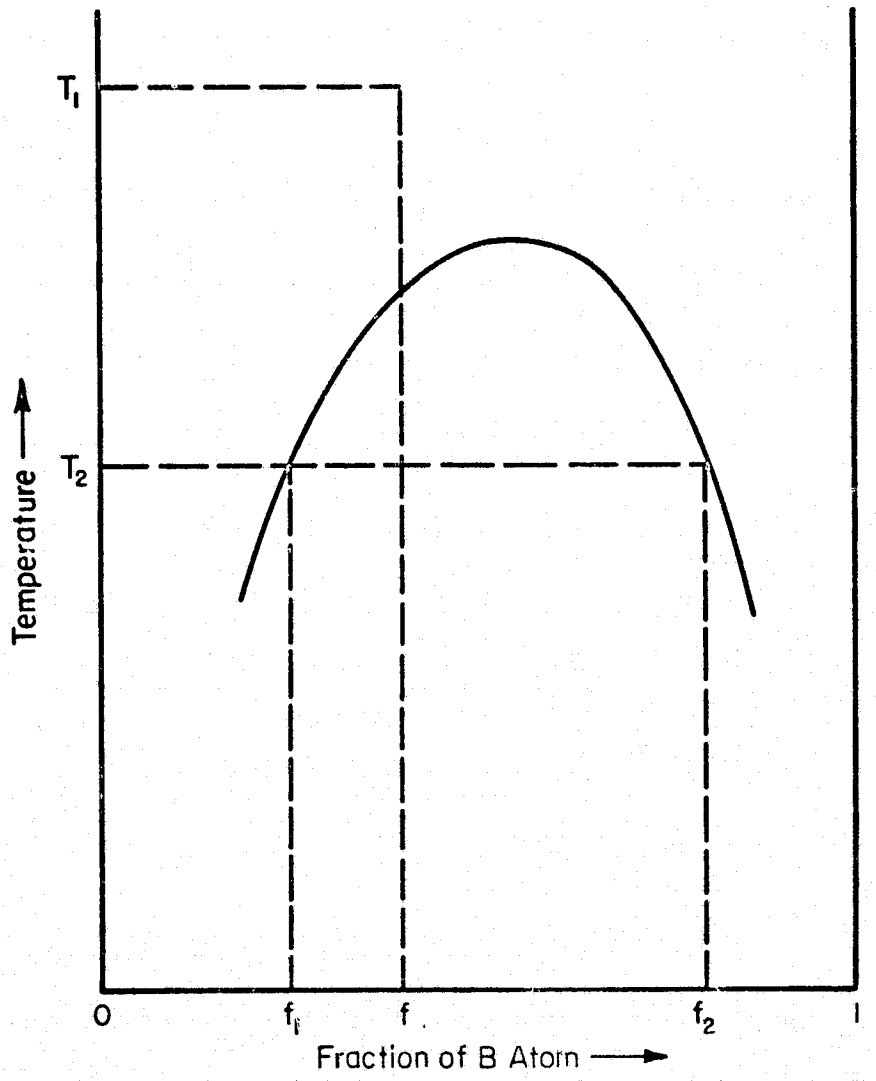

FIGURE 1. HYPOTHETICAL MISCIBILITY GAP, SHOWING EQUILIBRIUM COMPOSITIONS OF HOST PHASE AND SECOND PHASE (f_1 AND f_2, RESPECTIVELY) UPON COOLING FROM T_1 TO T_2 AT COMPOSITION f

with N_A and N_B being the respective numbers of atoms of types A and B in the system. (Extensive quantities, such as numbers of atoms, may be considered as referred-to-unit volume.) At temperature T_2, the equilibrium configuration of the system consists of a host phase and second phase characterized by atomic fractions f_1 and f_2 of B atoms, respectively, with

$$f_1 = \frac{N_{B1}}{N_{A1} + N_{B1}} \quad , \tag{6}$$

$$f_2 = \frac{N_{B2}}{N_{A2} + N_{B2}} \quad , \tag{7}$$

where N_{A1} and N_{B1} are the respective numbers of A and B atoms in the host phase and N_{A2} and N_{B2} are the numbers of A and B atoms in the second phase. Clearly, we must require that

$$N_A = N_{A1} + N_{A2} \quad , \tag{8}$$

$$N_B = N_{B1} + N_{B2} \quad . \tag{9}$$

One can use Equations (5) through (9) to derive the familiar "lever rule", i.e., that the equilibrium fractions F_1 and F_2 of all atoms within the host phase and second phases, respectively, are given by

$$F_1 = \frac{f_2 - f}{f_2 - f_1} \quad , \tag{10a}$$

$$F_2 = \frac{f - f_1}{f_2 - f_1} \quad . \tag{10b}$$

Obviously, this discussion of equilibrium compositions says nothing about the equilibrium morphology of the second phase. The computer-simulation study is devoted to evaluating the temporal evolution of the morphology of the second phase as thermodynamic equilibrium is approached.

2.132 Approach to Equilibrium. Clearly, a computer-simulation study deals with the nonequilibrium situation in the sense of using an

appropriate physical model to describe the kinetics of the approach of a system to its equilibrium configuration. In our case, we consider the growth of a system of second-phase droplets under the following simplifying assumptions:

(1) The system is cooled to a temperature T_2 within the miscibility gap, but outside the spinodal, such that diffusion coefficients remain positive[15].

(2) Nucleation occurs very rapidly and all nuclei are formed at essentially time $t = 0$.

(3) Growing second-phase droplets are situated at random positions throughout the volume of the host phase, and at any given instant, during the stage at which the host phase is decomposing, all droplets have the same size. (Thus, for example, effects due to collisions and subsequent coalescence of adjacent growing droplets are not included in the present treatment.)

(4) The growth stage occurs rapidly enough such that effects of droplet migration through the liquid need not be considered while growth is taking place.

(5) The second phase consists of droplets having composition f_2, and all growing droplets maintain this constant equilibrium concentration throughout the period of growth.

(6) Droplet growth occurs via the long-range diffusion of A and B atoms through the host phase, the diffusion of one of these atomic species being taken to be significantly slower than the other and, hence, rate controlling when atomic diffusion is the process governing droplet growth. In addition, the concentration field of diffusing atoms around each growing droplet is taken to be spherically symmetric with an otherwise uniform field of solute existing within the host phase.

(7) The composition of the host phase at the interphase boundaries is maintained at the equilibrium value (i.e., fraction f_1 of B atoms).

(8) The average atomic volume occupied by A and B atoms, denoted by Ω_A and Ω_B, respectively, does not change to a first approximation through the range of relative compositions within the given system.

Obviously, the validity of assumptions such as these must be tested both through comparison with experimental data and through demonstrated self-consistency within the physical model.

In simulating the approach of the system to thermodynamic equilibrium upon cooling to temperatures within the miscibility gap, two limiting cases can be considered: (1) cooling rate occurring very rapidly relative to the rate at which atoms can diffuse to droplets, and conversely, (2) cooling rate occurring very slowly relative to the rates of diffusive influx to droplets. In the former situation, decomposition of the host phase does not begin until cooling is virtually finished; in the latter, cooling occurs so slowly that the system is always in virtual equilibrium as defined by the phase diagram. Of course, cooling can also occur at intermediate rates, such that no process is rate controlling, but we shall not consider this significantly more complex problem at this time.

Very Rapid Cooling. Consider, first, diffusion-controlled growth kinetics. The system is rapidly cooled to temperature T_2 (after Figure 1) upon which n droplets nucleate from solution and begin to grow. We assume an initially homogeneous system, and also take the diffusion of B atoms to be rate controlling. Now let N'_{A2} and N'_{B2} be the instantaneous numbers of A and B atoms, respectively, in the second phase, and likewise, let N'_{A1} and N'_{B1} be the instantaneous numbers of A and B atoms in the host phase. Clearly,

$$N_A = N'_{A1} + N'_{A2} \quad , \tag{11}$$

$$N_B = N'_{B1} + N'_{B2} \quad , \tag{12}$$

and from assumption (5),

$$f_2 = \frac{N'_{B2}}{N'_{A2} + N'_{B2}} \quad , \tag{13}$$

and we define as f'_1, the instantaneous fraction of B atoms contained within the host phase, i.e.,

$$f'_1 = \frac{N'_{B1}}{N'_{A1} + N'_{B1}} \quad . \tag{14}$$

It is evident that f'_1 is equal to f initially and approaches f_1 as decomposition of the host phase approaches completion.

Let us assume the diffusion kinetics to be quasistationary, implying that the diffusion of B atoms to droplets can be described to a good approximation, using the time-independent diffusion equation (this will yield an underestimate of the instantaneous rate of influx of B atoms to droplets). One thus obtains the following expression for the rate at which N'_{B2} changes with time, t:

$$\frac{dN'_{B2}}{dt} = 4\pi n D_B (C'_{B1} - C^e_{B1}) + 4\pi n R^2 C^e_{B1} \frac{dR}{dt} \quad , \tag{15}$$

where D_B is the diffusion coefficient for B atoms in the host phase, C'_{B1} is the concentration of B atoms within the host phase at distances far from any droplets, C^e_{B1} is the equilibrium concentration of B atoms in the host phase at temperature T_2, and R is the instantaneous droplet radius. The first term on the right-hand side of Equation (15) represents the net rate of diffusive influx of B atoms into droplets, and the second term represents the rate at which B atoms already present in the host phase at the interface are collected into droplets.

Now one can use Equations (5) to (14) to show that

$$C'_{B1} = \frac{f'_1}{(1 - f'_1)\Omega_A + f'_1\Omega_B} \quad , \tag{16}$$

$$C^e_{B1} = \frac{f_1}{(1 - f_1)\Omega_A + f_1\Omega_B} \quad , \tag{17}$$

$$N'_{B2} = \frac{N_B f_2}{f} \left(\frac{f - f'_1}{f_2 - f'_1}\right) \quad . \tag{18}$$

In addition, the instantaneous total volume occupied by the second-phase droplets is just

$$\frac{4\pi nR^3}{3} = N'_{A2}\Omega_A + N'_{B2}\Omega_B \quad . \tag{19}$$

Combining Equations (13) and (19),

$$\frac{4\pi nR^3}{3} = \frac{N'_{B2}}{f_2} [(1 - f_2)\Omega_A + f_2\Omega_B] \quad , \tag{20}$$

from which we obtain

$$4\pi nR^2 \frac{dR}{dt} = \frac{1}{f_2} [(1 - f_2)\Omega_A + f_2\Omega_B] \frac{dN'_{B2}}{dt} \quad . \tag{21}$$

Differentiating Equation (18) with respect to time and substituting the result, together with Equations (16), (17), and (21) into (15), we obtain

$$\frac{df'_1}{dt} = -\lambda (f_2 - f'_1)^{5/3} (f - f'_1)^{1/3} \left[\frac{f'_1}{(1 - f'_1)\Omega_A + f'_1\Omega_B} - \frac{f_1}{(1 - f_1)\Omega_A + f_1\Omega_B}\right] \quad , \tag{22}$$

where

$$\lambda \equiv \frac{3^{1/3} D_B}{f_2(f_2 - f)\alpha} \left(\frac{4\pi nf}{N_B}\right)^{2/3} [(1 - f_2)\Omega_A + f_2\Omega_B]^{1/3} \quad ,$$

with

$$\alpha \equiv 1 - \frac{f_1}{f_2} \left[\frac{(1 - f_2)\Omega_A + f_2\Omega_B}{(1 - f_1)\Omega_A + f_1\Omega_B}\right] \quad .$$

Integration of Equation (22) by some appropriate method will yield the explicit variation of f'_1 with time.

Also, one can combine Equations (18) and (20) to obtain

$$\frac{4\pi nR^3}{3} = \frac{N_B}{f}\left(\frac{f - f_1'}{f_2 - f_1'}\right)\left[(1 - f_2)\Omega_A + f_2\Omega_B\right] \quad . \tag{23}$$

Equation (23) is a direct relation between the total volume of droplets (or volume fraction, if we refer n and N_B to unit volume) and the parameter f_1'.

We have solved Equation (22) numerically using a fourth-order Runge-Kutta method and using the following representative numerical values*:

$$f_1 = 0.3,\ f = 0.4,\ f_2 = 0.7 \quad ,$$

$$\Omega_A = \Omega_B = 3 \times 10^{-23}\ \text{cm}^3 \quad ,$$

$$N_B = (4/3) \times 10^{22}\ \text{cm}^{-3} \quad ,$$

$$D_B = (4/7) \times 10^{-5}\ \text{cm}^2/\text{sec} \quad .$$

The results are plotted in Figure 2 for three different droplet concentrations. Note that growth proceeds faster as the droplet concentration increases. This is what one would expect, since higher droplet concentrations mean that solute atoms have smaller distances, on the average, to diffuse in order to reach droplets. The times predicted here for growth to take place (of the order of a tenth of a second or less for these particular cases) are roughly consistent with the predictions of Lindborg and Torssell[14] and of Turkdogan[10] for the growth of deoxidation products within a liquid metal. One can show, by substituting appropriate numerical values into Equation (23), that the net volume fraction occupied by second-phase droplets at the conclusion of growth is 0.25 for all three cases (noting that $f_1' = f_1$ when growth is completed).

Very Slow Cooling. At the opposite extreme of the limiting case discussed above is that corresponding to a cooling rate so slow that the distribution of atoms between host phase and second phase always remains in quasiequilibrium, relative to the phase diagram, as the temperature is lowered into the miscibility gap. The instantaneous volume occupied by the droplets is still given by an expression analogous to Equation (23), i.e.,

---

* These values are typical of liquid metals, and so the results are representative for this class of materials.

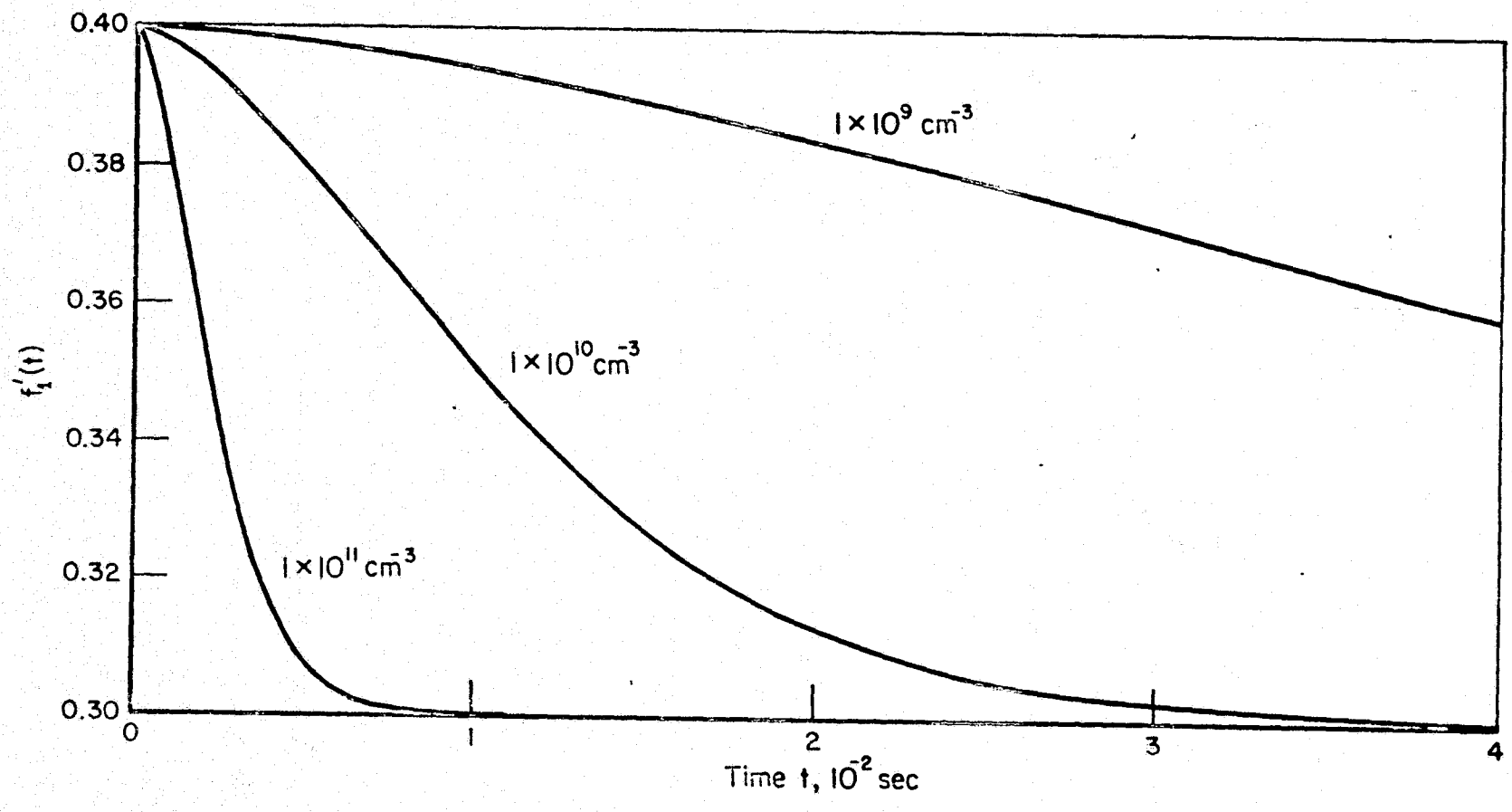

FIGURE 2. VARIATION OF f_1' WITH TIME DURING DROPLET GROWTH FOR THREE DIFFERENT DROPLET CONCENTRATIONS

$$\frac{4\pi nR^3}{3} = \frac{N_B}{f}\left(\frac{f - f_1'}{f_2' - f_1'}\right)\left[(1 - f_2')\Omega_A + f_2'\Omega_B\right] \quad , \tag{24}$$

where now f_1' and f_2' represent the atomic fraction of B atoms at the lower and upper compositional limits of the miscibility gap corresponding to the instantaneous temperature T. As T is slowly lowered to its final value T_2 (see Figure 2), f_1' and f_2' follow the miscibility-gap limits and finally reach values f_1 and f_2, respectively, at the final temperature T_2.

Equation (24) can be differentiated with respect to time, noting that

$$\frac{df_i'}{dt} = \dot{T}\frac{df_i'}{dT} \quad ,$$

where $\dot{T}$ is the cooling rate and where $i = 1,2$ with the derivative df_i'/dT being the local slope measured along the locus of points defining the limit of the miscibility gap. One thus obtains

$$4\pi nR^2\frac{dR}{dt} = \frac{N_B|\dot{T}|}{f(f_2' - f_1')^2}\{(f - f_1')\left[(1 - f_1')\Omega_A + f_1'\Omega_B\right]\frac{df_2'}{dT}$$

$$+ (f_2' - f)\left[(1 - f_2')\Omega_A + f_2'\Omega_B\right]\frac{df_1'}{dT}\} \quad . \tag{25}$$

We see from Equation (25) that the geometry of the miscibility gap (in composition-temperature space) becomes an important factor in determining droplet growth kinetics at very slow cooling rates.

2.14 Droplet Coalescence

Once the growth of liquid droplets from the host phase is completed, the structure of the two-phase system can undergo continued changes resulting from droplet coalescence. Coalescence can potentially occur by any of the several processes previously described, although it is likely that not all of these processes contribute significantly under a given set of conditions. Except for the direct overlap of growing droplets, coalescence processes generally occur on a larger time scale compared to

nucleation and growth processes and, if such is the case, can be assumed to occur, to a significant extent, only after the separation of the system into its two component phases has been virtually completed. Let us assume here (1) that coalescence is indeed important only after growth is completed, (2) that coalescence occurs principally by the collision of moving droplets, and (3) that the size distribution of droplets is, on the average, independent of spatial coordinates. In this case, Equation (1) reduces to

$$\frac{\partial f}{\partial t} = \psi_c + \psi_a \quad , \tag{26}$$

where ψ_c and ψ_a are given by Equations (3) and (4), respectively. Equation (26) can be integrated numerically once appropriate velocity functions are selected to describe the droplet-migration kinetics [see Equation (2)].

Our computer-simulation study of droplet-collision kinetics consists essentially of an integration of Equation (26) using a form of the Gaussian quadrature procedure. To permit the accuracy of the integration to be altered in a convenient way, a five-term quadrature was modified to include a variable integration interval, i.e., the total integration interval was subdivided into a number (which could be varied) of smaller intervals. The accuracy of the procedure could be tested by computing the total volume of droplets which should be invariant in time.

Among the useful features of the final version of the computer program we have developed are the following:

(1) The initial droplet size distribution (assumed to exist at the onset of the collision stage) is taken to be based on the familiar binominal distribution, truncated at both "tails" to conserve computational expense. Such factors as the distribution skewness, standard deviation, mean droplet radius, and volume fraction occupied by droplets can easily be selected by appropriate choices of the input parameters. This initial size distribution has a relatively general unimodal form and is most useful for testing the

effects of initial properties of the system on subsequent coalescence kinetics.

(2) Gross properties of the droplet size distribution are calculated as time progresses, including droplet concentration and mean radius. Also, the volume fraction occupied by droplets is continuously calculated to provide a check on the mathematical accuracy of the numerical approximations. This latter factor should be invariant in time, so that any observed variations are indicative of inaccuracies in the procedure.

(3) We have included a method by which the time increment δt for the finite-difference calculations is a variable parameter and is altered as the computation proceeds. In this regard, we recall that the solution to the complex integrodifferential equation, describing the evolution of the droplet size distribution, is generated by considering successively the changes which occur during these small increments of time. The problem we encountered was that, with arbitrary selection of δt by the user, it was likely that changes in the droplet system would occur either too slowly (i.e., δt too small, in which case excessive amounts of computer time are used) or too quickly (i.e., δt too large, in which case significant errors are introduced into the calculated results). We, therefore, decided to permit the selection of δt to be made within the calculation itself. There are innumerable ways of doing this (see, for example, Reference 16), but we chose one which is quite simple, as follows: the calculation treats the droplet size distribution essentially as a series of discrete size groups. We inserted a requirement in the program that the time increment for

each cycle be selected such that the concentration of drops in the size group corresponding to the smallest droplet radii would change by a selected percentage. It is clear that, in general, the time increment selected within the computer will be different for each cycle of the calculation. This criterion for selecting δt appears to work relatively well in governing the rate at which changes occur within the droplet distribution. For situations in which this criterion is found to be inadequate, appropriate alterations (e.g., lessening the selected percentage change) can easily be made.

Two examples of output obtained with the simulation are given in Figures 3 and 4. A terrestrial environment is assumed for these simulations, and both Stokes migration and velocity-gradient-induced migration of droplets are included. Data for the velocity functions* are those of Lindborg and Torssell[14], and the volume fraction occupied by droplets was assumed to be 0.25. The total time interval required for the size-distribution changes depicted in these figures was just a few tenths of a second. It is interesting to observe the formation of a bimodal distribution from one which was initially unimodal. (This is consistent with the experimental data of Lindborg and Torssell[14].) In particular, the second "peak" of the distribution is much more pronounced for the case illustrated in Figure 4, for which the initial distribution is much narrower than that for the case illustrated in Figure 3. This shows that the morphology of the initial distribution is indeed an important factor, and that some conclusions about the initial distribution could, therefore, be drawn from experimental data describing a size distribution at a later

---

* This particular set of data was chosen on the basis of ready availability and to permit some comparison to be made of predicted (i.e., simulated) kinetics with existing experimental data. It should be emphasized, however, that the input data can be easily altered in order to simulate the behavior of other systems that may be of interest, assuming the physical model is appropriate. The viscosity data used is typical of molten metals. Velocity gradients were based on a container size of 4.5 cm, and Stokes migration was based on a matrix-particle (droplet) density difference, $\Delta\rho = 4.6$.

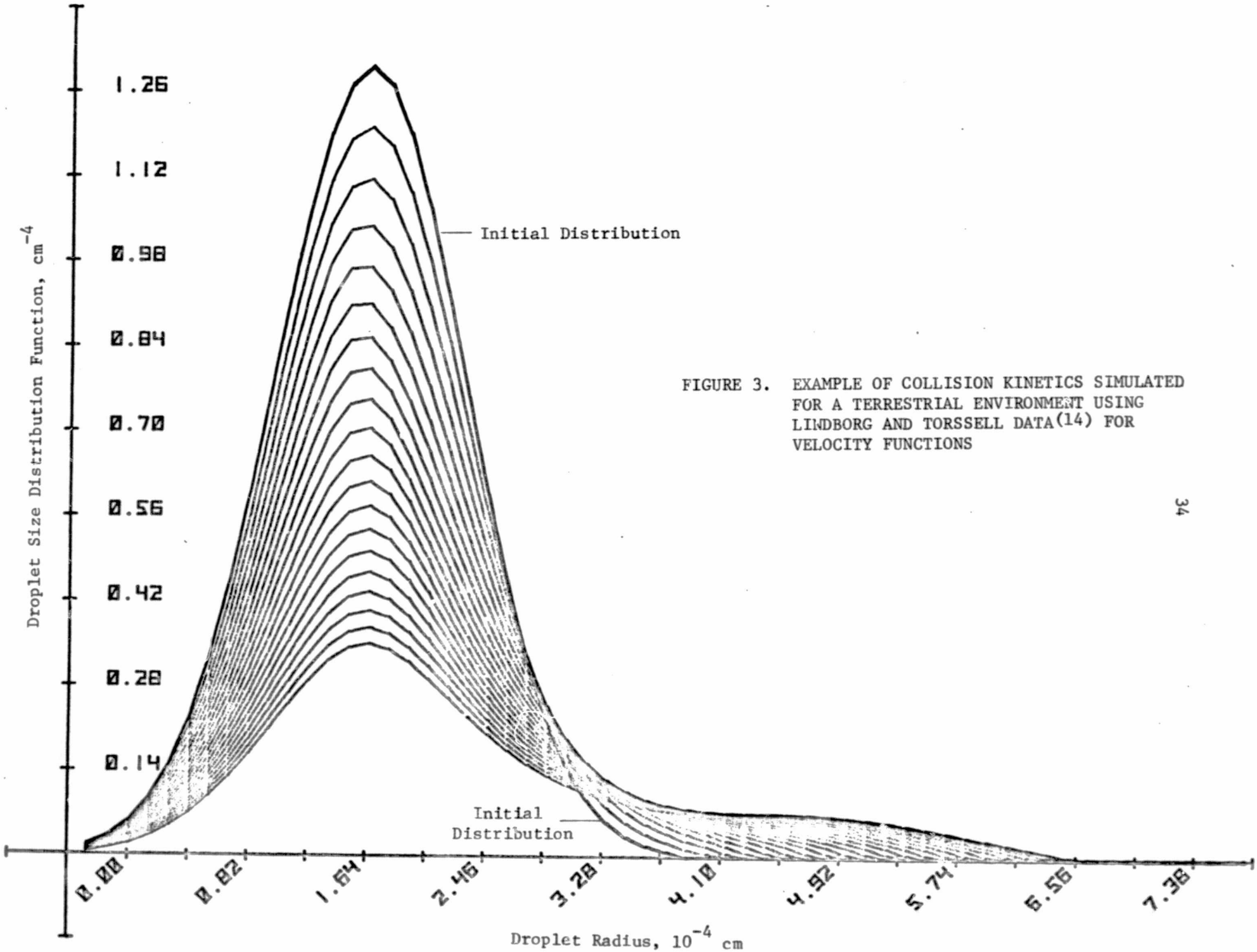

FIGURE 3. EXAMPLE OF COLLISION KINETICS SIMULATED FOR A TERRESTRIAL ENVIRONMENT USING LINDBORG AND TORSSELL DATA[14] FOR VELOCITY FUNCTIONS

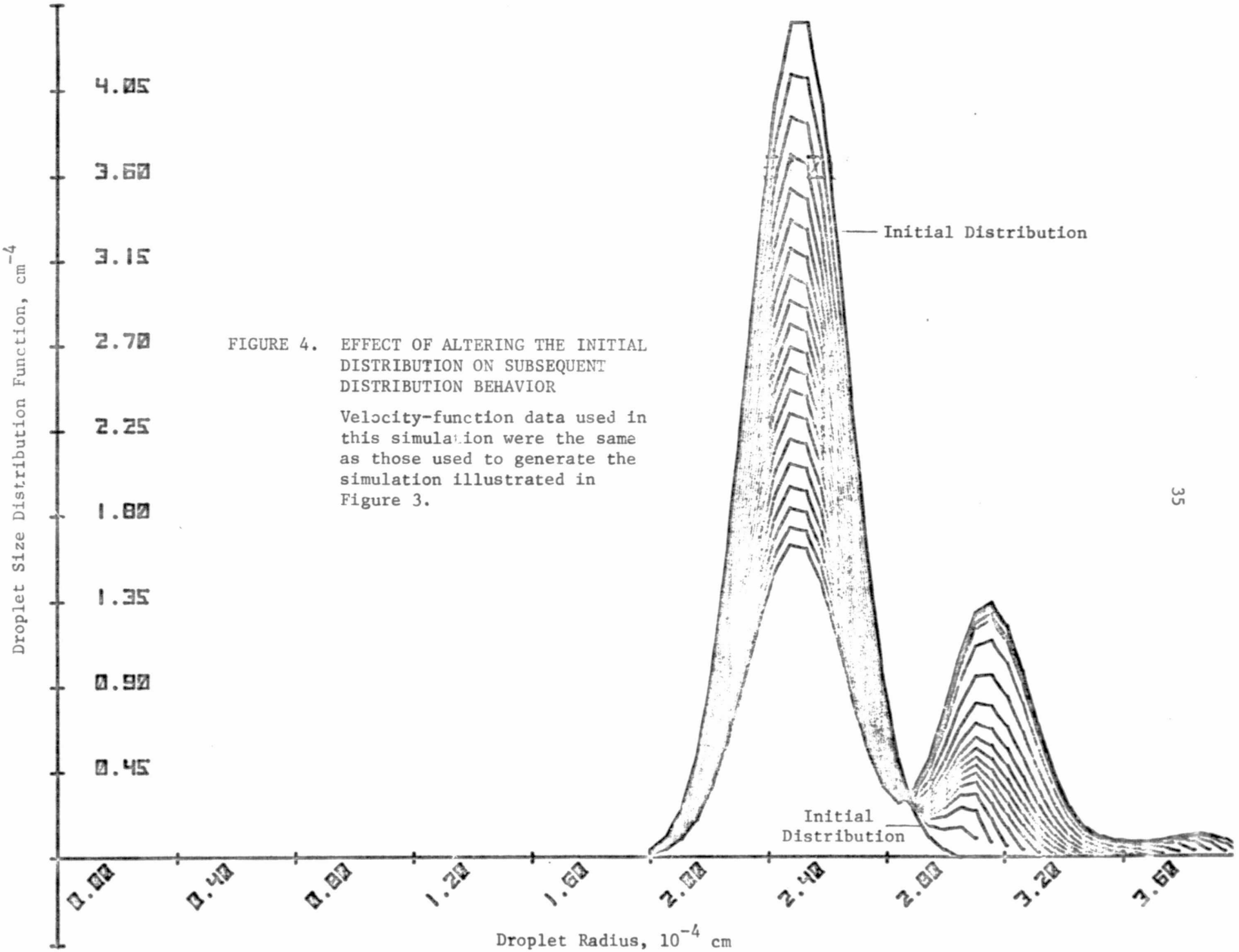

FIGURE 4. EFFECT OF ALTERING THE INITIAL DISTRIBUTION ON SUBSEQUENT DISTRIBUTION BEHAVIOR

Velocity-function data used in this simulation were the same as those used to generate the simulation illustrated in Figure 3.

time. We also note the formation of a third peak for the case shown in Figure 4. The placement of the initial distribution, relative to the droplet-size origin, might also be an important factor in determining subsequent coalescence kinetics, although we have not investigated this possibility.

It is interesting to note that the placement of the second peak in Figure 4, relative to the droplet-radius axis, can be predicted in a semiquantitative manner as follows: we see that the initial size distribution is relatively "narrow" in droplet-radius space, with most of the droplets having their radius, at this initial time, roughly equal to the mean radius (about 2.5 μ). When collisions first begin to take place, the new droplets most likely to be formed will simply be a combination of two of these 2.5-μ-radius droplets. The radius of these new droplets (since total volume is conserved) is just $(2.5\ \mu) \times 2^{1/3} \approx 3.1\ \mu$. It can be seen from Figure 4 that the maximum in the distribution function, occurring at the second peak, is positioned at about this value of droplet radius.

2.15 Analysis of Skylab 4 Experiment TV102

The stability of mixtures of immiscible liquids in low g was studied by the crew of Skylab 4, and the results thus obtained were compared to analogous experimental studies carried out on earth. A detailed description of these experiments has been given by Lacy and Otto[17]. Basically, the mixtures consisted of three samples containing 25, 50, and 75 vol % degassed Krytox 143 AZ oil, the remaining volume containing degassed water. The samples were contained in vials, and a small brass nut was included in each vial in order to disperse the liquids when the vials were shaken.

What is presented below is an analysis of droplet coalescence in space for these oil-water systems, in terms of possible coalescence mechanisms, including Brownian motion, Ostwald ripening, and velocity-gradient-induced collisions; in addition, a discussion of possible causes for the observed, and apparently anomalously high[5], stability of the dispersions in space is also presented.

2.151 Brownian Motion. The coagulation of droplets in a colloidal suspension, via Brownian motion, is an old problem which has been treated by many investigators (see, for example, References 17 to 19). One particularly pertinent result, which relates the concentration of droplets at time t to that at initial time t = 0 (assuming an initially uniform size distribution), i.e., N(t) and N(0), respectively, is the following:

$$\frac{N(t)}{N(0)} = \left(1 + \frac{t}{\tau_B}\right)^{-1} \quad , \tag{27}$$

where τ_B is a characteristic time which is indicative of the relative rate at which coalescence proceeds by Brownian motion, and is given by

$$\tau_B = \frac{3\mu}{4kTN(0)} \quad , \tag{28}$$

where μ is the viscosity of the host fluid, k is Boltzmann's constant, and T is the absolute temperature. Clearly, any numerical estimate for τ_B requires an estimate for N(0). The latter estimate can be made if one has some knowledge of the initial mean radius, $\langle R \rangle_o$, as follows: Assuming an initially uniform size distribution, the volume fraction f_v occupied by droplets is related to N(0) and $\langle R \rangle_o$ through the equation

$$f_v = 4\pi N(0)\langle R \rangle_o^3/3 \quad ,$$

in which case

$$N(0) = \frac{3f_v}{4\pi\langle R \rangle_o^3} \quad .$$

Let us take $f_v = 0.25$ and consider two possible choices for $\langle R \rangle_o$ so that we may determine the dependence of the kinetics upon initial droplet size. Thus, we find for $\langle R \rangle_o = 10\mu m$, $N(0) \approx 6 \times 10^7 cm^{-3}$, and for $\langle R \rangle_o = 50\mu m$, $N(0) \approx 5 \times 10^5 cm^{-3}$. Taking T ≈ 300 deg K, and μ = .63 and .01 poise[17] for Krytox oil and water, respectively, we obtain

Host phase: Krytox Oil

$\tau_B \approx 2 \times 10^5$ sec for $\langle R \rangle_o = 10\mu m$

$\tau_B \approx 2 \times 10^7$ sec for $\langle R \rangle_o = 50\mu m$

Host phase: Water

$$\tau_B \approx 3 \times 10^3 \text{ sec for } \langle R \rangle_o = 10\mu m$$

$$\tau_B \approx 4 \times 10^5 \text{ sec for } \langle R \rangle_o = 50\mu m.$$

We see that even for the smaller of the two initial sizes and for Krytox droplets moving through water, which has relatively low viscosity, the distribution of droplets remains relatively free of changes wrought by Brownian-motion coalescence for substantial times.

In addition, it is clear from Equations (27) and (28) that for asymptotic times (i.e., $t >> \tau_B$) the instantaneous droplet concentration becomes independent of initial conditions, that is

$$N(t) \approx \frac{N(0)\tau_B}{t} = \frac{3\mu}{4kTt} \quad ,$$

and the droplet concentration, in units of cm^{-3}, becomes

Host phase: Krytox Oil

$$N(t) \approx 1.14 \times 10^{13}/t(sec)$$

Host phase: Water

$$N(t) \approx 1.81 \times 10^{11}/t(sec) \quad .$$

Thus, for example, if the host phase is water and the initial droplet size was 10μm, then after 5×10^4 sec (for which the asymptotic-time approximation holds relatively well) we find $N(t) \approx 4 \times 10^6 cm^{-3}$.

2.152 Ostwald Ripening. Our quantitative understanding of the kinetics of Ostwald ripening has been developed, to a great extent, much more recently than that for Brownian motion; nevertheless, the theory is presently well advanced and we shall make use here of some established results. We shall assume that the kinetic process controlling the rate at which Ostwald ripening proceeds (if, indeed, it does occur to any significant extent) is the volume diffusion of solute atoms through the host liquid rather than an interfacial-reaction process occurring at the interphase boundaries [see Wagner[20] or Markworth[21]].

Essentially two different stages of second-phase evolution via Ostwald ripening have been dealt with theoretically: that occurring at

"early" times, for which the second-phase size-distribution is assumed to be relatively "narrow" in radius space[20,22] and that occurring at asymptotic times, for which the distribution is relatively "wide", and has a time-dependent shape, in droplet-radius space, that can be described mathematically in terms of similarity solutions[21,23]. For the latter situation, one can show that the droplet concentration varies, for the diffusion-controlled limiting case, according to the relation

$$\frac{N(t)}{N(0)} = \left(1 + \frac{t}{\tau_0}\right)^{-1} \quad , \tag{29}$$

if the distribution at the initial time has the asymptotic form; here, the characteristic time is given by

$$\tau_0 = \frac{9kT}{8\gamma\Omega^2 C_o D} \langle R \rangle_o^3 \quad , \tag{30}$$

where γ is the interphase surface energy, Ω is the atomic volume of the second phase, C_o is the equilibrium solubility of the second phase in the host phase, and D is the diffusivity of the solute in the host phase. It has been shown[22], for the situation in which the size distribution is relatively narrow, that the "width" (or standard deviation) of the distribution increases exponentially with time, the time constant τ_C being simply

$$\tau_C = 4\tau_0/9 \quad .$$

It is interesting to observe that the mathematical form of Equation (29) is completely analogous to that of Equation (27), the only difference being the form of the characteristic time.

As far as our present analysis of the Skylab experiment is concerned, we limit our considerations to the ripening of water droplets within a Krytox-oil host phase. It is felt that the dissolution and diffusion mechanisms characterizing the large-atomic-weight Krytox oil in water are too little understood[7] to permit relatively good quantitative estimates to be made of ripening kinetics. For the water droplets we assume

$\gamma = 50$ erg/cm^2 (assumed interfacial energy between Krytox oil and water)

$\Omega = 3 \times 10^{-23}$ cm^3 (molecular volume of water)

$C_o = 3 \times 10^{18} cm^{-3}$ (assumed equilibrium solubility of water in Krytox oil)

$D = 10^{-5} cm^2/sec$ (assumed diffusivity of water molecules in Krytox oil).

We see that most of these numerical values are "educated" assumptions, so that our resulting estimates for τ_o are subject to corresponding uncertainty. Substituting these numerical values into Equation (30) we find

$$\tau_o \approx 3 \times 10^7 \text{ sec for } \langle R \rangle_o = 10\mu m \quad ,$$

$$\tau_o \approx 4 \times 10^9 \text{ sec for } \langle R \rangle_o = 50\mu m \quad .$$

It can be seen that, for Krytox oil as the host phase, the characteristic times for Ostwald ripening are much larger than the corresponding times for Brownian motion, which would imply that Brownian motion would be the dominant of the two processes. Our view of this situation could change, of course, if more reliable values for various physical quantities (e.g., C_o and D) were known.

2.153 Velocity-Gradient-Induced Collisions. Velocity-gradient-induced collisions between droplets are collisions which result from the presence of velocity gradients within the host fluid. In the Skylab experiment on oil-water mixtures, for example, such gradients were established as a result of shaking the vials; the velocity fields thus established then tended to decay with time as a result of the finite viscosity of the host fluid. Velocity gradients arise from essentially two sources: (1) frictional interaction of the fluid with the container walls and (2) existence of turbulent eddy currents within the fluid. A detailed, quantitative evaluation of these phenomena and their contribution to droplet coalescence kinetics was clearly beyond the scope of the present research; however, recognizing that such effects could, in this experimental situation, have been the dominant cause of droplet coalescence, at least within the time interval that such gradients existed to an appreciable extent, we did obtain a semiquantitative means for describing these effects within the framework of our computer simulation.

We based our formulation upon the work of Lindborg and Torssell[14], who expressed the magnitude of the average velocity gradient, $|\text{grad } v|_{avg}$, as a sum of two contributions, i.e.,

$$|\text{grad } v|_{avg} = \frac{5v}{\ell} + \frac{v^{3/2}}{\nu^{1/2}\ell^{1/2}} \quad , \tag{31}$$

where v is the macroscopic flow velocity within the host fluid, ℓ is a characteristic length (taken to be the vessel diameter by Lindborg and Torssell), and ν is the kinematic viscosity of the host fluid. The first and second terms on the right-hand side of Equation (31) represent contributions arising from boundary-layer effects and turbulence effects, respectively. For conditions corresponding to the Skylab experiment, however, we must assume that v decreases with time. As a first approximation, we assumed that v decreases exponentially with increasing time according to the relation

$$v = v_o \exp\left(-\lambda\nu t/\ell^2\right) \quad . \tag{32}$$

Here, v_o is the value of v at time $t = 0$, and ℓ^2/ν is a characteristic damping time for fluid currents. The quantity λ is a dimensionless numerical parameter, the magnitude of which must be selected such that the resultant predicted velocity damping is in good agreement with experimental data.

Following Lindborg and Torssell[14], if the velocity gradient is in the x direction, then the relative velocity between two droplets separated by distance x along this direction (assuming velocity-gradient-induced migration only) is just

$$|x| \cdot |\text{grad } v|_{avg} \quad ,$$

and it follows[14] [making use of Equation (2)] that, for this situation,

$$Q(R',R'') = \frac{4}{3} |\text{grad } v|_{avg} (R' + R'')^3 \quad . \tag{33}$$

Equations (3), (4), (26), (31), (32), and (33) can be combined and the result solved numerically, as described above, to yield a description of the evolution of the droplet size distribution in time. Of course, appropriate selection must be made of the initial size distribution and of the quantities, ℓ, ν, λ, and the initial value of v.

It is clear that the model, summarized in Equations (31) to (33) is quite crude and represents only a first attempt at estimating the contribution of velocity-gradient effects to droplet-collision kinetics. Nevertheless, we have used this model to estimate the effect of velocity-gradient-induced collisions on the droplet size distributions for situations corresponding to the Skylab experiment. We examined both the case in which water and Krytox constituted the host phase. In each simulation, we assumed a droplet volume fraction of 0.25, v_o = 1 cm/sec, and ℓ = 1.2 cm (the inner diameter of the vials). Viscosities for Krytox and oil are well known[5].

The quantity remaining to be selected was the dimensionless parameter λ. Our estimate of this quantity was based upon visual observations of movement of the brass nut following shaking, taken from filmed recording of the Skylab experiment. We, thereby, deduced that λ is of the order of 10, and although we carried out simulations of collision kinetics for various values of λ, we report here only the results for λ = 10.

Illustrated in Figures 5 to 8 are some results obtained from the simulations. Figures 5 and 6 represent results for water as a host phase and 7 and 8 for Krytox as a host phase. The initial size distribution was taken to be the same for both cases, and its properties are illustrated in Figures 5 and 7. The changes shown in the respective size distributions have taken place over about the same time interval as the changes shown in corresponding plots of droplet concentration. As expected, the changes in the droplet distribution for water as host phase are much more pronounced and take place over a longer time interval than the corresponding changes for the case in which Krytox is the host phase. Indeed, velocity-gradient-induced collisions bring about, on the basis of this

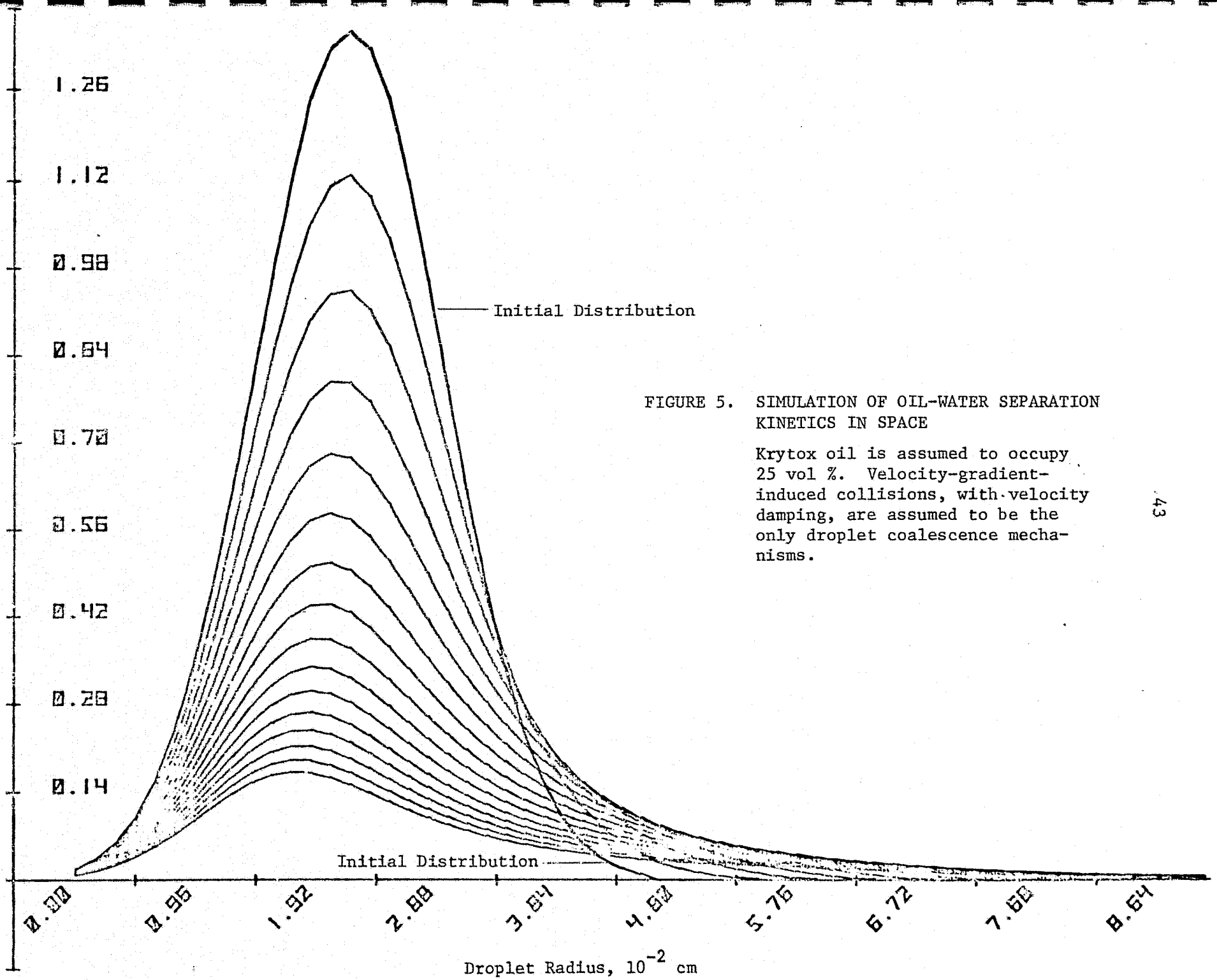

FIGURE 5. SIMULATION OF OIL-WATER SEPARATION KINETICS IN SPACE

Krytox oil is assumed to occupy 25 vol %. Velocity-gradient-induced collisions, with velocity damping, are assumed to be the only droplet coalescence mechanisms.

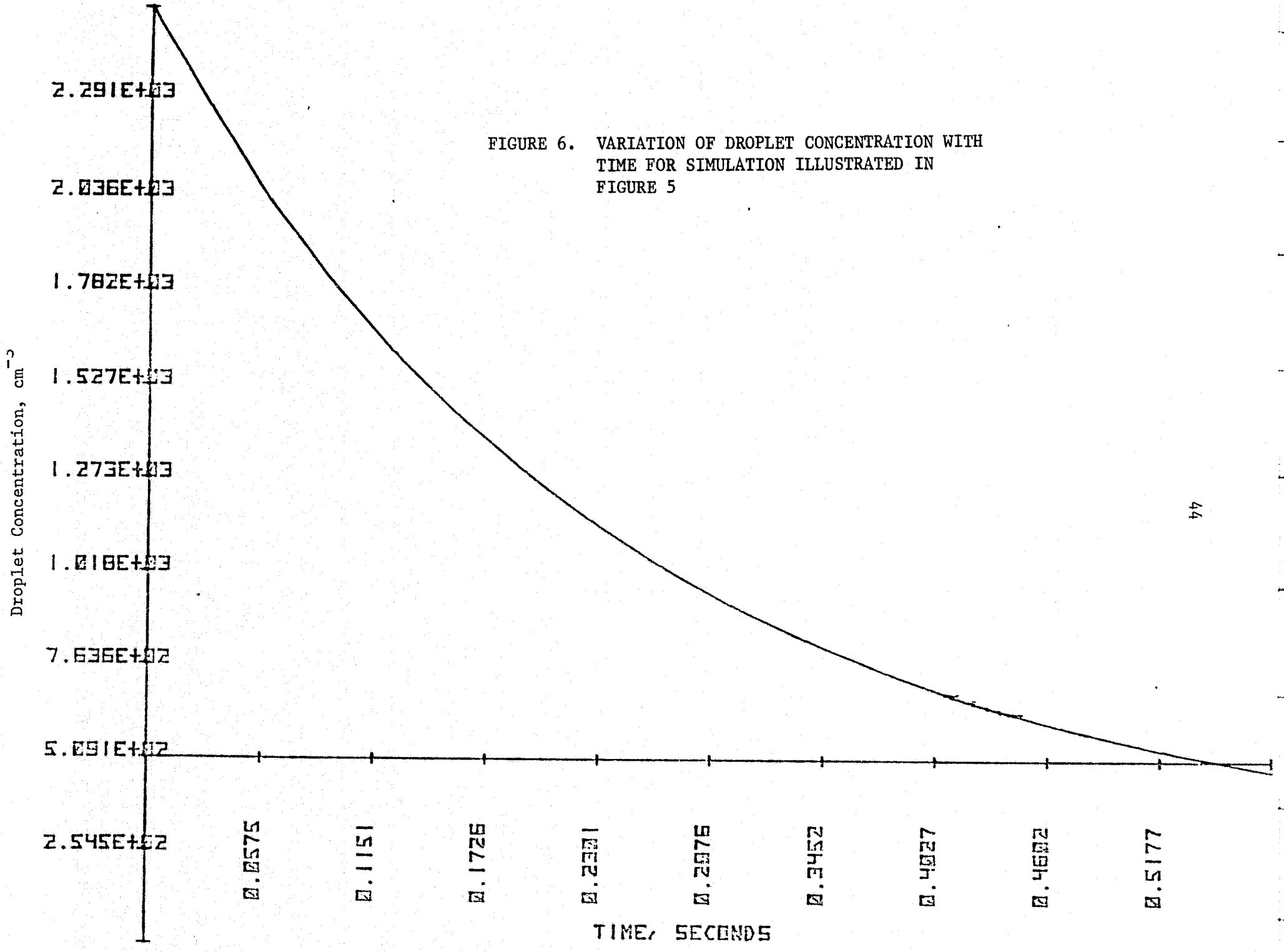

FIGURE 6. VARIATION OF DROPLET CONCENTRATION WITH TIME FOR SIMULATION ILLUSTRATED IN FIGURE 5

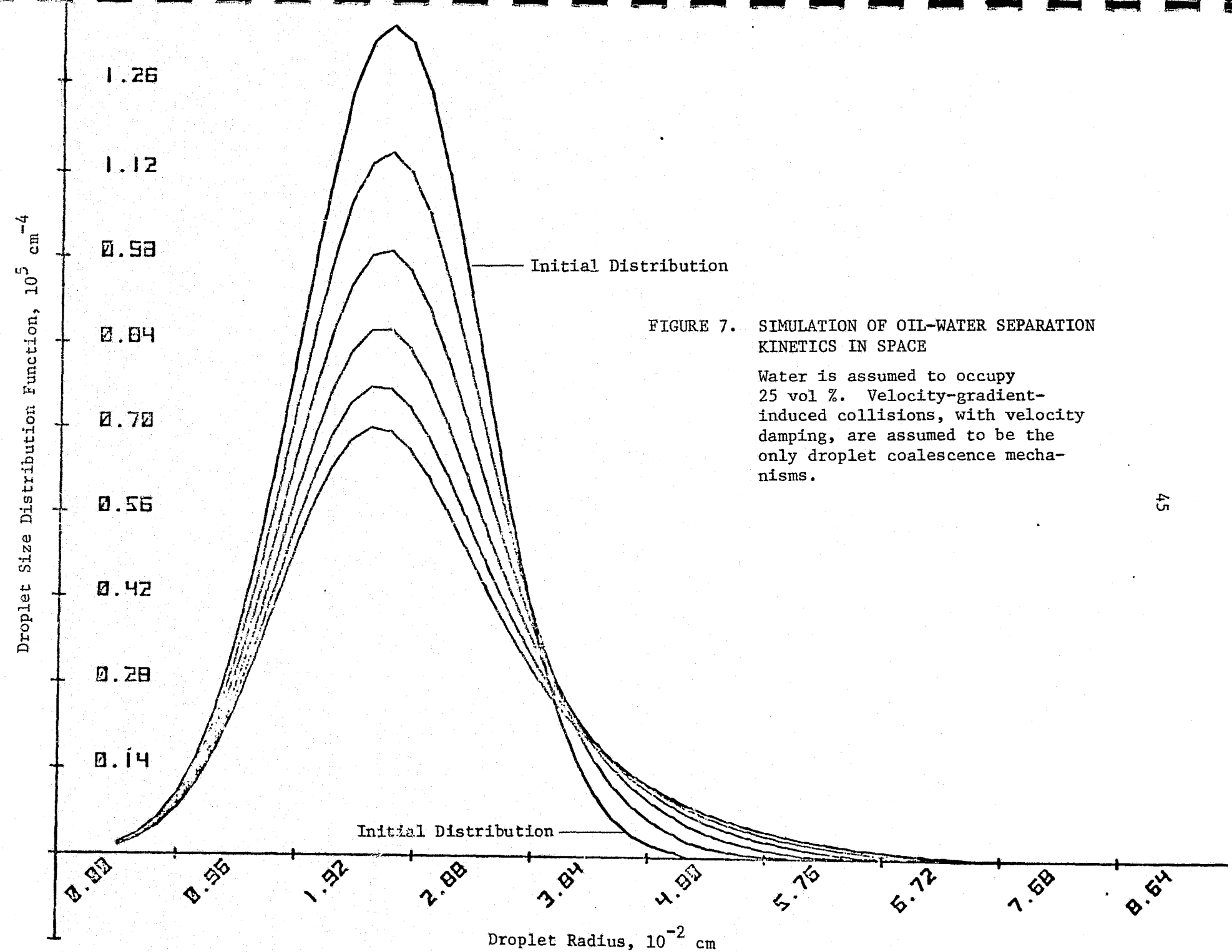

FIGURE 7. SIMULATION OF OIL-WATER SEPARATION KINETICS IN SPACE

Water is assumed to occupy 25 vol %. Velocity-gradient-induced collisions, with velocity damping, are assumed to be the only droplet coalescence mechanisms.

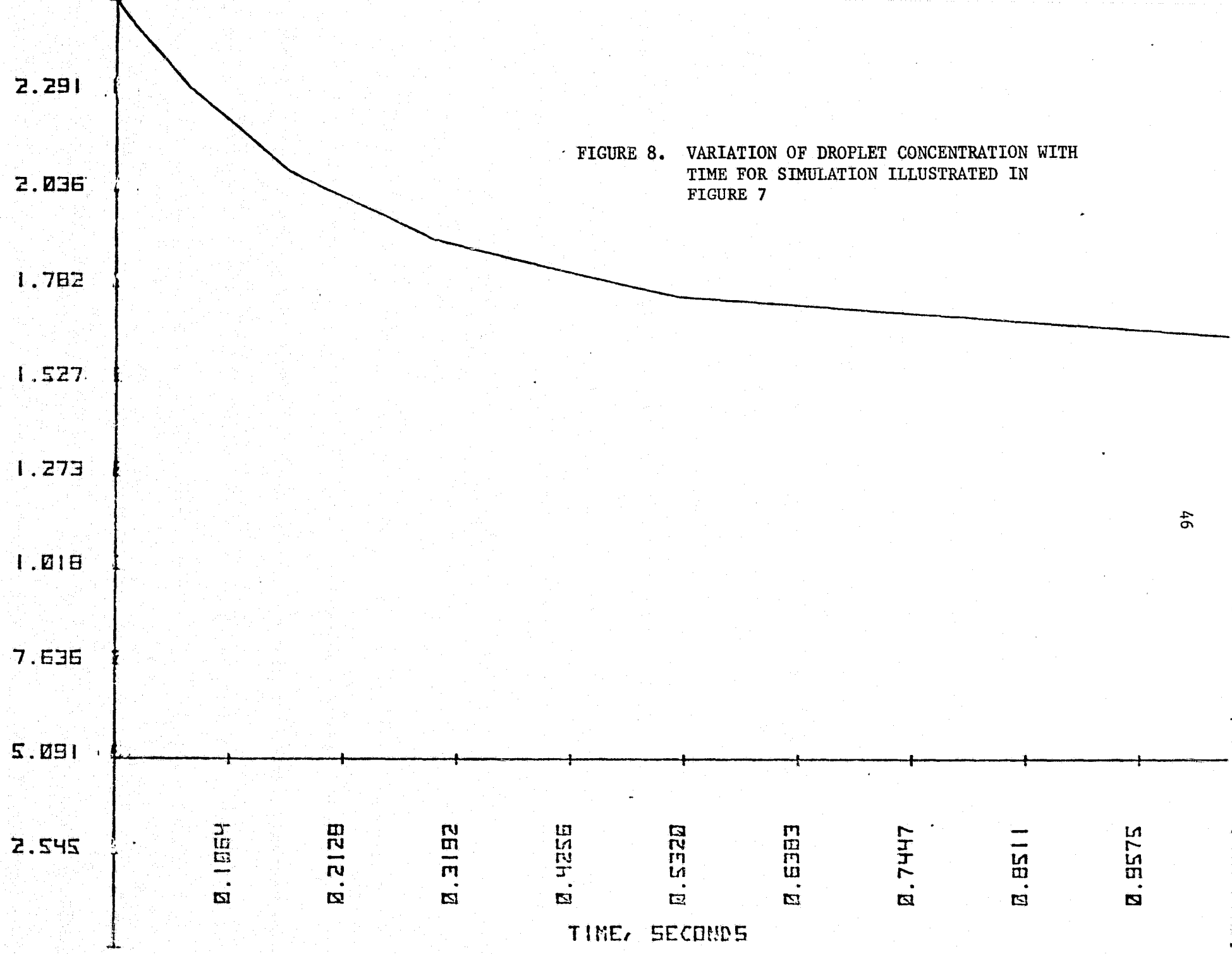

FIGURE 8. VARIATION OF DROPLET CONCENTRATION WITH TIME FOR SIMULATION ILLUSTRATED IN FIGURE 7

physical model, significant coarsening of the droplet distribution when water is the host phase, indicating that great care must be taken in future experiments to avoid such effects if the finest possible second-phase dispersion is desired. In the initial interval of about 1/2 second, the concentration of Krytox droplets is reduced (for this case see Figure 6) by roughly a factor of five. In both cases it can be seen that the rate of decrease of droplet concentration approaches zero with increasing time as the host-fluid velocity currents decay.

One point of interest regarding these simulations should be noted. We found that as time progressed the calculated volume fraction of droplets tended to decreases instead of remaining constant as conservation of matter would require. This decrease resulted from a "loss" of droplets at the large-radius tail of the distribution due to the fact that the computational field comprised radii only up to a certain selected maximum value. Once droplet sizes exceeded this value, these droplets were "lost" from the computation. However, this effect should be only slight as far as the results illustrated in Figures 5 to 8 are concerned, since only relatively few droplets appeared to be "lost". The effect on volume fraction would naturally be much more pronounced since this quantity is proportional to the third algebraic moment of the size distribution. This artifact of the computation could easily be alleviated by extending the maximum radius to a larger value. This was not felt to be necessary in the present case.

2.154 Long-Term Stability of Oil-Water Mixtures. The experimental studies of the stability of the oil-water mixtures in space indicated[5] that the emulsions were between one and two orders of magnitude more stable in the low-g environment than was expected. One possible explanation for this phenomenon lies in the "collision-efficiency" effect[10,25] which we now describe.

The model, upon which our calculations of droplet-collision kinetics were based, does not take into account the fluid-flow field in the host liquid around the moving droplets. Our model is based upon

the assumption that two moving droplets that are approaching each other will definitely collide if the distance between their centers, measured perpendicular to the relative velocity vector, is less than the sum of their radii. However, the droplets actually tend to follow the streamlines in the host liquid and, hence, may move around each other with no collision taking place. Inertial effects can, however, be sufficiently great to cause collisions to occur[10], depending upon such factors as Reynolds number and the densities of the primary and second phase. [Other factors may also influence collision rates, such as the finite time required to drain the liquid film separating two droplets in close proximity[10].] The tendency of approaching droplets not to collide can be described in terms of a "collision-efficiency" factor which would equal unity for the simple model we used in our calculations, but which could be appreciably smaller in practice[10]. In fact, this effect may be particularly pronounced in the low-g environment for which the droplet velocities are relatively low. This would lead to higher stability as was observed. Collision-efficiency factors of the order of 10^{-3} have been reported[10], so this effect could be of sufficient magnitude to account for the high stabilities observed in space. Clearly, a more quantitative treatment of this problem than we have hitherto carried out is required, particularly if space processing is decided upon as a means for the manufacture of mixtures of immiscible materials for practical applications.

2.16 Simulation of Collision Kinetics in Liquid Aluminum-Indium

Discussed elsewhere in this report are the results of experimental studies of the separation kinetics of immiscible liquid Al-In alloys. We shall now describe the results of computer-simulation studies of this system, assuming conditions corresponding to those characterizing the experimental situation. In addition, we assume that the only mechanism contributing to second-phase coalescence is simple Stokes migration of droplets without modification for interfacial energy effects, which tend

to reduce migration velocities[9]. For this case one can readily show[26] that the terminal velocity v of a droplet of radius r along a gravitational field is given by

$$v = \frac{2}{9} g r^2 \frac{\Delta\rho}{\mu} \quad , \tag{34}$$

where g is the acceleration due to gravity; μ, the viscosity of the host fluid; and $\Delta\rho$, the difference in density between droplet material and host-phase material. Of course, the droplets move parallel to the gravitational field if their density is greater than that of the host fluid, and antiparallel to the field if their density is less than that of the host fluid.

Equations (2) and (34) can be combined, and subsequent calculations yield

$$Q(R',R'') = \frac{2\pi g \Delta\rho}{9\mu} (R' + R'')^3 \left|R' - R''\right| \quad . \tag{35}$$

We can now combine Equations (3), (4), (26), and (35), using appropriate values for g, $\Delta\rho$, and μ, and an appropriate initial size distribution, to evaluate the evolution of the droplet distribution. In particular, we examined the behavior of an Al-In alloy contaning 40 wt % In at a temperature just above the monotectic temperature (639 C). Figure 9 presents the equilibrium-phase diagram for the Al-In system[27]. After the droplet-growth stage has been completed, the system contains 14.1 vol % of In-rich droplets, the Al-rich primary phase contains 17.5 wt % In, and the In-rich droplets contain 96.8 wt % In. The droplet density is estimated as 6.42 g/cm^3, and the primary-phase density is estimated as 2.67 g/cm^3, so that $\Delta\rho$ = 3.75 g/cm^3. (We are not interested in the sign of $\Delta\rho$.) The value we used for μ was taken in an approximation to be that for pure Al at 639 C. Now the viscosity of Al at 660 C and 800 C is .045 poise and .025 poise, respectively; a linear extrapolation of these values to 639 C yields a value for viscosity of .048 poise, which was the value for μ substituted into Equation (35). The value used for g was 980.665 cm/sec^2. (One can show that these values, substituted into Equation (34), yield $v = 17025\ r^2$, where units for v and r are cm/sec and cm, respectively.)

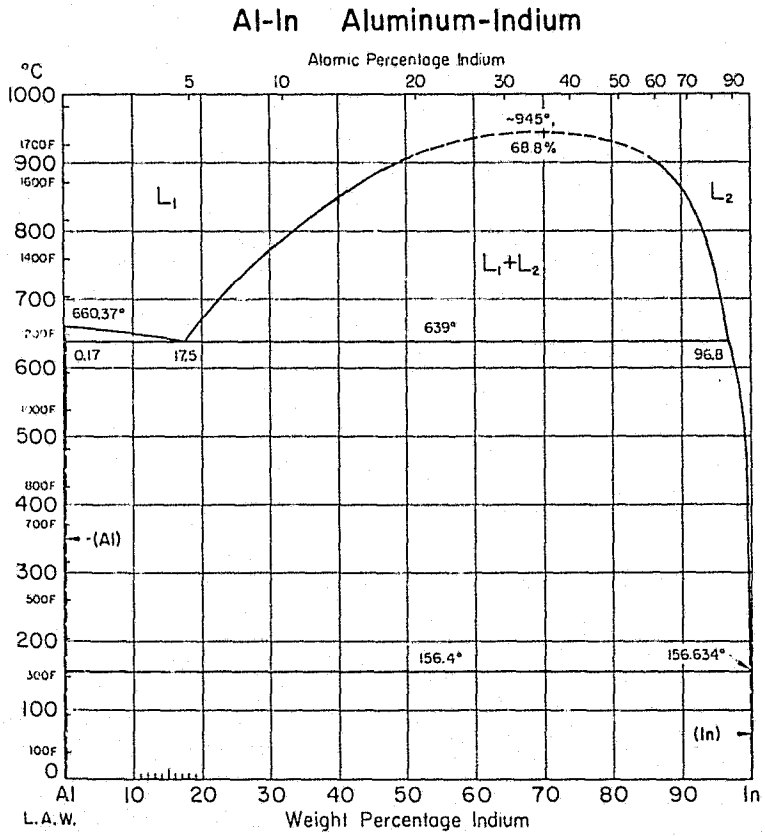

FIGURE 9. ALUMINUM-INDIUM EQUILIBRIUM SYSTEM[27]

Results of one simulation are illustrated in Figures 10 and 11. Properties of the assumed initial droplet size distribution can be seen in Figure 10; these properties were selected to correspond roughly with experimental data. The changes in the size distribution shown in Figure 10 correspond to the same time scale as the droplet concentration changes shown in Figure 11. From these two figures, it can be seen that substantial changes take place in the droplet size distribution over the interval analyzed (less than 2 seconds from the assumed onset of the collision stage). For example, the droplet concentration is decreased by more than half its original value, and the size distribution, while remaining unimodal, becomes considerably skewed, developing a long "tail" at the larger radii. This manner in which skewness is predicted to develop is consistent with experimentally obtained size-distribution data for this system illustrated in the following section of this report.*

2.2 Aluminum-Indium Experimental Studies

2.21 Background

The work on the Al-In system has as its objective the study of agglomeration of liquid In droplets in a liquid Al matrix under various thermal conditions at 1 g and at 0 g. These experimental results are to be used to check the self-consistency of the computer simulation and thus provide a check on the adequacy of our understanding of the processes involved.

The Al-In system shown in Figure 9[27] was selected because of the convenient melting temperatures, the relatively large temperature spread of the miscibility gap, and the potential ease of metallographic preparation in the Al-rich region.

The alloy composition, Al-In (40 wt %), was selected for the initial studies. During cool-down from the homogeneous liquid field

---

* The material values used in this analysis are those for the Al - 40 wt % In alloy. The results should be qualitatively similar for other metallic systems. The quantitative results, however, will depend on the initial size distribution chosen, the viscosities, and $\Delta\rho$, the difference in density between matrix and droplets.

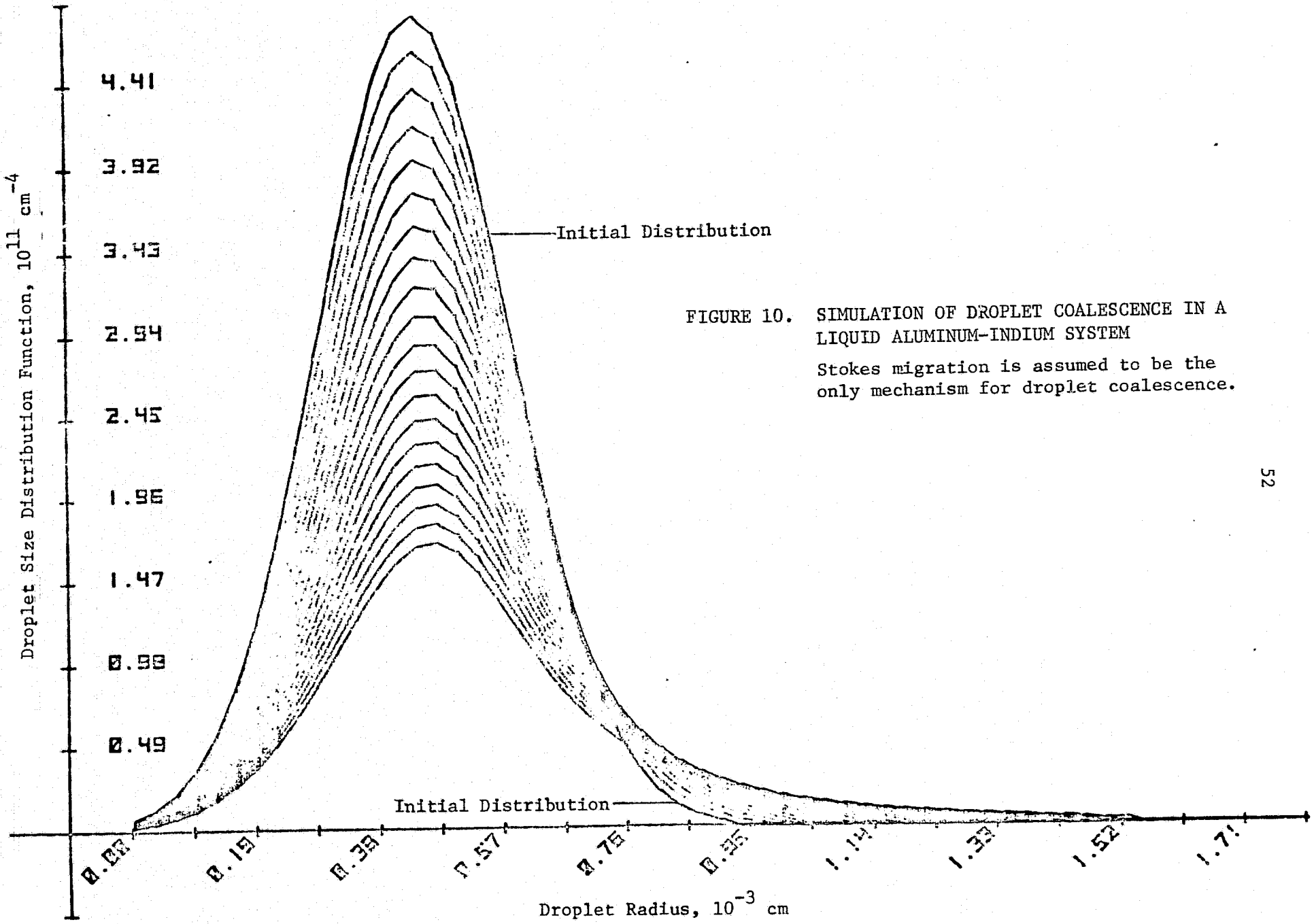

FIGURE 10. SIMULATION OF DROPLET COALESCENCE IN A LIQUID ALUMINUM-INDIUM SYSTEM

Stokes migration is assumed to be the only mechanism for droplet coalescence.

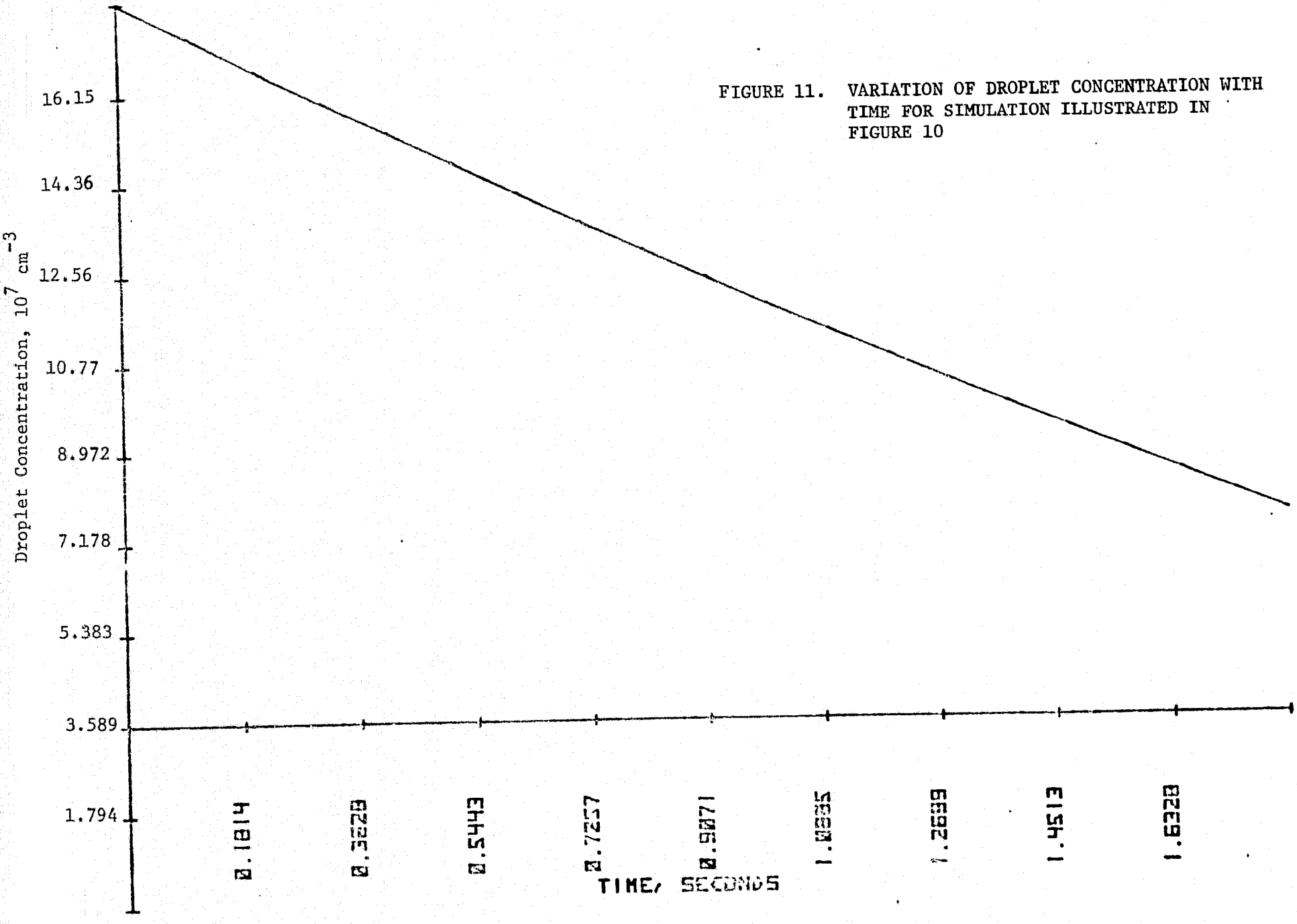

FIGURE 11. VARIATION OF DROPLET CONCENTRATION WITH TIME FOR SIMULATION ILLUSTRATED IN FIGURE 10

(> 850 C), In-rich liquid (L_2) droplets are expected to precipitate in an Al-rich host liquid (L_1). Under equilibrium conditions, the host liquid will undergo a monotectic reaction, L_1 (17.5 wt % In) → Al (solid) + L_2 (96.8 wt % In) at 639 C. The liquid, L_2, distributed as primary droplets formed in the miscibility gap and as a secondary phase formed by the monotectic reaction, solidifies when cooled below 156 C. The theoretical volume fraction of the In phase under equilibrium conditions just below the monotectic temperature is ∿ 23 percent. Approximately 62 percent of the volume of this phase or 14.1 vol % is made up of the primary In droplets, i.e., the droplets formed within the miscibility gap.

The specific experiments carried out were aimed at determining the droplet size distribution as a function of cooling rate through the miscibility gap. The cooling process began from a temperature above the miscibility gap (1000 C) in a homogeneous single-phase liquid field.

2.22 Experimental

2.221 Alloy Preparation. High-purity Al-In (40 wt %) alloy in the form of two 20-cm lengths of ∿ 1-cm-diam rod was produced by vacuum induction melting the required weights of 99.999 percent pure Al and In in a zirconia crucible and pouring the molten alloy into a massive Cu mold having two ∿ 1-cm-diam x 20-cm-long cylindrical channels. Transverse sections taken near the bottom, middle, and top of each length of rod have been macroscopically examined and found to be somewhat segregated. In some sections, massive agglomerates of what appears to be an In-rich phase have been found near the axial center of the rod.

The agglomeration is probably caused by the low-melting liquid In flowing into the voids produced by the solidification shrinkage. This possibility was recognized at the outset, and attempts were made to prevent it through use of the massive Cu mold and the relatively small diameter channels to provide a relatively fast solidification rate.

2.222 Thermal Analysis. Thermal analysis samples were taken from a more uniform portion of the 1-cm-diam cast rod. The samples were

1.14 cm in diam by 1.26 cm long and had 5-mm-diam cylindrical holes machined into their bases to accommodate thermocouple wells in the Ta or graphite crucibles used to contain the alloy.

Experiments were conducted in the thermal analysis equipment previously described[28]. These were intended to determine the size and space distribution of In-rich droplets formed in the miscibility gap as a function of cooling rate through the gap. Basically, the equipment consists of an electrically heated furnace that is supported by a pulley arrangement and can be positioned around the sample contained in a fused silica container. The latter is attached to a vacuum system capable of achieving 10^{-6} Torr.

In all the experiments the furnace was preheated to $\sim$ 1000 C and then lowered around the sample contained in the Ta or graphite crucible and supported by a thermocouple which allowed the continuous recording of temperature. After the sample reached a temperature of $\sim$ 1020 C, well above the miscibility gap (see Figure 9), and was held for 4 minutes, it was either rapidly cooled by raising the furnace away from the sample or slowly cooled by leaving the furnace in place around the sample and simply shutting off the power to the furnace.

Initial experiments were conducted with the alloy contained in Ta crucibles. However, after metallographic observations revealed that some reaction had occurred between the Ta crucible and molten alloy, the experiments were repeated in graphite crucibles. The latter were machined from a spectrographic Grade CZ82 graphite purchased from Poco Graphite and then outgassed in high vacuum at 2000 C. The Al-In experiments are summarized in Table 1 and show that the fast and slow cooling rates used approximated 4 and 0.12 C/sec, respectively.

A thermal arrest corresponding to the monotectic reaction in the Al-In system at 639 C was observed on cooling in all the experiments. The arrest on heating was not consistent, probably due to lack of intimate contact between the sample and thermocouple well. As expected, the observed temperature range of the thermal arrest was lower than the equilibrium temperature and varied with cooling rate.

TABLE 1. SUMMARY OF THERMAL TREATMENT EXPERIMENTS CONDUCTED ON ALUMINUM-INDIUM ALLOYS

Sample No.	Crucible Material	Maximum Sample Temperature, C	Monotectic Arrest Temperature, C	Cooling Rate to Monotectic Temperature, C/sec	Time to Cool to Monotectic Temperature, minutes
Al-In-1	Ta	1034	(a)	3.72	1.6
Al-In-2	Ta	1015	637-625	0.12	51.7
Al-In-3	C	1019	620-594	4.75	1.4
Al-In-4	C	1020	630-625	0.12	53.5

(a) Inaccurate calibration of sensor. Temperature reading in error.

2.223 Metallography. After the indicated thermal treatment, the samples were sectioned longitudinally for metallographic observations. Initial attempts to metallographically prepare the samples by conventional techniques proved futile. Thus, some effort was expended in developing a metallographic technique for observing and analyzing the microstructure of the Al-In (40 wt %) alloys cooled at different rates through the miscibility gap.

The technique developed for metallographic preparation of this alloy consists of

- Grinding through 600 grit SiC paper with a wax lubricant
- Polishing on a Syntron automatic polishing unit with 1-1/2-μ diamond paste and kerosene lubricant on a silk microcloth combination for 2 days
- Final polishing with 1/4-μ diamond paste containing a kerosene lubricant on a microcloth.

The polishing method produces a reasonably satisfactory product, especially for characterizing the larger droplets. However, there are still some problems associated with measurement of the distributions of droplets $< \sim$ 5-μ diam, owing to the somewhat mottled background of the matrix, the lack of a sharp interface between some of the smaller droplets and the matrix, and the difficulty in removing of all the scratches.

2.23 Results

2.231 Microstructural Observations. Photomicrographs of three regions from both Sample Al-In-3, cooled through the miscibility gap at 4.75 C/sec, and Sample Al-In-4, cooled through the miscibility gap at 0.12 C/sec, are shown in Figures 12 and 13. The regions shown are from one side of each of the sectioned samples and were situated at different levels above the bottom of the specimen.

The tabulation given below lists the position of each of the micrographs shown in Figures 12 and 13.

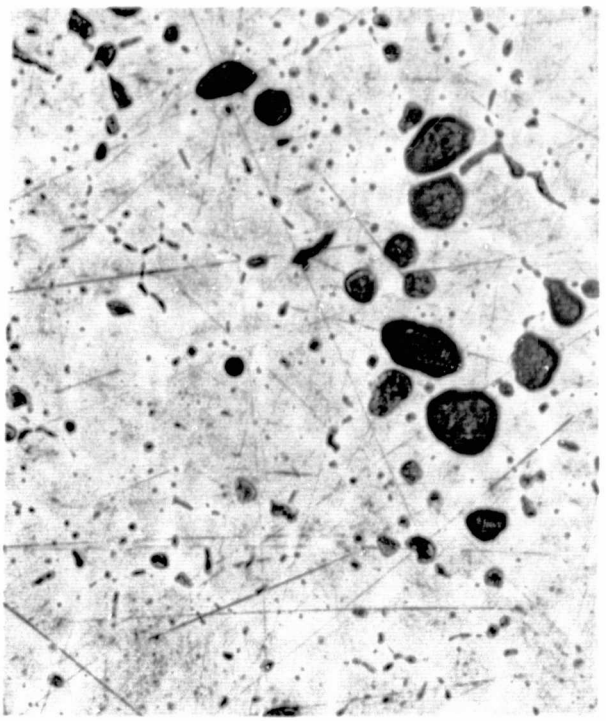

OH910

a. Top

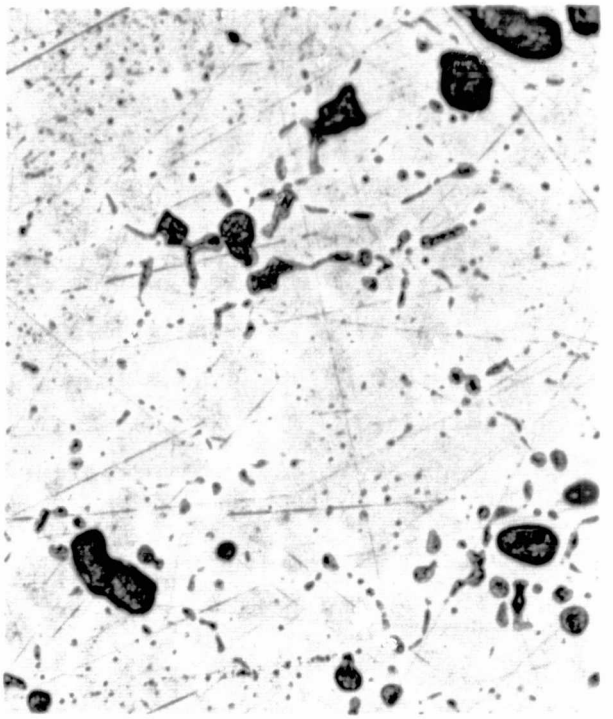

OH909

b. Middle

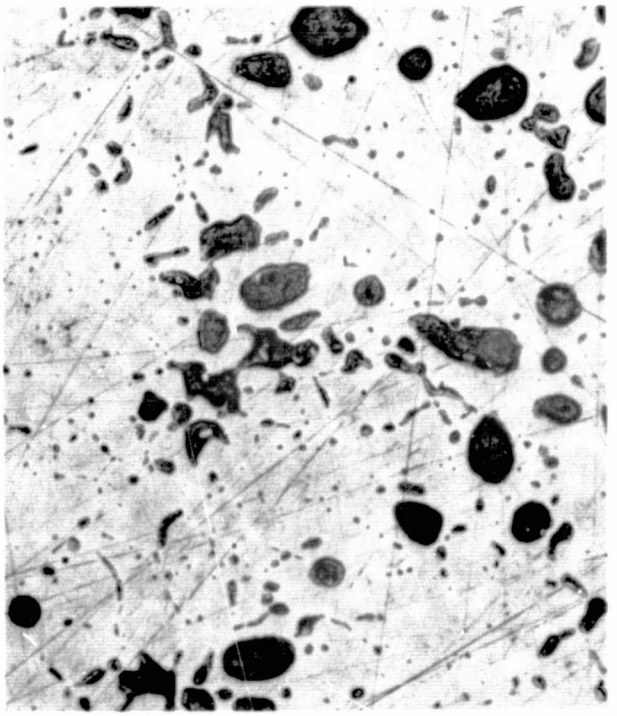

OH908

c. Bottom

FIGURE 12. PHOTOMICROGRAPHS OF Al-In-3 RAPIDLY COOLED (4.75 C/SEC) THROUGH MISCIBILITY GAP (100X)

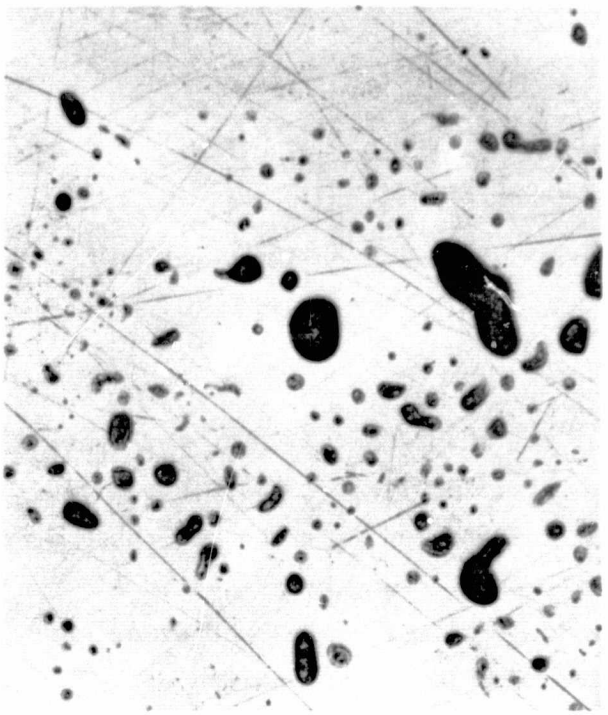

OH913

a. Top

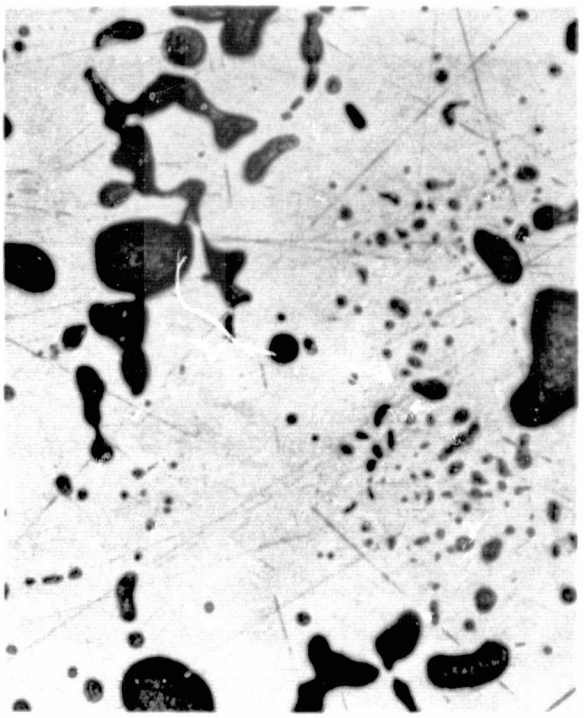

OH912

b. Middle

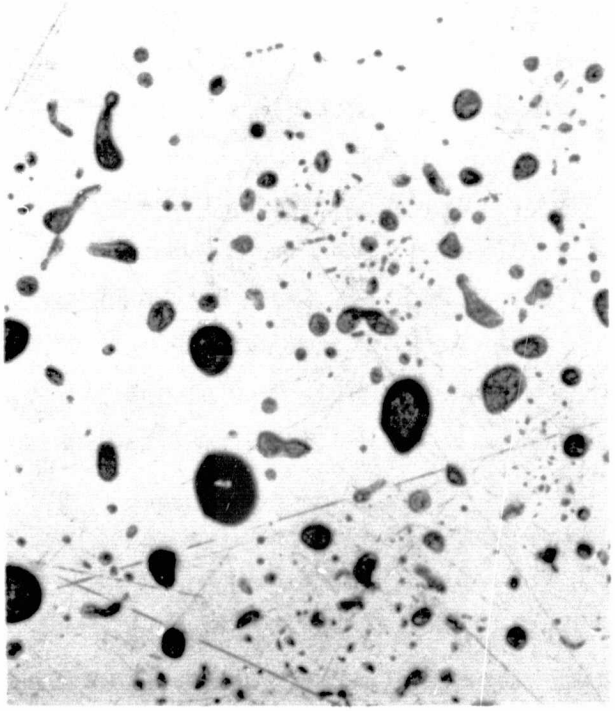

OH911

c. Bottom

FIGURE 13. PHOTOMICROGRAPHS OF Al-In-4 SLOWLY COOLED (0.12 C/SEC) THROUGH MISCIBILITY GAP (100X)

Sample No.	Nominal Distance from Sample Base, mm		
	Bottom	Middle	Top
Al-In-3	3	6.5	10
Al-In-4	4	8	12

In general, the micrographs of Figures 12 and 13 show the type of microstructure anticipated. The dark circular features correspond to the In-rich spherical droplets formed during cooling into the two-phase liquid field. Some of the droplets have been deformed by the solid Al formed during the monotectic transformation, while the shape of others is obviously due to collisions of two or more droplets. Comparison of Figures 12 and 13 shows that the concentration of fine droplets is much smaller in the slower cooled specimen, Figure 13, than in the more rapidly cooled specimen, Figure 12. In addition, it should be mentioned that In-rich particles $\sim$ 2 mm in diam were present at the bottom of each of the specimens. Subsequent droplet size distribution analysis ignored the very bottom sample regions in which the large particles were present.

2.232 Droplet Size Distribution Analysis. Droplet size distribution analysis has been carried out by means of the Quantimet and the Zeiss Particle Size Analyzer. Six areas on both Samples Al-In-3 and Al-In-4 were directly analyzed by the Quantimet. Three of the areas were identical to those shown in Figures 12 and 13, and the three others were at the same distance from the bottom of the specimens but were on the opposite side of the samples.

In the Quantimet analysis, the image of the region to be analyzed is projected onto a television screen, and the microstructural features, in this case the droplets, are detected because of their contrast with the matrix, and their size distribution and volume fraction are determined electronically.

The photomicrographs of Figures 12 and 13, as well as some additional ones taken at higher magnification, were analyzed by means of the

Zeiss Particle Size Analyzer. This technique is a much more tedious one than the Quantimet, but because of its simplicity, is less subject to error. Individual droplets are sized and recorded by comparing their size with that of a circular cross-section light of variable diameter which is projected on the photomicrograph. Adjustment of the light beam diameter to approximate the droplet diameter and punching a hole through the particle on the photomicrograph ensure that the particle and its diameter are recorded. The hole punched through the particle alerts the operator to the fact that the particle has already been counted.

Table 2 presents the Quantimet In droplet size data for the six areas of each of the Samples Al-In-3 and Al-In-4. Region 1 corresponds to the areas shown on the photomicrographs of Figures 12 and 13; Region 2 is from areas on the opposite side of the sample section but at corresponding heights above the bottom. The quantitative data support the earlier observation that the number of droplets in the very fine size range is greater in Al-In-3, the rapidly cooled sample, than in Al-In-4, the slower cooled sample. In addition, it is also observed that the opposite is true for the coarser droplets. The percentage of In as determined by the Quantimet shows some tendency for the In to segregate toward the bottom of the melt.

It should also be noted that the average volume fraction of In-rich droplets in Sample Al-In-3 is somewhat higher (13.5 vol %) than in Sample Al-In-4 (12.8 vol %). This difference is probably due to the longer time allowed for settling of a portion of the In-rich phase into a separate layer in the slower cooled sample. Because of this layering, the droplet concentrations in the interior of the sample are somewhat less than that expected theoretically under equilibrium conditions just above the monotectic temperature (14.1 vol %). All in all, the results are quite reasonable.

In order to improve the counting statistics, the number of particles in the various size ranges has been summed for the three levels in each region and presented in Table 3. It should be noted that the agreement between the droplet size distributions of Regions 1 and 2 is quite good.

TABLE 2. RESULTS OF INDIUM DROPLET SIZE DISTRIBUTION AS DETERMINED BY THE QUANTIMET[a]

	Number of Particles in Designated Range											
	Al-In-3[b]						Al-In-4[c]					
	Bottom		Middle		Top		Bottom		Middle		Top	
Range, μ	1[d]	2	1	2	1	2	1	2	1	2	1	2
< 3	99	88	126	125	108	126	50	73	44	93	87	87
3-6	68	49	70	76	47	47	43	59	36	54	68	27
6-9	31	37	25	27	36	27	29	32	28	31	20	15
9-12	16	28	15	21	19	17	20	16	12	15	10	14
12-15	19	13	17	6	15	13	9	16	12	9	10	6
15-18	10	10	12	9	10	12	16	14	11	8	7	6
18-21	11	7	5	3	10	10	15	8	7	5	5	6
21-24	7	6	5	4	7	8	15	7	8	7	7	4
24-27	8	6	4	0	5	4	13	5	5	5	3	4
27-30	2	4	3	1	4	6	13	5	7	4	4	3
30-33	4	4	1	5	5	2	3	4	4	6	6	2
33-36	1	5	5	3	2	2	3	4	6	3	2	1
36-39	3	3	3	3	2	0	4	3	3	1	1	2
39-42	1	3	2	0	2	2	2	3	2	2	1	0
42-45	4	3	1	2	3	0	2	3	3	4	2	1
45-48	4	4	1	0	2	2	2	2	4	2	0	0
48-51	4	2	1	2	2	1	2	4	3	1	0	1
51-54	4	0	0	1	3	1	4	2	2	1	0	0
54-57	4	2	0	1	0	1	2	1	5	2	1	0
57-60	4	2	2	1	1	1	0	0	3	0	0	0
60-63	2	1	2	1	1	0	2	1	3	2	1	0
63-66	0	0	2	0	1	0	2	0	2	0	0	0
66-69	2	1	0	0	1	0	1	1	1	0	0	0
69-72	0	0	0	0	0	0	1	1	3	0	0	0
72-75	1	2	0	2	0	0	0	1	3	0	0	0
75-78	0	0	1	0	0	0	1	1	1	0	1	0
78-81	2	2	1	0	1	0	1	2	1	1	1	1
81-84	0	2	2	1	1	0	0	1	1	1	0	1
84-87	1	0	0	0	0	0	0	1	0	1	0	0
87-90	1	1	0	1	2	0	1	1	0	1	0	0
90-93		1	1	0		0	1	1	1	0	0	0
93-96		0	0	1		0	0	0	2	1	1	1
96-99		0	1	0		0	0	1	2	0	0	0
99-102		2	1	1		0	1	1	2	0	0	0
102-105		0	1			0	0	0	0	0	0	0
105-108		2				1	0	0	2	0	1	0
108-111		0					0	2	0	0		0
111-114		0					1	1	1	0		0
114-117		0						1	1	0		0
117-120		0						0	1	0		0
120-123		1						0	1	0		0
> 125		1						2	6	1		1
Vol Frac. In., pct	16.0	22.4	12.5	10.5	11.4	8.5	15.7	15.1	20.9	10.1	8.6	6.2

(a) Data obtained supersedes data presented in Table 1, Reference 8.

(b) Cooled at 4.8 C/sec.

(c) Cooled at 0.12 C/sec.

(d) Regions 1 and 2 are at the same height above the bottom but on opposite sides of the sample.

TABLE 3. INDIUM DROPLET SIZE DISTRIBUTION IN SAMPLES Al-In-3 AND Al-In-4 (a)

Size Range, μ	No. of Particles in a Given Size Range			
	Al-In-3 (b)		Al-In-4 (c)	
	1 (d)	2	1	2
< 3	333	339	181	253
3-6	185	172	147	140
6-9	92	91	77	78
9-12	50	66	42	45
12-15	51	32	31	31
15-18	32	31	34	28
18-21	26	17	27	19
21-24	21	18	30	18
24-27	17	10	21	14
27-30	9	11	24	12
30-33	10	11	13	12
33-36	8	10	11	8
36-39	8	6	8	6
39-42	5	5	5	5
42-45	8	5	7	8
45-48	7	6	6	4
48-51	7	5	5	6
51-54	7	2	6	3
54-57	4	4	8	3
57-60	7	4	3	0
60-63	5	2	6	3
63-66	3	0	4	0
66-69	3	1	2	1
69-72	0	0	4	1
72-75	1	4	3	1
75-78	1	0	3	1
78-81	4	2	3	4
81-84	3	3	1	3
84-87	1	0	0	2
87-90	3	2	1	2
90-93	1	1	2	1
93-96	0	0	3	2
96-99	1	0	2	1
99-102	1	3	3	1
102-105	1	0	0	0
105-108		2	3	0
108-111		0	0	2
111-114		0	2	1
114-117		0	1	1
117-120		0	1	0
120-123		1	1	0
> 125		1	6	4

(a) The effect of position in the melt relative to the base (level) is ignored. Number of particles at the various levels is added together.

(b) Cooled at 4.8 C/sec.

(c) Cooled at 0.12 C/sec.

(d) 1 and 2 represent regions on the left and right sides of the section respectively. Region 1 of both samples has already been analyzed on the Zeiss Particle Size Analyzer. See Table 2, Reference 8, and Table 3 of present report.

The droplet size distributions obtained from the Quantimet are shown graphically for Region 1 of both samples in Figure 14. The differences in size distributions in the two samples as previously noted can readily be seen in this figure.

The results of analyzing regions identical to Region 1 by the Zeiss Particle Size Analyzer are summarized in Table 4 and Figure 15. As has been previously shown (see Figure 14 for the Quantimet data), the fast-cooled sample, Al-In-3, shows a much larger number of very small particles compared to the slow-cooled sample, Al-In-4. The size distributions in the large droplet size range for the two samples are similar, although there is some tendency for there to be a larger concentration of the very largest particles in the slower cooled sample.

Although the droplet size distributions as measured with the Zeiss Particle Size Analyzer were qualitatively in agreement with those determined by the Quantimet, there was a substantial quantitative difference noted in the very fine particle size regions of the distributions. The number of very fine droplets as determined by the Zeiss Particle Size Analyzer was substantially larger than that determined by the Quantimet. This is apparently due to lack of sensitivity in the Quantimet for the very fine particles at the magnification used. It would be expected that use of higher magnifications would ease this problem.

The larger number of very small droplets (<6 μ) and the sensitivity of this portion of the size distribution to cooling rate has made it necessary to concentrate at least some of our efforts on the droplet size distribution in the fine size range. Accordingly, Zeiss Particle Size analyses were carried out on 500X photomicrographs of specimens Al-In-3 and Al-In-4. The analyses are shown in Table 5 and once again demonstrate the larger number of fine particles which are present in the rapidly cooled sample compared to the slowly cooled one.

The work to date has thus demonstrated that cooling rate through the miscibility gap within the range 0.1 to 5 C/sec alters the droplet size distribution in the expected way. However, we have been hampered in

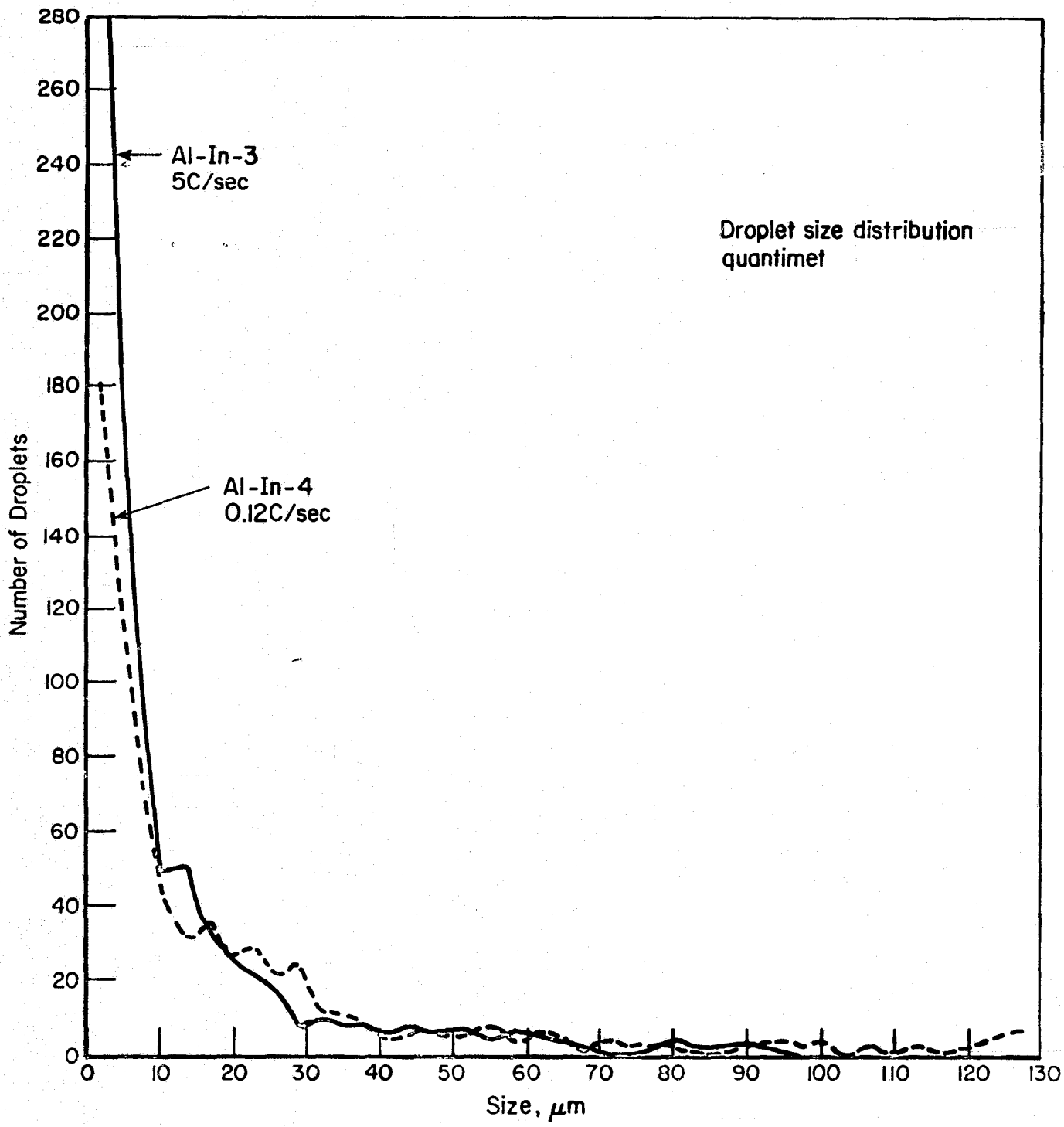

FIGURE 14. DROPLET SIZE DISTRIBUTION FOR SAMPLES Al-In-3 AND Al-In-4 AS DETERMINED ON THE QUANTIMET

TABLE 4. RESULTS OF PARTICLE SIZE ANALYSIS CARRIED OUT ON Al-In-3[a] AND Al-In-4[b]. ZEISS PARTICLE SIZE ANALYZER[c]

Interval Center, microns[d]	Number of Particles		Interval Center, microns[d]	Number of Particles	
	Al-In-3	Al-In-4		Al-In-3	Al-In-4
<5.9	527	285	49.1	0	2
6.8	242	127	51.0	2	1
8.6	225	112	52.8	4	2
10.5	131	87	54.6	3	4
12.3	90	73	56.5	5	1
14.2	68	62	58.3	1	4
16.0	44	45	60.2	4	0
17.8	27	30	62.0	1	1
19.7	21	22	63.8	1	1
21.5	16	23	65.7	3	0
23.4	26	32	67.5	5	1
25.2	16	19	69.4	0	1
27.0	11	11	71.2	5	1
28.9	16	11	73.0	2	0
30.7	15	5	74.9	1	0
32.6	9	9	76.7	0	2
34.4	10	7	78.6	0	2
36.2	7	3	80.4	1	0
38.1	11	5	82.2	1	2
39.9	5	4	84.1	3	0
41.8	3	6	85.9	0	1
43.6	1	3	87.8	1	2
45.4	3	0	89.6	3	1
47.3	11	2	>91.4	4	7

(a) Cooled at 4.8 C/sec.

(b) Cooled at 0.12 C/sec.

(c) Three areas, each 0.98 x 1.28 mm, analyzed per sample. Number of particles in each size range combined.

(d) Interval = Interval Center $\pm$0.93 μ.

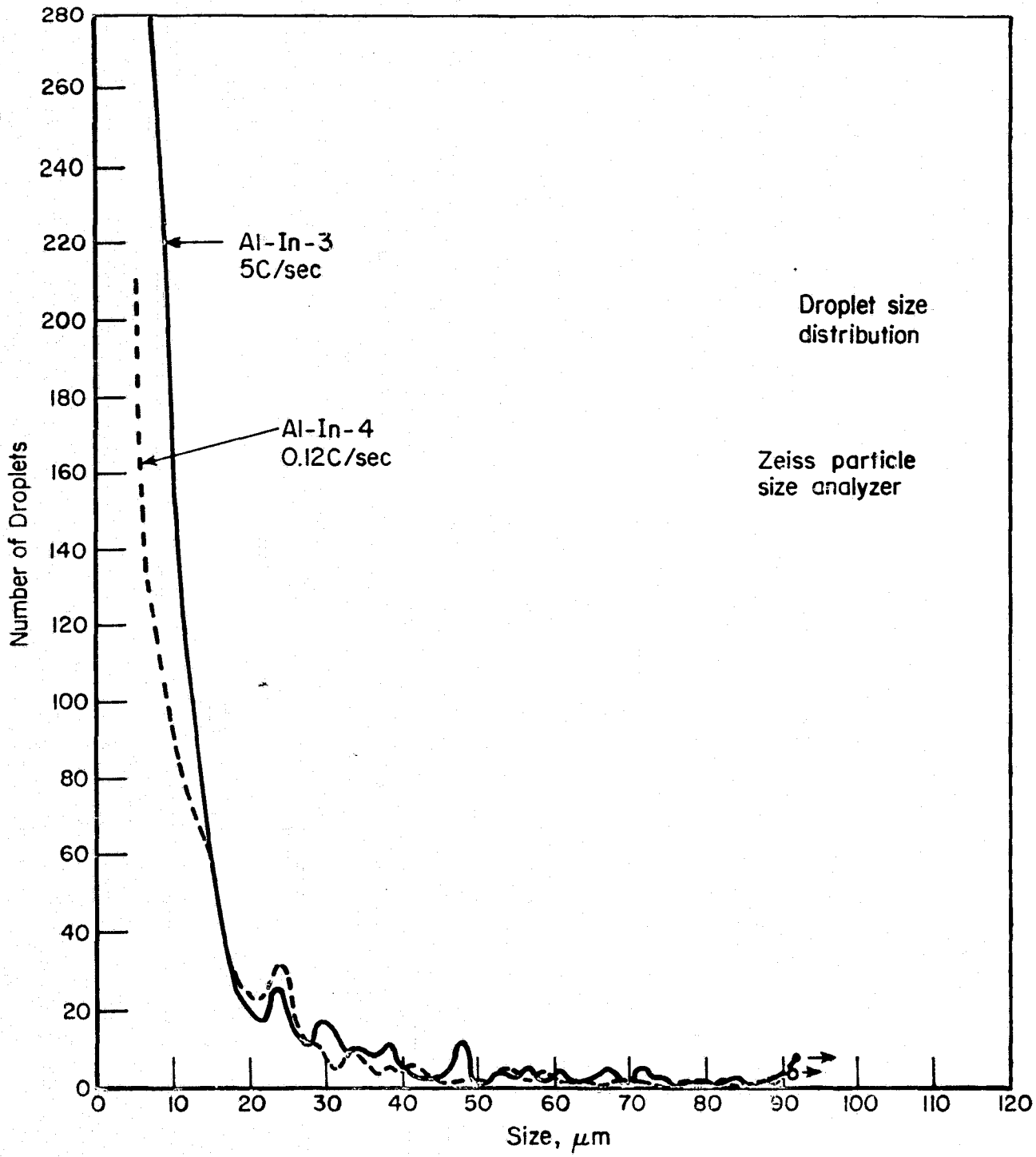

FIGURE 15. DROPLET SIZE DISTRIBUTION FOR SAMPLES Al-In-3 AND Al-In-4 AS DETERMINED ON THE ZEISS PARTICLE SIZE ANALYZER

TABLE 5. RESULTS OF PARTICLE SIZE ANALYSIS FOR Al-In-3[a] AND Al-In-4[b] ZEISS PARTICLE SIZE ANALYSIS CARRIED OUT ON 500X PHOTOMICROGRAPHS[c]

Interval Center, microns[d]	Number of Particles	
	Al-In-3	Al-In-4
<3.5	416	250
4.0	55	40
5.1	34	15
6.2	15	8
7.4	10	7
8.5	5	4
9.6	11	5
10.7	3	2
11.8	2	7

(a) Cooled at 4.8 C/sec.

(b) Cooled at 0.12 C/sec.

(c) Three areas each 0.25 x 0.20 mm were analyzed per sample. Number of particles in each size range combined. It should be noted that in order to compare the present droplet size distribution with that shown in Table 1, a normalization factor must be applied that accounts for the differences in area and interval sizes.

(d) Range Interval = Interval Center $\pm$0.55 μ.

our investigation to some extent by the large range of droplet sizes and the unanticipated large number of very small droplets. In addition, the metallographic preparation of the samples has not produced ideal contrast between the matrix and the finer particles. Future work should be aimed at somewhat improved metallographic preparation and the use of a range of magnifications from ∿ 100X to 2000X with both the Zeiss Particle Size Analyzer and Quantimet being applied to determine the size distribution from <1 μ and above. Other viewing techniques, such as scanning electron microscopy and polarized light metallography (Indium has a face-centered tetragonal crystal lattice and is thus expected to be optically active.) may further improve the contrast. Work along these lines was beyond the resources of the present contract and thus must await a future effort.

The results of the computer-simulation study conducted on the kinetics of droplet coalescence in the Al-In (40 wt %) alloy (see Section 2.16) qualitatively agree with those expected based on the experiments conducted thus far. This is in spite of the fact that the computer-simulation work conducted thus far on the Al-In alloys is a "first approximation" since it includes only one basic coalescence mechanism (Stokes migration) and does not account for the fact that the cooling conditions used experimentally were not the same as that assumed in the simulation. Future work in this area should include the introduction of other coalescence mechanisms, the experimental cooling conditions, the effect of low g, and a quantitative comparison between the simulation and experiment.

2.24 Low-G Experiments

Sufficient ground-base experimentation has now been performed to allow the design of low-g experiments, both in drop-tower tests and in rocket flights. The objective of this work would be to determine the effect of low g, cooling rate, and composition on the microstructure and, where applicable, on the droplet size distribution in Al-In alloys. The

low-g experiments should help us to better understand the types of structures achievable by space processing and the interaction of the effects of low g, cooling rate, and compositional effects.

Some of the questions that we would hope to answer in a study of this type are the following:

(1) How fine can liquid-phase immiscible materials be made when processed at low g?

(2) What effect does cooling rate have on the fineness of the structure?

(3) Is there a critical cooling rate beyond which convection currents are induced in the liquid so that agglomeration and a coarser structure results?

(4) What effect does composition have on the distribution of the immiscible phases and the fineness of the structure?

(5) Is there an effect in systems containing a liquid-phase miscibility gap that is comparable to the spinodal decomposition reaction that occurs in some solid-state miscibility gaps?

(6) Is metastability in space-processed liquid-phase immiscible alloys a real effect?[2]

Experiments in drop tower and in rocket flights would be complementary. Those samples run in the drop tower would be quenched (cooling rate $\sim$ 100 C/sec), while those in the rocket experiments would be cooled at as slow a rate as is compatible with the time at 0 g ($\sim$ 4 C/sec) and at an intermediate rate (20 C/sec). Three compositions of alloy should be examined, Al-In (40 wt %); Al-In (70 wt %); and Al-In (85 wt %). These have been chosen to produce, respectively, In-rich droplets in an Al-rich matrix, an intimate mixture of the two phases, and finally a mixture of Al-rich droplets in an In-rich matrix.

It is anticipated that in a typical low-g experiment the alloys contained in suitable capsules would be preheated on the ground to $\sim$ 1000 C, a temperature above the miscibility gap in a liquid single-phase field,

and allowed to sit at least 15 minutes at that temperature. This will insure that the samples are homogeneous before starting to cool through the miscibility gap. This latter operation will begin when the experiment enters the weightless mode.

The capsules would be designed to fit existing furnace facilities and would have to provide

- A nonreacting compatible environment for the liquid Al-In alloys
- Hermetical sealing in vacuum or inert gas
- Facility for introduction of a thermocouple by means of which cooling-rate information could be recorded.

A graphite-lined Ta crucible which had been evacuated and sealed would probably be suitable.

Both ground-base and low-g experiments would be run at the three compositions and would be analyzed metallographically to determine droplet size distributions and to quantitatively assess other microstructural features. X-ray diffraction should also be applied to determine whether metastable phases are present in the structure. In addition, other characterization tools, such as scanning and transmission electron microscopy, could be used where applicable.

2.3 Rapidly Cooled Immiscible Materials

This aspect of our effort on liquid-phase immiscible materials is aimed at simulating some of the features expected from processing such materials at low g. In particular, it is felt that the fine microstructure, which can be produced in bulk samples by processing at low g, could also be formed in wire or other high-surface-area form by very rapid cooling. If this proves to be the case, a low-cost technique might result which can be used as a tool for selecting immiscible systems with the most promising properties for further research at low g.

The technique selected to produce the rapidly cooled immiscibles is a Battelle-patented process called "Melt Extraction". The process makes use of a water-cooled spinning disc with a shaped periphery that

dips into a molten bath and extracts the liquid which is rapidly cooled and solidified during the short time it is in contact with the disc. The solidified filament can be continuous or "chopped", depending on the geometry of the wheel. In the extraction of fine wire, cooling rates as high as 10^6 C/sec should be achievable.

Two variations of the technique are available, Crucible Melt Extraction (CME) and Pendant Drop Melt Extraction (PDME)[29]. These are illustrated in Figures 16 and 17. The experiments conducted in the present program were limited to PDME since it is more amenable to the production of finer fibers and thus will produce the higher cooling rates desired and also because it can be more readily used to process small quantities of material. As is illustrated in Figure 17, PDME requires a feed rod (in our case $\sim$ 3-6 mm in diameter), the end of which is melted by a heat source. The apparatus we used for this application was contained in a vacuum chamber and made use of an electron beam as a heat source.

To fabricate the feed rods, it was necessary to prepare material with a minimum of compositional heterogeneities, a task which can be especially difficult terrestrially with liquid-phase immiscibles having components which have appreciable differences in specific gravity. To accomplish this task, equipment similar to that used previously[6] and shown in Figure 18 was assembled. The components, in their correct proportions, were induction melted either in vacuum or under a partial pressure of argon, and brought to a temperature in the single-phase liquid field above the miscibility gap. After a short time at this temperature, during which the eddy current stirring is homogenizing the melt, the closed-end fused silica tube, $\sim$ 4-mm ID, is dropped into the molten bath and at the same time the system is pressurized with $\sim$ 0.1 MPa ($\sim$ 1 atmosphere) of Ar. The pressurization forces some of the molten alloy up the fused silica tube where it is rapidly solidified. The tube is immediately withdrawn from the bath by the magnet positioned at the top of the apparatus. The alloy is subsequently removed from the silica tube by breaking the tube and/or leaching with HF.

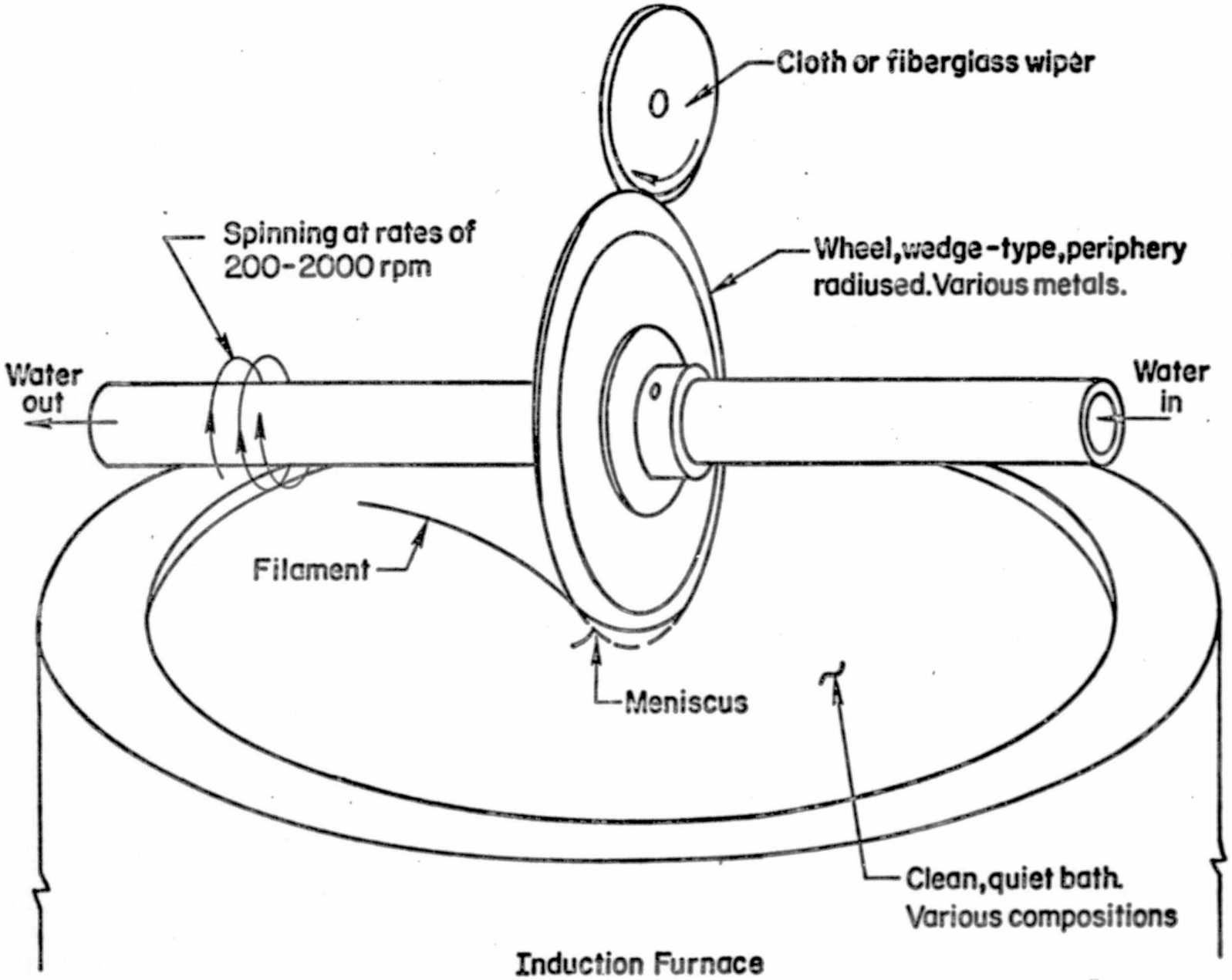

FIGURE 16. SKETCH ILLUSTRATING THE PRINCIPLES OF CRUCIBLE MELT EXTRACTION(29)

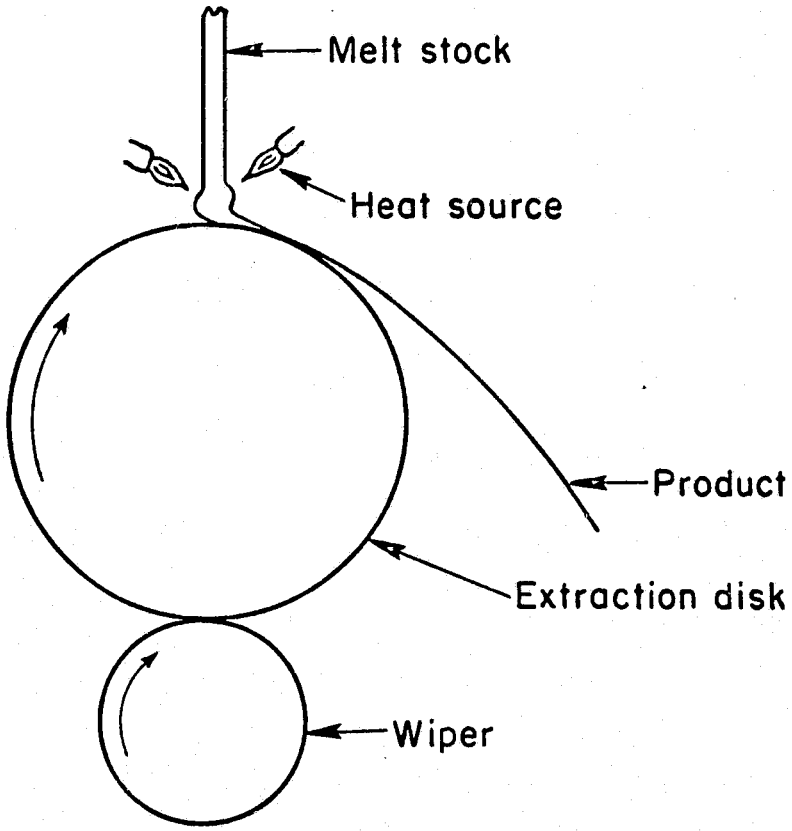

FIGURE 17. SCHEMATIC DIAGRAM OF PENDANT DROP MELT EXTRACTION APPARATUS[29]

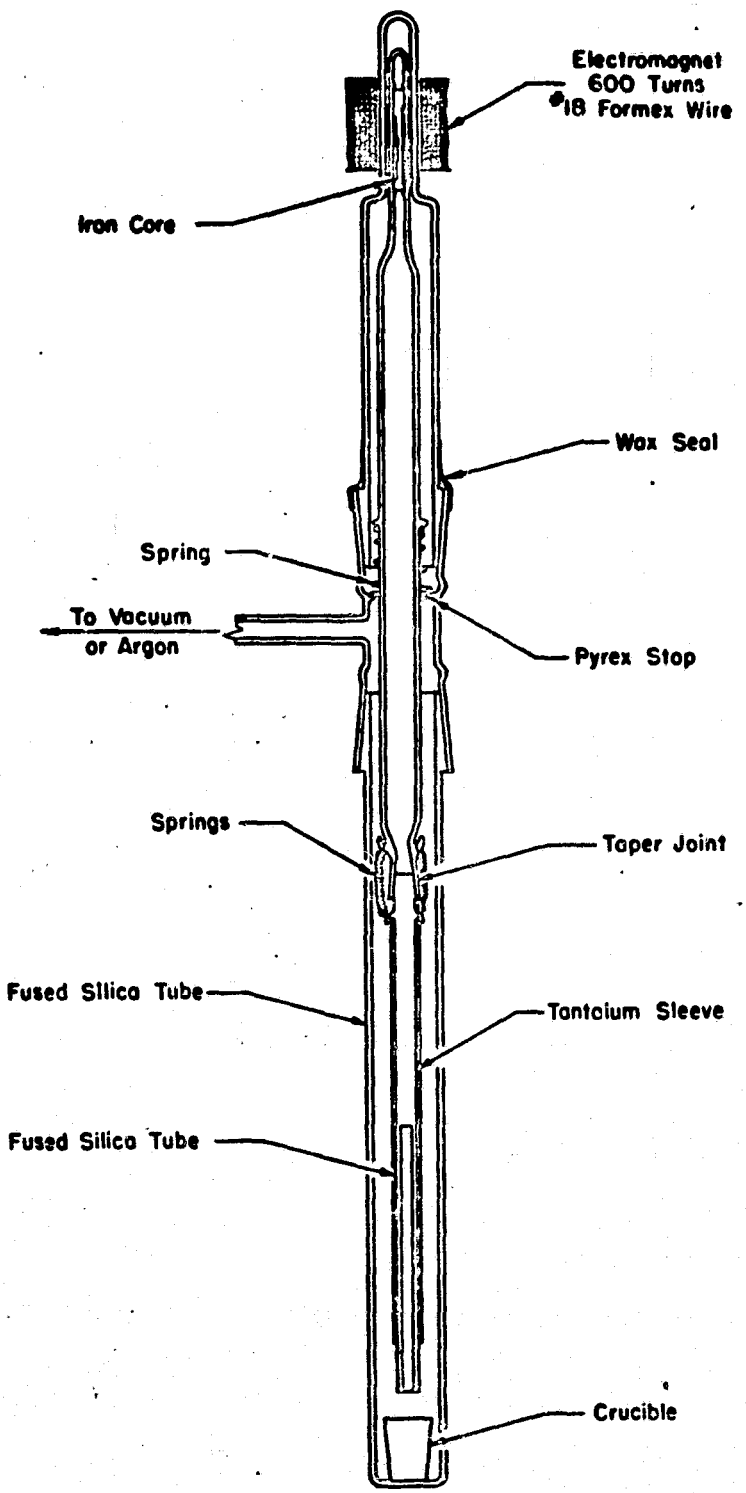

FIGURE 18. SCHEMATIC OF VACUUM-MELTING EQUIPMENT[6]

Since the molten alloy travels in the silica tube for ∿ 1 second, at which point its motion is halted because it solidifies, it is estimated that the cooling rate through the miscibility gap is on the order of 200 C/sec. This, of course, is very approximate but could be measured fairly easily if subsequently warranted.

A summary of the rods produced by the "Rod Extraction Technique" is presented in Table 6, where it is seen that the following six different alloys were fabricated.

- Al-In (40 wt %)
- Al-In (68.8 wt %)
- Al-In (85 wt %)
- Pb-Cu (23.5 wt %)
- Pb-Cu (40 wt %)
- Bi-Ga (25 wt %).

Metallographic observations have been carried out on two of the samples [Melt No. 5, Pb-Cu (23.5 wt %); and Melt No. 7, Al-In (40 wt %)], and portions of three rods have been provided to I. C. Yates (COR) for incorporating in drop-tower experiments [Melt No. 9, Al-In (85 wt %); Melt No. 10, Al-In (68.8 wt %); and Melt No. 14, Bi-Ga (25 wt %)]. Two samples have also been provided for PDME experiments [Melt No. 6, Pb-Cu (23.5 wt %); and Melt No. 15, Al-In (40 wt %)].

The photomicrographs of Figures 19 and 20 show the microstructures obtained in extracted Rods 5, Pb-Cu (23.5 wt %); and 7, Al-In (40 wt %), respectively. In general, the microstructures are quite uniform along the length of the samples. In the Pb-Cu alloy they generally consist of fine (∿ 10 μ) Cu-rich droplets in a Pb-rich matrix. The Cu-rich droplets which undergo a monotectic transformation.

$$\text{Liquid Cu-Pb (14.7 wt \%)} \rightarrow \text{Solid Cu} + \text{Liquid Pb-Cu (13 wt \%)} \quad ,$$

show evidence of this transformation, as seen in Figures 19d-f. Some non-uniformity in the structure was seen, especially at the bottom of the rod (Figure 19f). This generally took the form of appreciably larger Cu-rich droplets.

TABLE 6. SUMMARY OF ROD EXTRACTION EXPERIMENTS

Melt No.	Material	Remarks
1	Pb-Cu (23.5 wt %)	Melted in vacuum. Excessive Pb vaporization caused glow discharge. Crucible Failure. Unsuccessful run.
2	Pb-Cu (23.5 wt %)	Melted in vacuum. Excessive Pb vaporization caused glow discharge. Unsuccessful run.
3	Pb-Cu (23.5 wt %)	Melted in Ar at 0.05 MPa. Successful run except rod appears segregated. Suspect not high enough melt temperature.
4	Pb-Cu (23.5 wt %)	Melted in Ar at 0.05 MPa. Induction coil shorting. Unsuccessful run.
5	Pb-Cu (23.5 wt %)	Melted in Ar at 0.05 MPa. Used for metallography.
6	Pb-Cu (23.5 wt %)	Melted in Ar at 0.033 MPa. Used for PDME.
7	Al-In (40 wt %)	Melted in vacuum. Used for metallography.
8	Bi-Ga (25 wt %)	Melted in vacuum.
9	Al-In (85 wt %)	Melted in vacuum. Portion of rod provided to MSFC for drop-tower experiments.
10	Al-In (68.8 wt %)	Melted in vacuum. Portion of rod provided to MSFC for drop-tower experiments.
11	Pb-Cu (40 wt %)	Melted in Ar at 0.05 MPa.
12	Al-In (40 wt %)	Melted in vacuum. Run stopped when piece of In found outside crucible. Unsuccessful run.
13	Al-In (40 wt %)	Melted in vacuum. Tube formed rather than rod. Unsuccessful run.
14	Bi-Ga (25 wt %)	Melted in vacuum. Portion of rod provided to MSFC for drop-tower experiments.
15	Al-In (40 wt %)	Melted in vacuum. Used for PDME.

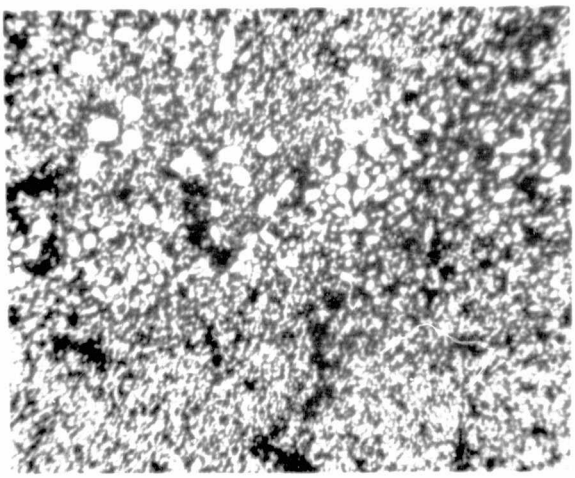

100X a. Top 847

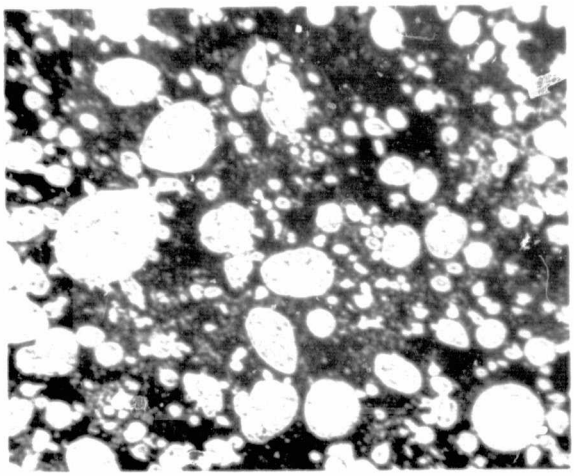

100X d. Center 851

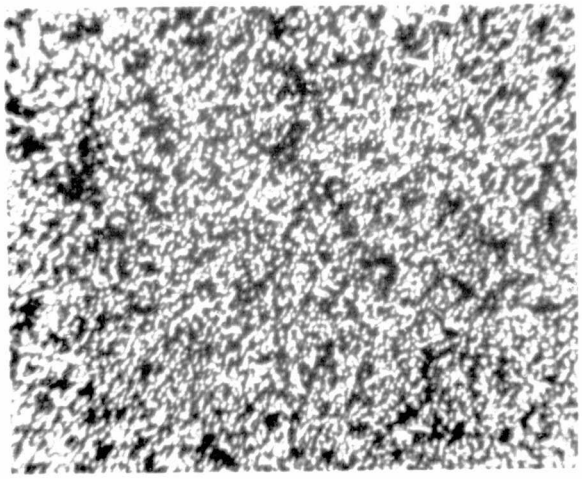

100X b. Center 849

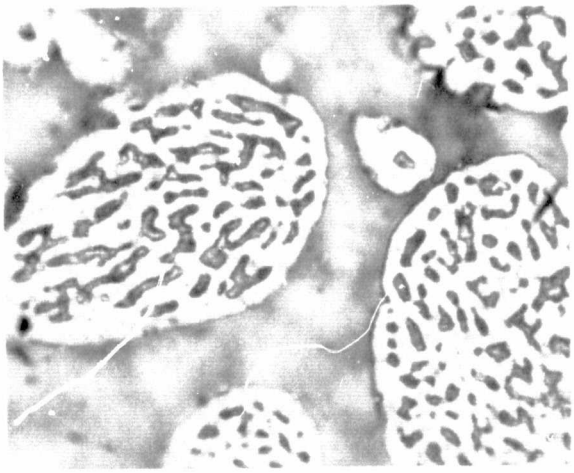

500X e. Center 852

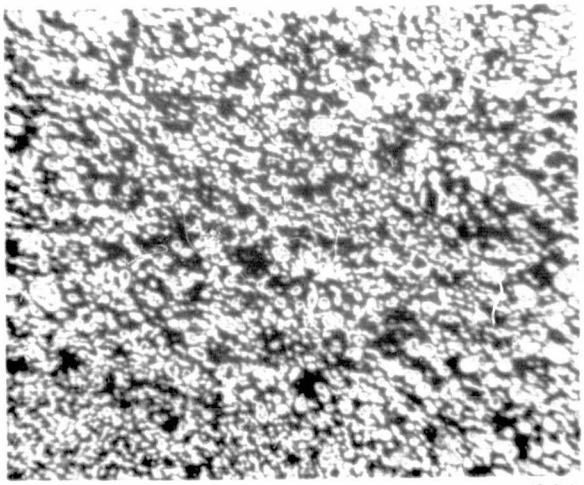

100X c. Bottom 843

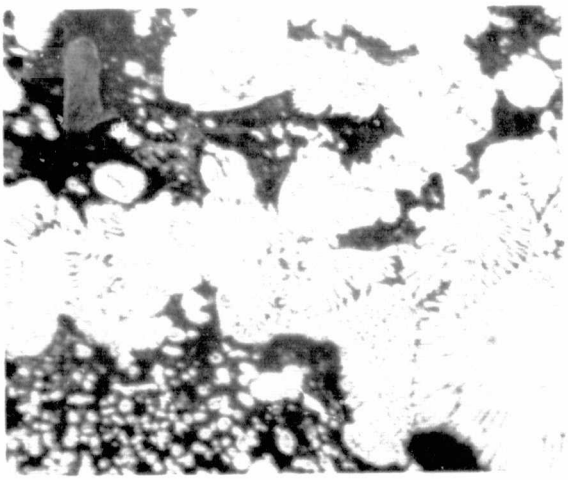

100X f. Bottom 870

FIGURE 19. PHOTOMICROGRAPHS OF EXTRACTED ROD NO. 5, Pb-Cu (23.5 WT %)

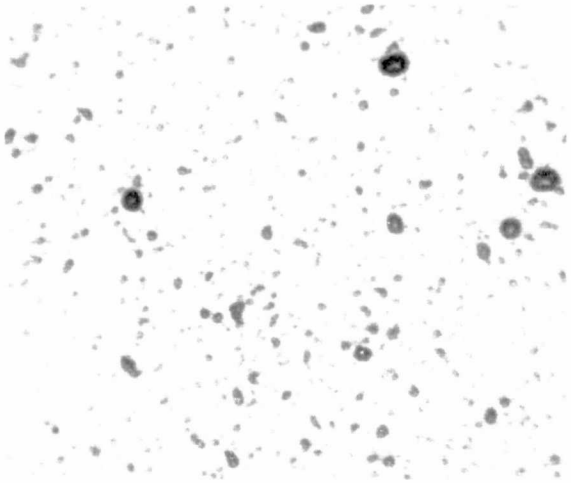

100X a. Top 858

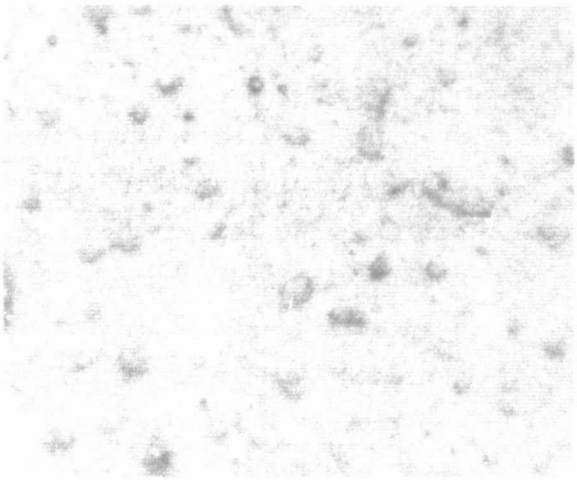

50CX d. Top 859

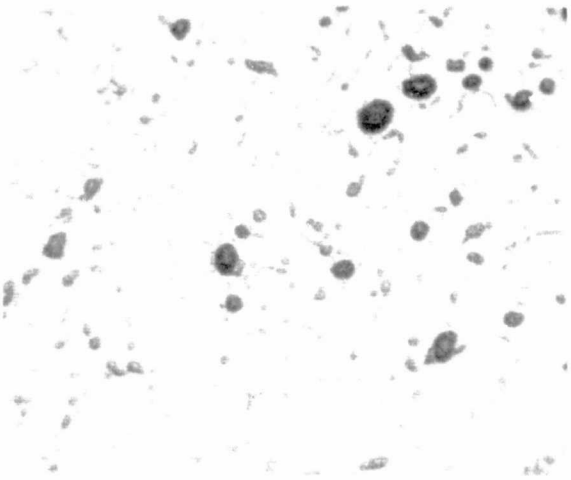

100X b. Top 857

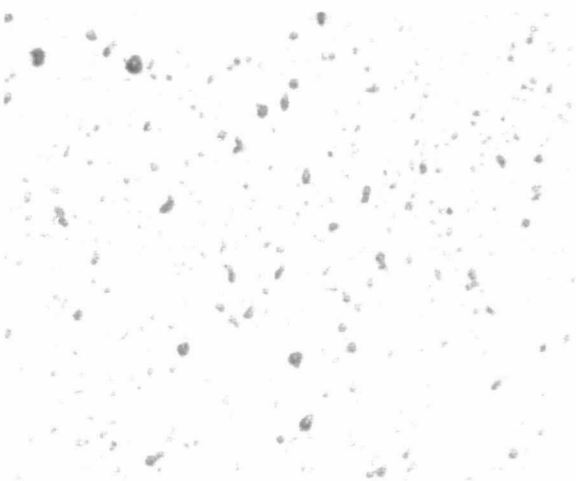

100X e. Center 860

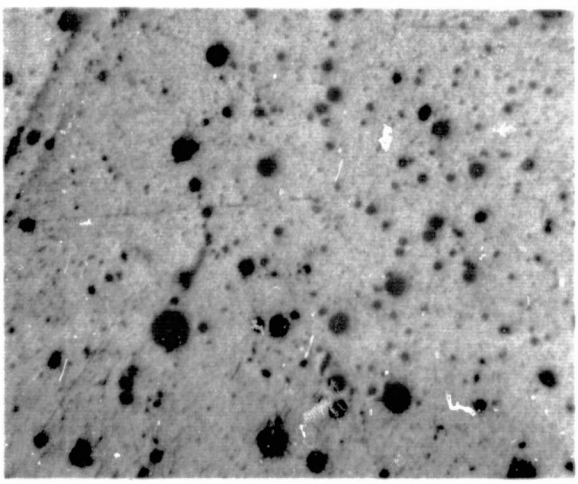

100X c. Bottom 864

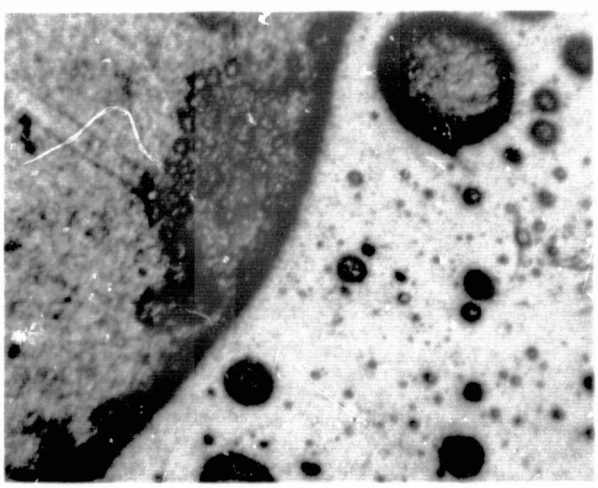

100X f. Bottom 867

FIGURE 20. PHOTOMICROGRAPHS OF EXTRACTED ROD NO. 7, Al-In (40 WT %)

The microstructure of extracted Rod 7, Al-In (40 wt %), generally consisted of a uniform dispersion of fine In-rich droplets in an Al-rich matrix. The latter should consist of Al and In phases produced by the monotectic transformation in this system. This feature has as yet not been seen in the photomicrographs of this alloy, presumably because of the less than ideal metallographic preparation techniques used. Some agglomeration or segregation was also noted at the bottom of this rod (see Figure 18f). This is probably due to the somewhat slower cooling rates in this region, although macrosegregation cannot be ruled out.

Comparison of the photomicrographs of Figure 20 with those in Figures 12 and 13 shows that the droplet size distribution is much narrower and has a higher concentration of fine particles in the extracted rod, where the cooling rate is at least twenty times faster than in the thermal analysis specimens. The narrower droplet size distribution and the higher concentration of fine particles are both predicted on the basis of the computer-simulation analysis.

Based on the preceding observations, it is evident that a uniform material of relatively fine microstructure can be obtained by the rod extraction technique. In addition to more rapidly cooled materials made by melt extraction or spinning methods, samples made by the rod extraction technique should also prove to be useful in helping to predict the properties of the liquid-phase immiscible materials processed in space.

Two attempts have been made to produce PDME fiber from extracted rod. Some success was achieved with extracted Rod 6, Pb-Cu (23.5 wt %), in producing an extremely fine microstructure. However, composition and drop stability were difficult to control. This is probably due to the fact that there is a region between the pendant drop and the solid rod, which is in the two-phase liquid region, wherein the Pb-rich and Cu-rich phases tend to segregate. There is not enough time for these regions to homogenize once they reach the pendant drop itself since they would be rapidly extracted from the melt as Cu-rich and Pb-rich fibers. Examples of these fibers are shown in the photomicrographs of Figures 21, where it may be seen that

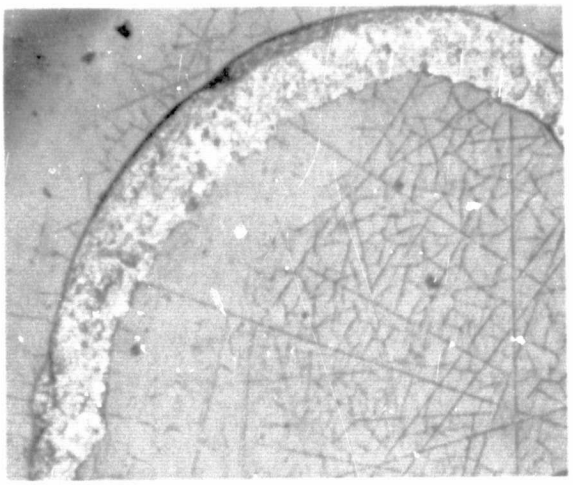

100X

a. Pb-rich particles in Cu-rich matrix

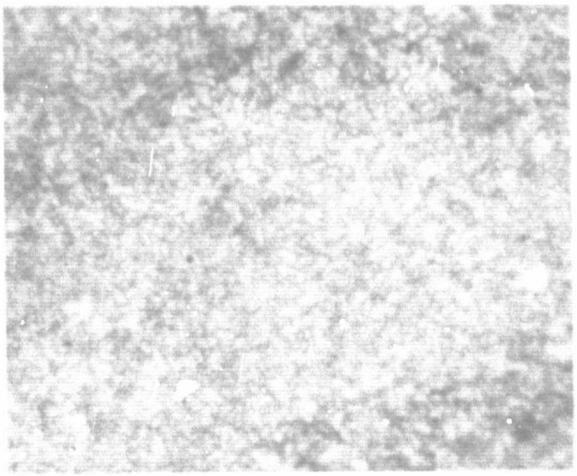

1000X

b. Pb-rich particles in Cu-rich matrix

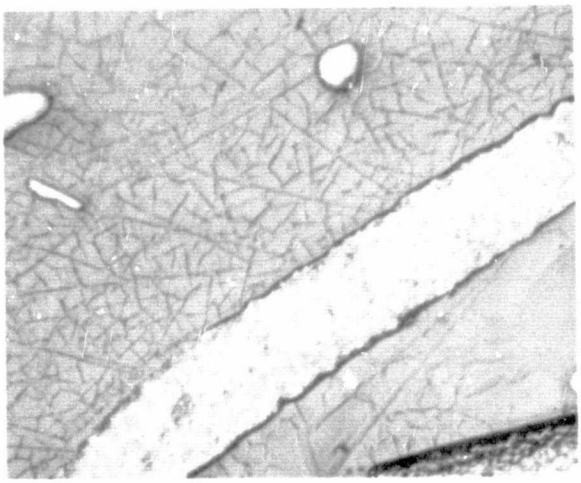

100X

c. Cu-rich particles

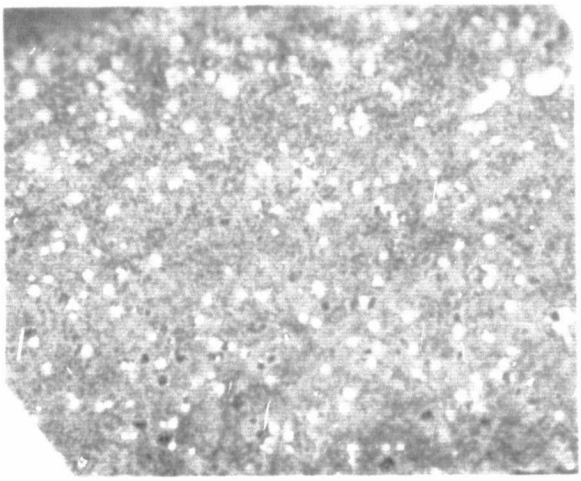

500X

d. Cu-rich particles

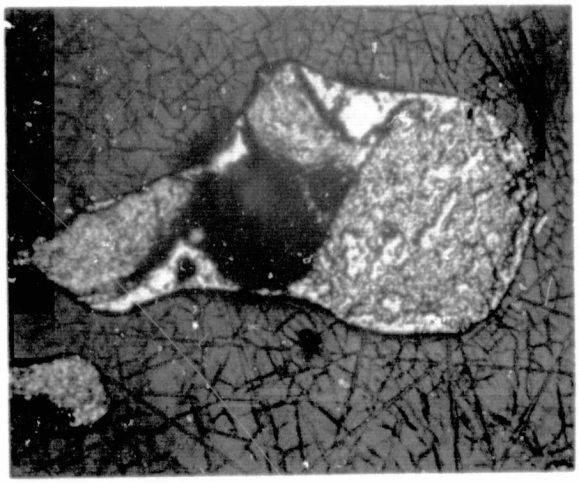

100X

e. Cu-rich particles

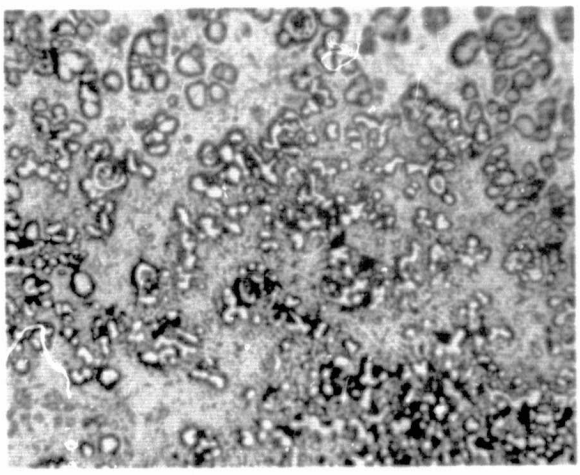

500X

f. Cu-rich particles

FIGURE 21. PHOTOMICROGRAPHS OF PENDANT DROP MELT EXTRACTED FIBERS PRODUCED FROM EXTRACTED ROD 6, Pb-Cu (23.5 WT %)

(1) The droplet size is extremely fine; e.g., Figure 21b shows droplets $\leq$ 1 μ.

(2) Depending on the composition of the particular fiber, the droplets may be Cu rich or Pb rich.

No success was achieved in the one attempt made to extract Al-In (40 wt %) fibers because of the droplet instability.

In the light of our experience using PDME, we would suggest that future attempts to produce rapidly quenched fibers or ribbon be directed to crucible melt extraction (CME) or a mode of melt spinning in which a pressurized stream of molten metal is allowed to impinge on a cooled moving disc or drum.

2.4 Analysis of Liquid Phase Immiscible Systems

This section addresses the question of candidate materials selection among the many possible combinations of liquid phase immiscible materials, and the potential unique properties which may be attained through processing in a gravity-free environment. Among the items to be discussed here are: (1) the readily available compendia of potential systems for consideration, (2) estimates of the usefulness of such systems, as grouped into various property and application categories, and (3) the characteristic features of such applications which suggest that zero-g processing may provide either unique structures or methods for readily achieving the necessary properties.

To set the stage for the following discussion on properties, it is necessary to make some preliminary statements regarding the morphologies and material properties which can result from the cooling of an originally homogeneous liquid through a liquid-phase miscibility gap. It is presumed that the initial configuration will be a homogeneous liquid phase, that nucleation of one phase within the host will occur on cooling and will result in a dispersion of a particulate phase in a continuous phase (matrix). Other portions of the present study have already shown that the distribution in size of such particles is a function of time and is influenced by a variety of diffusion and collision mechanisms.

Variations in composition across the miscibility gap and/or cooling rate may lead to other morphological forms in addition to that of fine particles embedded in a matrix. One possibility is a structure consisting of two interlocking phases, one of which may take the form of a fine filigree or "lace". Lastly, the dispersed phase may take the form of oriented or random needles in a solid matrix. For the purpose of the remaining discussion, these three separate forms (which can conceivably be attained in any given system, depending upon preparatory methods) will generally be considered as one, unless particular features in applications suggest that specific attention to any one of them be emphasized.

In determining the role space processing may play in providing unique or useful materials, three points must be recognized.

(1) Finer structures are achievable by space processing than by comparable treatment on the earth due to the absence of the gravity driven coalescence processes in the 0-g environment.

(2) Less segregated microstructures are likely in space-processed materials, and

(3) Non-equilibrium phases may form at 0-g.[2] These could alter the properties of the material and thus might lead to unique applications. Since this last effect is not understood, it is impossible at this time to incorporate it directly into our consideration of potential applications of space-processed materials. A further understanding of this phenomenon is certainly called for.

A key link in predicting potential applications for liquid-phase immiscible materials processed terrestically or in space is our understanding of the relations between properties and microstructures. In some cases this relationship is quite well understood but in others, the development is in its infancy. In most cases much more understanding is needed to effectively apply the knowledge of microstructural possibilities to the accurate predicition of material performance.

2.41 Potential Systems for Consideration

Much of the preliminary work on the evaluation of candidate materials for this study has drawn upon the compilations of Reger[4] of TRW. This survey of immiscible systems, drawn primarily from the standard literature, contains reference to 361 suggested metal/metal systems, as well as additional combinations, including metal/metal oxide, metal oxide-metal oxide/metal salt ceramic systems, metal-metal salt/element systems, and metal salt/metal salt systems. In addition, preliminary consideration had been given to the existence of a number of ternary and quarternary systems having a miscibility gap.

The TRW listing is, in part, incomplete in that insufficient data is presented which defines the characteristics or extent of the miscibility gaps. On the other hand, it is perhaps too complete in that there are included many systems where the gaps are unconfirmed. However, even with its deficiencies, the TRW collection proves an excellent starting point for consideration of the potential applications which might not otherwise be attained through more conventional processing methods.

2.42 Categories of Applicability

TRW has not only provided an "atlas" from which to begin a study of applications and properties, but has detailed possible applications in a number of different fields. Considering only the metallic binary systems, the TRW study has delineated potential applications for each of the 331 systems listed (some of which may, of course, be classified in more than one area), with the result that the following lists provide starting points for detailed study. In Table 7 we have listed the application areas and the numbers of systems falling in each category.

TABLE 7. POTENTIAL APPLICATIONS OF IMMISCIBLE MATERIALS

Applications	Number of Systems
Catalysts	263
Fine particle superconductors	246
Fine particle permanent magnets	46
Breeder-reactor fuel	42
Nuclear reactor structural materials	20
Electrical contact material	16
Nuclear reactor control rods	15
Bearing alloys	8
Dispersion strengthened alloys	6
Solid lubricants	2
III-V semiconductors	2
Extrinsic semiconductors	1
Other	1
TOTAL	668

In general, the grouping of the materials systems into the various categories has apparently been predicated on a knowledge of the properties of one or both of the materials in the two component systems. No effort has been made to consider the potential applications as they might vary depending upon whether one of the components is the continuous or discontinuous phase, or what form any dispersion might take. To be sure further consideration of the kinetics and thermodynamics of the systems would provide additional guidance on the forms expected in any given experimental system, and more detailed investigation of the phase diagrams would infer some practical limitations on the quantitative aspects of the choices made. For the purposes of the present discussion, however, we shall continue with the TRW qualitative aspects of the argument, and will present preliminary evaluations of the potential applications.

2.43 Characteristic Features of Suggested Applications

Thus far, only some of those categories listed in Table 7 have been considered. However, another category, superplastic materials, has been added and discussed below. The discussion below is limited to identification of selected features which will determine whether the applications anticipated can be realized in practice.

2.431 Superconducting Materials. The large list of potential superconducting materials (see Table 8) presents an ambitious number of systems in which either one or both of the elements has been verified to undergo a superconducting transition, and where selected alloys within the total system have demonstrated superconducting properties. To be sure, not all of the elements listed have demonstrated superconducting properties in normal bulk form; bismuth, for example, has no verified superconducting transition except in very thin films. The inclusion of such special conditions, however, is in keeping with the general direction of this discussion, for it is the unique properties which may be attained only through specialized processes or structures which are of primary interest.

TABLE 8. SYSTEMS OF IMMISCIBLE MATERIALS SUGGESTED FOR SUPERCONDUCTING PROPERTIES[4]

Ag-Cb	B-Bi	Bi-Ru	Cb-Pb	Cr-Sn	Ga-Hg	La-Ta	Mo-Sb	Pu-Ta
Ag-Ir	B-Cd	Bi-Si	Cb-Pu	Cs-Ga	Ga-K	La-Ti	Mo-Sc	Re-Sn
Ag-Mo	B-Ga	Bi-U	Cb-Sc	Cs-In	Ga-Pb	La-U	Mo-Sn	Re-Zn
Ag-Re	B-Hg	Bi-V	Cb-Sn	Cu-Mo	Ga-Te	La-V	Mo-Y	Ru-Zn
Ag-Ru	B-In	Bi-W	Cb-Y	Cu-Os	Ga-Tl	La-Yb	Na-Ta	S-Sn
Ag-Ta	B-Pb	Bi-Zn	Cb-Yb	Cu-Pb	Ga-W	La-Zr	Na-U	S-Tl
Ag-U	B-Sn	C-Cd	Cd-Cr	Cu-Re	Gd-Mo	Li-Mo	Na-Zn	Sc-U
Ag-V	B-Tl	C-Hg	Cd-Fe	Cu-Ru	Gd-Ta	Li-Ta	Na-Zr	Sc-V
Al-As	Be-Bi	C-Pb	Cd-Ga	Cu-Ta	Gd-U	Li-Ti	Nd-Ta	Se-Sn
Al-Bi	Be-Ga	C-Sn	Cd-K	Cu-Tl	Gd-V	Li-U	Nd-Ti	Se-Tl
Al-C	Be-Ge	C-Tl	Cd-Pu	Cu-U	Gd-W	Li-V	Nd-U	Se-Zn
Al-Cd	Be-Hg	C-Zn	Cd-Se	Cu-V	Ge-Hg	Li-Zr	Nd-V	Si-Tl
Al-Cs	Be-In	Ca-Cb	Cd-Si	Dy-Mo	Hg-Se	Lu-Ta	Ni-Pb	Sm-U
Al-In	Be-Mg	Ca-Cd	Cd-Tc	Dy-Ta	Hg-Si	Lu-U	Os-Sn	Sm-V
Al-K	Be-Pu	Ca-Gd	Ce-Mo	Dy-Ti	Hg-Ta	Lu-V	P-Sn	Sm-W
Al-Na	Be-Sn	Ca-La	Ce-Ta	Dy-U	Hg-V	Mg-Mo	P-Tl	Ta-Tb
Al-Pb	Be-U	Ca-U	Ce-Ti	Dy-V	Hg-W	Mg-Ti	Pb-Pm	Ta-Y
Al-Rb	Bi-C	Cb-Ce	Ce-U	Er-Mo	Ho-U	Mg-U	Pb-Se	Tb-U
Al-S	Bi-Cb	Cb-Cu	Ce-V	Er-Ta	In-S	Mg-V	Pb-Si	Te-Tl
Al-Tl	Bi-Co	Cb-Er	Ce-Zr	Er-Ti	In-Se	Mg-Zr	Pb-U	Th-U
As-Hg	Bi-Cr	Cb-Gd	Co-Hg	Er-U	In-Te	Mn-Pb	Pb-W	Th-Yb
As-Tl	Bi-Fe	Cb-K	Co-Pb	Er-V	K-Mo	Mn-Tl	Pb-Zn	Tl-Zn
Au-Ir	Bi-Ga	Cb-La	Co-Tl	Eu-U	K-Zn	Mo-Nd	Po-Ta	Tm-U
Au-Os	Bi-Ge	Cb-Li	Cr-Gd	Fe-Hg	La-Mn	Mo-Pb	Pr-Ta	U-Y
Au-Re	Bi-Mn	Cb-Mg	Cr-Hg	Fe-Pb	La-Mo	Mo-Po	Pr-Ti	U-Yb
Au-Rh	Bi-Mo	Cb-Na	Cr-Ta	Fe-Sn	La-Pu	Mo-Pr	Pr-U	U-Zn
Au-Ru	Bi-Os	Cb-Nd	Cr-Pb	Fe-Tl	La-Re	Mo-Pu	Pr-V	V-Y
								V-Yb
								W-Zn

The existence of mixed phases in a superconducting system can produce either detrimental or beneficial effects, depending upon the nature and distribution of the phases. For example, induced superconductivity of normally non-superconducting materials (e.g., bismuth, as seen above), whether it be through thin film, granular or deformation effects, is usually associated with significant perturbations in the local vibration modes of the crystal lattice, and a resultant enhanced phonon contribution to the electron-electron coupling responsible for superconductivity. It would be expected that such enhanced superconductivity (as seen principally through effects on the transition temperature) would result from a configuration in which there was a high surface/volume ratio, as would be the case in systems composed of a filigree supported by a matrix.

Such composite structures have been proposed earlier wherein porous ceramic or glass systems have been infiltrated with liquid aluminum, indium, lead or other relatively low-melting superconductors, and have been proposed as well for bismuth-containing composites. Enhancement (raising) of transition temperatures through applications of this approach offers the potential for creating superconducting materials or systems based almost entirely upon morphological contributions.

Fine particles of superconducting material if dispersed closely enough together have also been found to act as a continuous superconducting network as a result of a proximity effect. A case in point has been the work on a Cu-Nb(0.6 At. pct.)[30] alloy containing a dilute dispersion of superconducting Nb in a Cu matrix. Although the particles were isolated, the material showed superconducting properties that could be explained in terms of a continuous filamentary network.

Poisoning effects on the transition temperature may result from the presence of non-superconducting particles dispersed in a superconducting matrix. In such cases, a lowering of the transition temperature (or complete conversion to the normal state) results from the presence of high densities of particles sized on the order of the coherence length (several hundred angstroms).

The above considerations have dealt only with the transition temperature aspects of potential materials systems. There are, to be sure, additional effects which can be beneficial, such as flux pinning which can produce a resultant net enhancement of the total superconducting properties. While decreases in transition temperature can result from the inclusion of non-superconducting particles, evenly spaced particles produce a spreading of the transition over a range of temperatures, particularly where the included phase is ferromagnetic or insulating. These inclusions which act as flux pinners (similar to dislocation pinning in metals) retard the penetration of magnetic flux lines into the superconducting regions of the structure and thus increase critical fields and currents. In addition to the effect upon "intrinsic" superconducting properties, the presence of dispersed phases can also contribute to the mechanical strength of materials.

The relationship between superconductivity and the distribution of phases in a multiphase alloy is only poorly understood. We would recommend that further work be conducted to evaluate and understand the superconducting properties of model systems with the aim of improving this situation. Work in such systems as Bi-Ga or Pb-Zn in which the microstructure is varied by changing composition, cooling rate or by processing at 0-g is recommended. Other recommended areas for study are in the Pb-Cu system wherein it should be possible to directionally grow fine (< 1μ diameter) continuous Pb rods in a copper matrix[31] or else to produce diamagnetic copper rich dispersions in a Pb matrix. For comparison with the latter structure, the Fe-Pb system may be chosen to deduce the effects of a dispersion of ferromagnetic Fe particles on the properties of Pb.

2.432 III-V Semiconductors. The suggestion[4] that new semiconducting materials derived from the two immiscible systems As-Tl and Al-Bi has apparently been drawn from mere examination of the positions of these elements in the periodic table, and does not reflect more fundamental consideration of the basic phenonema which contribute to the properties of the III-V semiconductors. Judging from common band structural features which are associated with the more common III-V semiconducting compounds (such as AlAs, InSb, InAs, GaAs, etc), it is not anticipated that the suggested combinations would provide the essential fundamental features which contribute to normal semiconducting behavior. However, the unexplained electrical behavior of an alloy consisting of intimately mixed Ga and Bi phases would warrent further work on this syste and the related systems As-Tl and Al-B in order to understand the phenomenon.

2.433 Electrical Contact Materials. At the present time, immiscible materials are used extensively for electrical contacts. In fact, on a weight basis such materials comprise an estimated 75-80 percent of total contact material usage.

The materials systems of present commercial interest are relatively few. These are (1) Ag-CdO, (2) Ag-Ni, (3) Ag-W, and (4) Cu-W. Several others are used but in low volumes. These include Ag-Fe, Ag-Mo, and Ag-WC.

Such materials are used almost exclusively for switch, circuit breaker, and motor control applications above about 5-10 amperes. The objectives in their use are for (1) high conductivity, (2) low arc erosion, (3) resistance to electrical welding, and (4) contact resistance stability.

All of these materials are produced by classical powder metallurgy techniques. This includes liquid infiltration in the case of Ag-W and Cu-W.

While Ag-CdO materials are also produced by powder metallurgy, no more than 10 percent of present usage is in this type of product. Most of the Ag-CdO is produced by internal oxidation of silver-cadmium alloys.

One objective in the processing of all of these materials is to obtain a fine, uniform/random dispersion. This feature is generally desired for optimum performance but for reasons which are still not totally understood. Subtle changes in process and microstructural variables are known to result in performance differences of at least a factor of three for a given composition.

While 0-g processing offers unique opportunities for producing a uniform distribution of fine particles in a conducting matrix by:

(1) Cooling through a liquid phase miscibility gap

(2) Introducing stable particles or fibers directly into the molten bath (Al_2O_3, Ni, etc).

it is impossible to predict the magnitude of these and other effects on performance. This is due to the fact that the interrelation of variables is imperfectly understood and that studies in this field have proceeded largely on an experimental rather than theoretical basis.

In spite of this, immiscible systems have considerable promise in application. Here there are three factors to be considered. In the first place, absence of miscibility or compound formation will permit maintenance of the high conductivity for which the matrix material was initially selected. Secondly, even in that case where the included second phase (which contributes to mechanical properties enhancement) is an insulator, the volume fraction of the second phase is usually small enough that only insignificant effects upon total bulk conductivity result, and the enhanced mechanical integrity more than compensates for decreased conductivity. And third, the structure which appears to have the greatest promise is that in which the second dispersed phase is metallic and completely noninteractive with the matrix. For it is this latter case that the mechanical integrity is improved, and the losses to electrical conductivity are minimized.

Sixteen systems were listed by Reger[4] in his compilation of liquid phase immiscible systems as being potentially applicable as electrical contact materials. These are listed in Table 9.

TABLE 9. SUGGESTED ELECTRICAL CONTACT MATERIALS DERIVED FROM IMMISCIBLE SYSTEMS[4]

Ag-Cr	Ag-Ru	Au-Re	Cr-Cu
Ag-Ir	Ag-W	Au-Rh	Cu-Os
Ag-Re	Au-Ir	Au-Ru	Cu-Re
Ag-Rh	Au-Os	Co-Cu	Cu-Ru

The rationale for the choice of these systems was the presence of a good conductor (Cu, Ag, Au) and a dispersion of a second phase which could add good wear, erosion, or corrosion resistance. Using the same criteria, a few other possibilities could be added to the list among which are the electrical contact materials currently being utilized, Ag-Ni, Ag-Mo, Ag-Fe and Cu-W and the as yet unexplored systems Ag-Cb, Ag-Co, Ag-Mn, Ag-Ta, Ag-V, Cu-Mo, Cu-V. Ag-C and Cu-C are presently being employed where the lubricating property of the graphite improves resistance to sticking.

The potential of all these systems needs further exploration in terms of the technical and economic benefits to be derived from superior performance by the as-yet unexplored material systems or by materials produced by space processing.

2.434 Catalysts. The TRW classification lists 263 immiscible systems which are deemed to have applicability in the field of catalysts. In almost all of these cases, it is apparent that the primary rationale in assigning "catalysts" as an area for development was derived from the characteristics of one or both of the metal constituents. For example,

it has been well established that nearly all transition metals (those having incomplete d- or f- shells) can result in catalytic activity associated with electron transfer mechanisms. In addition, oxides and other compounds of many of these transition metals are similarly effective in catalysis.

There is, however, an additional criterion which must be met in the development and use of catalysts: intrinsic catalytic activity must, to be effective, be augmented by high surface areas in order that effective processes may be realized. These two criteria and the possibility of space processing constitute the principal thrusts of this section.

There is little in the list of suggested catalytic material systems which would indicate that entirely new intrinsic materials would result from the space processing approach. However, it is more important to note that the second criterion, that of phase morphology, offers more promise. To be specific, consideration must be given to the use of a zero-g preparation scheme that would result either in extremely fine particles or a highly porous filigree structure. Either of these would contribute to the attainment of high surface/volume ratios. For either configuration, the preparation of a catalyst from an immiscible system would involve the leaching or dissolving of one phase in an interconnected system or the complete dissolution of the matrix phase of a two-phase system containing a fine dispersion of the catalyst sought. A present, both of these methods are used, in principle. The infiltration of porous glasses or metals, followed by the dissolution of the initial framework (similar to the production of superconducting materials as mentioned above) produces a network having high surface/volume ratios. In addition, foaming techniques are presently employed for the preparation of porous structures which have high surface/volume ratios and result in either filigrees or precursor "containers" for infiltration of metals. Likewise, products of aqueous reactions or precipitation from molten salts have been used to prepare fine dispersions of selected materials to be used in a variety of forms, including agents for

dispersion strengthening, aerosol applications and catalysts. It is anticipated that use of a zero-g environment can similarly provide suspensions of particles which can meet the necessary criteria for applications as catalysts, and can be produced in a form which would only require extraction from the carrier.

The requirement for a high surface/volume ratio precludes much consideration of bulk materials for application as catalysts. In only limited cases is there the potential that special electronic characteristics of interfaces between contiguous immiscible materials would contribute a catalytic role to any chemical reaction. However, were this feasible, it is suggested that the "lineal density" of interfaces which can be realized from materials prepared at 0-g would have to be sufficiently high and of necessary significance to warrant efforts in this direction.

2.435 Nuclear Reactor Control Rods. The TRW classification of suggested applications has delineated 15 systems which show promise for application to nuclear reactor control rods, as summarized in Table 10.

TABLE 10. SUGGESTED IMMISCIBLE SYSTEMS FOR APPLICATION TO NUCLEAR REACTOR CONTROL RODS(4)

Al-Cd	Dy-Ta	Gd-Ta
B-Cd	Dy-Ti	Gd-V
Cb-Gd	Dy-V	Gd-W
Cd-Fe	Dy-W	Hf-Mg
Dy-Mo	Gd-Mo	Sm-V

In each of these systems, at least one component has a sufficiently high neutron capture cross-section to play a significant role in poisoning of nuclear reactions and in the control of reactor rates. Based simply upon the materials selection, it apparent that composites using a distribution of the absorber material may be (and, in fact, have been) used in this application. It is yet to be determined, however, what critical parameters must be satisfied in order that control rods so prepared are most effective, both in terms of physical performance and cost effectiveness.

Specifically, it has not yet been ascertained whether the configurations and distributions expected from a zero-g preparation would provide more efficient utilization of the suggested poisons; whether a controlled size and shape distribution of dispersant can reduce problems associated with swelling; or whether reduction in attack on cladding materials (or other support strucutre materials) can be achieved. These questions must be answered first in order to determine the potential of space processing in this application area.

2.436 Permanent Magnet Materials. In this section, consideration has been given to the immiscible mixtures identified by TRW[4] which suggest application as fine particle permanent magnet materials. The systems that have been selected, purely on the basis of phase diagram data and the known ferromagnetic behavior of at least one of the components, are listed in Table 11.

Before considering the applicability of any of these systems specifically, it is necessary to briefly discuss selected factors which are presently influencing materials development for permanent magnets, including critical elements contributing to coercive force, size and shape considerations, the role of impurities and other defects, recent advances in miniaturized magnets based upon "standard" materials, and new developments in high energy-product materials.

In large part, the critical parameters of coercivity, energy product, etc. (all being grouped under the so-called "second quadrant" properties), are basically dependent upon magnetic domain structures and movement. The impediments to domain motion which arise from pinning

TABLE 11. FINE PARTICLE PERMANENT MAGNET MATERIAL CANDIDATES

Ag-Co	Cu-Fe[a]	Fe-Se
Ag-Fe	Cs-Fe	Fe-Sn
Ba-Ni	Dy-Mo	Fe-Sr
Bi-Co	Dy-Ta	Fe-Tl
Bi-Fe	Dy-Ti	Gd-Mo
Ca-Fe	Dy-U	Gd-Ta
Ca-Dy	Dy-V	Gd-U
Ca-Gd	Dy-W	Gd-V
Cb-Gd	Fe-Hg	Gd-W
Cd-Fe	Fe-K	K-Ni
Co-Cu[a]	Fe-Li	Li-Ni
Co-Hg	Fe-Mg	Na-Ni
Co-Pb	Fe-Na	Ni-Pb
Co-Se	Fe-Pb	Ni-S
Co-Tl	Fe-Rb	Ni-Tl
Cr-Gd	Fe-S	

[a] Miscibility gap occurs in undercooled melts. (32)

effects (impurities, grain boundaries) will govern the utility of permanent magnet materials for a broad variety of applications. High coercivities in almost all materials are directly associated with such "extrinsic" parameters influencing domain motion.

In addition, of course, there are the physical effects associated with shape of magnetic particles and the intrinsic magnetic crystal anisotropy. The former is a controlling feature in recent commercial improvements in classical magnetic materials, and the latter has a strong influence in new materials developed by the Air Force Materials Laboratory.

Consider first the size effects that might arise in experiments performed in the absence of gravitational fields, where we treat the situation in which fine magnetic particles are nucleated in a molten metal bath during cooling through a miscibility gap. First, it is necessary that particle sizes be at least as great as the domain size in the magnetic material, for below the threshhold dimensions (on the order of 0.1 micron), permanent ferromagnetic domain structures cannot be supported. In the region below the critical domain size, superparamagnetism becomes the dominant factor determining the properties of the materials.

Once the critical size has been achieved, the next most important parameter is the shape, for the highest coercive forces, energy products and retentivity, are associated with the shape anisotropy of the magnetic particles, with elongated and oriented particles showing the greatest effects. In present practice, the shaping of magnetic particles after mass preparation is generally accomplished through secondary working at temperatures sufficiently high to promote particle deformation but low enough to preclude the disolution of precipitated particles or impurities (where these latter contribute to the pinning effects noted above).

A second procedure, and one which may be considered as a candidate experiment for zero-gravity conditions, employs the production of ultrafine iron-cobalt single-domain particles by electrolysis and/or electrodeposition, and thermal treatment to produce elongated shapes*. In actual application, the fine particle permanent magnet domains are dispersed in a nonmagnetic (lead) matrix.

---

* The commercial product, Lodex (Registered Trademark of the General Electric Company), is presently available in a wide variety of sizes and shapes for special purpose applications.

The "individual treatment" experienced by the single domain particles permits tailored sizes, shapes, and distributions in a matrix such that predetermined magnetic properties may be achieved in components far smaller than those formerly available. Miniaturized magnets having higher energy products and coercivities have found commercial markets and industrial applications, particularly where space- and weight-savings are required.

One may extrapolate from this experience to consideration of zero-gravity conditions, in view of the existence of the immiscible systems Fe-Pb and Co-Pb. Under proper experimental conditions, it is anticipated that Fe-Co alloys could provide a model for investigation, particularly since there is presently a viable commercial material with which to contrast behavior.

In addition, it is suggested that selected compositions in the Alnico series of magnet materials may well be amenable to zero-gravity processing. The high-energy products associated with Alnico V (51 Fe/ 24 Co/14 Ni/8 Al/3 Cu), coupled with the fact that each of the elements exhibits immiscibility with Pb, suggest that this system should be investigated, taking into account several established observations. First, Alnico V has a higher reported energy product than any of the standard iron-base alloys (more will be said later regarding the rare earth-cobalt alloys), a large residual magnetic induction and a high coercive force. These intrinsic properties are generally achieved through domain-pinning effects arising from precipitated and dissolved impurities.

For the most part, this suggested system and method of preparation is directed more toward the use of the materials system as a convenient tool for process assessments and potentials, rather than upon an expressed need for improved materials. Commercial processes for the production of "standard" magnetic materials (such as the Lodex process) have been advanced to the point where useful materials can be fabricated at relatively low cost, taking advantage of well-developed techniques. However, the ability to duplicate existing methods or materials through processing in a different environment provides an experimental tool that reduces one of the variables: namely, the properties of existing materials have been well established, and the resultant space-processed materials have a standard with which to compare preparation variables.

There is an increasing demand for magnetic materials having improved properties such as coercive force, residual magnetism, high-energy product, etc. Applications range from needs in miniaturized commercial products (toys, hearing aids, video stimulators for minimally sighted persons, and the like) and in military equipment (communications, high-powered microwave equipment, etc.). Over the past few years, significant advances have been accomplished in terms of improved classical materials and crystallite size and shape. Such improvements have generally capitalized upon the advances available through alterations and control of the extrinsic shape anisotropies that contribute to overall behaviour. However, the most promising breakthroughs most recently found are associated with the series of compounds formed from cobalt and the rare earth elements, with the general formula $(RE)Co_5$. Pioneering work at the Air Force Materials Laboratory, followed by commercial research and development, has established several of these compounds as being far superior for permanent magnet applications. With the basis for advancement being use of the intrinsic crystal anisotropy of the materials, the most widely used system to date has been the $SmCo_5$ compound, where energy products of 20×10^6 gauss-oersteds (compared with 5×10^6 GOe for Alnico V) have been achieved.

Comparisons among a few permanent magnet materials, as shown in Table 12, show quite markedly the advances that have been made through new processing methods and basic material research over the past few years. To be sure, the Lodex commercial products display significant improvements over many of the Alnico series, although not nearly so dramatic as the cobalt alloys or compounds. However, it must be emphasized that for the purposes of the present investigation, the model preparation method for the Lodex materials offers a more direct comparison between the commercial and the experimental approaches considered here.

The major advances displayed by the rare earth cobalt series do not appear to be extendable by zero-gravity processing in the context of this study, principally because of the limited numbers of systems believed to show immiscibility. In review of the best available data, it is apparent that the three-component system Pb-Co-Pm combines immiscibility of both cobalt and a rare earth metal in a single common third element, and that this would constitute the most reasonable candidate at

TABLE 12. PROPERTIES OF SELECTED PERMANENT MAGNET MATERIALS

Material	Coercive Force, oersteds	Residual Induction, gauss	Energy Product, million gauss-oersteds
Alnico IV	700	5,500	1.3
Alnico I	440	7,200	1.4
Alnico XII	950	5,800	1.5
Lodex 33	860	8,000	3.2
Lodex 31	1140	6,250	3.4
Lodex 32	940	7,300	3.4
Vicalloy II	510	10,000	3.5
Alnico VI	750	10,000	3.5
Alnico V	550	12,500	4.5
Platinum Cobalt	3600	5,900	6.5
Samarium Cobalt	ca. 8000	ca. 8,000	ca. 16-20

the present. There is no information relative to the immiscibility of any $(RE)Co_5$ compound with another material, nor the thermodynamic stability of any of these compounds in relation to compound formation in the experimental configurations envisioned for this program.

In conclusion of this section, it is apparent that candidates for experimental evaluation are confined principally to permanent magnet materials of the Alnico type, taking advantage of the immiscibilities of the components with Pb, and directing efforts toward the preparation of suspended particles which take advantage of the shape anisotropies available. While it would be desirable to augment such studies to take better advantage of the crystalline anisotropies of the newer permanent magnet materials, such studies should be deferred until more complete information is available on the immiscibility of these compounds with other components.

2.437 Bearing Materials. In considering the various candidates suggested as immiscible materials for bearing applications, it is first important to note that there is considerable controversy regarding the influence of composition variables on the performance of bearings.* Overall performance surely is influenced by the size, distribution, and nature of included phases; the surface chemistry that affects the distribution of lubricants; the thermal diffusivity properties in the participating materials; the operating temperatures of the system; and the physical morphological properties before, during, and after the "wearing-in" process.

Following the TRW classification,[4] candidate systems showing potential promise are listed in Table 13. In addition to those noted, some additional consideration should be given to suggested solid lubricants, such as C-Cd and C-Pb.

In spite of the vast amount of research that has been directed toward the field of plain bearing materials, major developments have been more the result of empirical observations and correlations than detailed studies on the effects of individual variables on the performance of structures and devices. As a consequence, it is difficult to assess

---

* For the purposes of the present program the discussion will be limited exclusively to plain bearings, rather than ball or roller bearings.

TABLE 13. IMMISCIBLE MATERIALS SYSTEMS FOR BEARING ALLOYS[4]

Al-Cd	Cb-Pb	Fe-Pb
Al-In	Cd-Fe	Cu-Pb
Al-Pb	Mo-Sb	Ni-Pb

the specific importance of a difference in materials characteristics, preparation procedures, or secondary working on the ultimate behaviour of a plain bearing. One can only rely upon selected generalities that have been drawn from limited controlled research, and estimate the effect that such changes might have on operating modes.

Perhaps the most widely accepted hypotheses, which have been fairly well substantiated by microscopic examination, are: (1) the presence of soft inclusions--including those materials which do not significantly work-harden--as a free and available second phase enhances the applicability of a material for a plain bearing; and (2) for lubricated bearing surfaces, the surface chemistry should be manipulated such that sufficient wetting by a lubricant can be maintained. The second factor here has, for the most part, been relegated to a position of lower importance in research and development on bearing materials, with the first having been of primary consideration. Surely the presence, for example, of lead inclusions on bronze bearings and its availability at the bearing surface has contributed to the widespread use of this system. The somewhat detailed experiments by de Gee et al.[33] have clearly demonstrated that the availability of a lead film on a bearing surface is critical to the performance, in either the lubricated or unlubricated case.

However, while the presence of lead is an undisputed attribute for such materials, there is remaining a question and controversy as to whether the free lead should be present in the form of a coarse or fine distribution. It has been argued that chill-cast materials (having a fine distribution, perhaps very similar to that which could be achieved in a gravity-free environment) possess better mechanical properties, with

a reduced tendency to wear. However, an overriding feature of sand cast materials (where the lead distribution is coarser) relates to the surface chemistry in bearings with a layer of lubricant. In this case, it is noted that the free surface lead interrupts the continuity of adsorbed films of polar compounds in the lubricants, and that for a given volume of dispersed lead, the lineal density of matrix/inclusion interfaces will be smaller for the coarse than for the fine particles. It is thus presumed that the coarse particles are preferred for the plain bearing materials.

If this argument is correct, it would tend to minimize the importance zero-gravity processing in the preparation of plain bearing materials that depend upon the second phases of lead in a hard matrix. Based purely on the question of the properties of lubricating agents, the argument favors the use of sand-cast (or more slowly cooled) materials with coarse inclusions. In addition, even with unlubricated bearings, it has been determined that lead contents up to about 10 weight percent improve the wear characteristics, but that additions above this level are unnecessary. As seen from the TRW classification of immiscible systems, the miscibility gap in the Cu-Pb system exists in the range of lead concentration on the order of 36-87 weight percent, somewhat above the maximum found to be effective in bearing materials.

Some care should be exercised here in relying too heavily upon results obtained from the limited detailed work reported on the science of bearing materials. In an extensive review by Pratt [34], considerable coverage is devoted to discussions of Cu-Pb alloys with lead concentrations in the range of 30-40 weight percent. These have, in fact, found use in a variety of plain bearing applications, particularly in internal combustion engines.

Among the materials listed in Table 13, there may be some limited interest in developments of the Mo-Sb system, particularly in view of the high thermal diffusivity of molybdenum. In this case, the thermal diffusivity (or thermal conductivity) is important in reducing

the equilibrium temperature attained at operating bearing interfaces, and thus preventing the decomposition of lubricant. and the subsequent formulation of undesirable residue.

Aside from a few special features which characterize the properties of individual components in the immiscible systems given in Table 6, it does not appear that any of the suggested systems would offer significant improvements either in the preparation or in the properties of existing plain bearing materials. A single exception may be found with the Al-Pb system, said by Pratt to have attractive potential as an alternate to Al-Sn (this being based on the lower costs of Pb relative to Sn) but complicated by the fact of the gravitationally induced separation of Pb from the matrix. Zero-gravity preparation would, of course, obviate this problem. Furthermore, Pratt noted that a number of applications for the Al-Pb bearing system (even including designs which capitalize upon the Pb segregation) have been found, and that compatibility with other metals in overall design is exceptionally good. It must be noted, of course, that pure aluminum matrix materials have limited appeal as bearing materials due to the low yield strength and high thermal expansion coefficient. A few aluminum alloys have been developed to circumvent these intrinsic problems.

In the light of the above discussion and the confusion as to the type of microstructure which leads to superior bearing properties, we would recommend that bearing materials having fine Pb dispersions produced by space processing be fabricated and tested. These materials could be in the Cu-Pb or Al-Pb systems.

2.438 Superplastic Materials. Superplasticity is a phenomenon characterized by the following:

(1) Extensive ductilities. Tensile elongations of several hundred percent to > 1,000 percent are commonly observed.
(2) Low values of flow stress.
(3) Viscous flow behavior.

Superplasticity occurs at intermediate temperature ranges ($\sim 0.5\ T_m$) and is very sensitive to strain rate. An example of this behavior taken from Reference 35 is shown in Figure 22 and demonstrates the effect of strain rate $\dot{\varepsilon}$ on elongation, flow stress, σ, and strain sensitivity index, m. σ and m are related to $\dot{\varepsilon}$ by the equation

$$\sigma = k\dot{\varepsilon}^m \quad ,$$

where k is a constant.

For a superplastic material, m is normally > $\sim$ 0.2 rather than < 0.1, the usual value found in normal-behaving metals and alloys. The curves shown in Figure 22 are for the eutetoid alloy 78 percent Zn - 22 pct Al, tested in the range 260 to 270 C. The structure of this material consists of a fine mixture of zinc and aluminum-rich phases.

The fineness of structure is a common feature of superplastic materials since the basic flow mechanisms (grain or interphase boundary shear coupled with grain boundary accommodation) depend greatly on interfacial effects. It is not only important that the structure be fine initially but also remain fine during heating to the superplastic temperature and during subsequent deformation at this temperature. Pure metals are the least stable in this regard since they have no barriers to grain growth. Mixtures of phases which have very limited mutual solubility are the most stable. Thus, immiscible systems with limited mutual solid solubility appear to be good candidates for demonstrating superplasticity if they can be produced as an extremely finely divided dispersion (on the order of 1 μ).

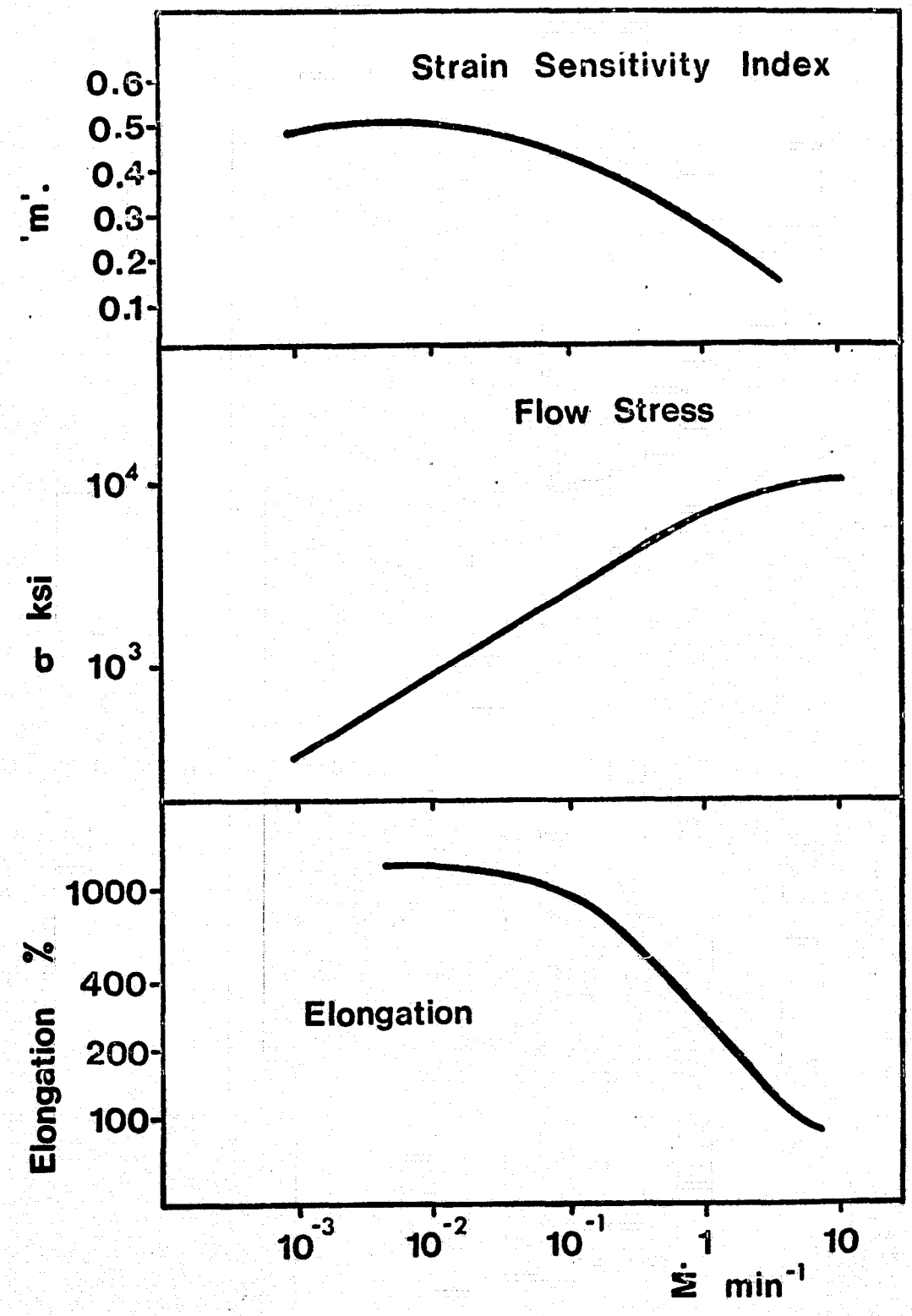

FIGURE 22. TYPICAL PROPERTIES OF SUPERPLASTIC Al-Zn ALLOY(35)

Superplastic materials have a number of advantages over conventional materials. The most important of these is their ability to be formed into extremely intricate shapes. What is also important is the low stress required in forming these materials.* This allows less expensive, lower capacity-forming equipment to be used in the forming operations. In addition, the viscous nature of superplastic material coupled with the low flow stresses allows us to draw on the forming technology which exists in the plastics and glass industry. Thus, vacuum-forming and glass-blowing techniques can be directly applied to the forming of superplastic materials. Aside from the economic considerations which have not been addressed as yet, space processing of immiscible materials appears to be ideally suited for production of materials with the desired fine structure and superplastic properties. As previously discussed, finer structures are expected and, indeed, have been observed[2,4] in low-gravity-processed systems containing a liquid-phase miscibility gap compared to terrestrially processed materials. It is, thus, concluded that alloys containing a liquid-phase miscibility gap, when processed in a zero-gravity environment, would readily produce alloys exhibiting superplastic behavior.

Accordingly, we have started with Reger's compilation[4] of systems containing a liquid-phase miscibility gap and added the following conditions:

(1) The mixture of phases involves only the pure components and not compounds.

(2) The components have melting points which are reasonably close to each other.

(3) The mutual solid solubility of the components is relatively small.

(4) The components are relatively common materials.

---

* It should be noted that although the flow stress is low in the superplastic temperature and strain rate region, at ambient temperature the fine structured materials would normally have high strength and good ductility.

Criteria (1) and (2) were imposed to ensure that the flow properties of both phases in the mixture would be similar in order that the flow of the alloy be uniform. Criterion (3) has been imposed to better ensure that the structures remain fine grain during heating and deformation. Lastly, the fourth condition insures that the system selected is a practical one.

The systems selected on the basis described above are listed in Table 14. The further selection of one system over another will depend not only on the formability where the superplasticity properties are of importance but also on the properties desired in the formed component (strength, magnetic properties, bearing properties, etc.).

TABLE 14. SELECTED LIST OF CANDIDATE SYSTEMS WITH POTENTIAL SUPERPLASTIC BEHAVIOR

Ag-V	Cu-Fe[(a)]
Bi-Zn	Pb-Zn
Co-Cu[(a)]	Tl-Zn
Cr-Y	

(a) Miscibility gap in Co-Cu and Cu-Fe systems occurs in undercooled liquid alloys. (33)

REFERENCES

(1) Markworth, A. J., Gelles, S. H., Duga, J. J., and Oldfield, W., in Proceedings of the Third Space Processing Symposium, NASA Report No. 74-5 (June, 1974) p. 1003.

(2) Reger, J. L., and Yates, I. C., Jr., "Preparation and Metallurgical Properties of Low-G Processed Immiscible Materials", AIAA Paper No. 74-207, presented at AIAA 12th Aerospace Sciences Meeting, Washington, D.C. (January 30 - February 1, 1974).

(3) Lacy, L. L., and Otto, G. H., "The Electrical Properties of 0-G Processed Immiscibles", AIAA Paper 74-208, presented at AIAA 12th Aerospace Sciences Meeting, Washington, D.C. (January 30 - February 1, 1974).

(4) Reger, J. L., "Study of Processing Immiscible Materials at 0 G", Interim Report to NASA-MSFC, Contract NAS8-28267 (May, 1973).

(5) Lacy, L. L., and Otto, G. H., "The Stability of Liquid Dispersions in Low G", AIAA Paper No. 74-1242.

(6) Gelles, S. H., and Nowak, W. B., "Cryotron Alloy Development", Nuclear Metals, Inc., Report NMI 4900 (September 20, 1957).

(7) Kenning, D.B.R., "Two-Phase Flow with Nonuniform Surface Tension", Appl. Mech. Rev., 21 (1968) 1101.

(8) Markworth, A. J., "The Kinetic Behavior of Precipitate Particles Under Ostwald Ripening Conditions", Metallography, 3 (1970) 197.

(9) Bodsworth, C., and Bell, H. B., Physical Chemistry of Iron and Steel Manufacture (Second Edition), Longman Group Limited, London (1972), Section 13.6: "Formation and Removal of the Deoxidation Products", 418-427.

(10) Turkdogan, E. T., "Deoxidation of Steel", in Chemical Metallurgy of Iron and Steel, Iron and Steel Institute, London (1973) 153-170; also in J. Iron Steel Inst., 210 (1972) 21.

(11) Present, R. D., Kinetic Theory of Gases, McGraw-Hill Co., Inc., New York (1958) Section 11-3: "The Boltzmann Integrodifferential Equation", 224-232.

(12) Baroody, E. M., "Calculations on the Collisional Coalescence of Gas Bubbles in Solids", J. Appl. Phys., 38 (1967) 4893.

(13) Drake, R. L., "Processes Influencing Evolution of Droplet or Aerosol Spectrum", in Precipitation Scavenging (1970), Coordinated by R. J. Engelmann and W.G.N. Slinn, USAEC Report CONF-700601 (December, 1970) 385.

(14) Lindborg, U., and Torssell, K., "A Collision Model for the Growth and Separation of Deoxidation Products", Trans. Metall. Soc. AIME, 242 (1968) 94.

(15) Miejering, J. L., "Precipitation", J. Less-Common Metals, 28 (1972) 419.

(16) Markworth, A. J., and Oldfield, W., "Precipitation Kinetics of Inert-Gas Bubbles in Solids; A Computer Model", Mater. Sci. Eng., 10 (1972) 159.

(17) Smoluchowski, M. V., "Versuch einer Mathematischen Theorie der Koagulationskinetik Kolloider Lösungen", Z. Physik. Chem., 92 (1917) 129.

(18) Chandrasekhar, S., "Stochastic Problems in Physics and Astronomy", Rev. Mod. Phys., 15 (1943) 1.

(19) Baroody, E. M., "Calculations on the Collisional Coalescence of Gas Bubbles in Solids", J. Appl. Phys., 38 (1967) 4893.

(20) Wagner, C., "Theorie der Alterung von Niederschlagen Durch Umlösen", Z. Elektrochem., 65 (1961) 581.

(21) Markworth, A. J., "The Kinetic Behavior of Precipitate Particles Under Ostwald Ripening Conditions", Metallography, 3 (1970) 197.

(22) Markworth, A. J., "Ostwald Ripening of a Narrow Precipitate Size Distribution", Ber. Bunsenges Phys. Chem., 75 (1971) 533.

(23) Markworth, A. J., "Approaches to Describing the Kinetic Behavior of Distributions of Second-Phase Inclusions", in Defects and Transport in Oxides, Edited by M. S. Seltzer and R. I. Jaffee, Plenum Press, New York (1974) 397.

(24) Miller, C., Du Pont (Wilmington, Delaware), personal communication.

(25) Fuchs, N. A., The Mechanics of Aerosols, The Macmillan Company, New York (1964) 338 ff.

(26) Constant, F. W., Theoretical Physics-Mechanics of Particles, Rigid and Elastic Bodies, Fluids, and Heat Flow, Addison-Wesley Publ. Co., Inc., Reading, Massachusetts (1954) 236-237.

(27) Metals Handbook, American Society for Metals, Vol. 8 (1973).

(28) Gelles, S. H. and Malik, R. K., "Process Development for Producing Fine-Grain Castings in Space", Final Report to NASA-MSFC (February 24, 1975).

(29) Maringer, R. E., and Mobley, C. E., "Casting of Metallic Filament and Fiber", Proceedings of the Vacuum Metallurgy Conference held June 17-20, 1974, American Institute of Physics (1974) 1067.

(30) Gupta, A. D., Mordike, B. L., and Schultz, L., "Superconductivity in a Dilute Copper-Niobium Alloy", Materials Science and Engineering, 18 (1975) 137-142.

(31) Livingstone, J. D. and Cline, H. E., "Monotectic Solidification of Cu-Pb Alloys", Trans Met Soc AIME, 245 (1969) 351.

(32) Nakagawa, Y., "Liquid Immiscibility in Copper-Iron and Copper-Cobalt Systems in the Supercooled State", Acta Met, 6 (1958) 704.

(33) deGee, W. J., Vaessen, G. H. G., and Begeliner, A., ASLE Transactions, 12 (1969) 44.

(34) Pratt, G. C., "Materials for Plain Bearings," International Metallurgical Reviews (1973).

(35) Hundy, B. B., "Exploitation of Plasticity and Superplasticity in the Sheet Metal Industry", Plasticity and Superplasticity, Institution of Metallurgists, Review Course, Series 2, Number 3, 212-69-T.